State of Global Water Resources 2024

Report

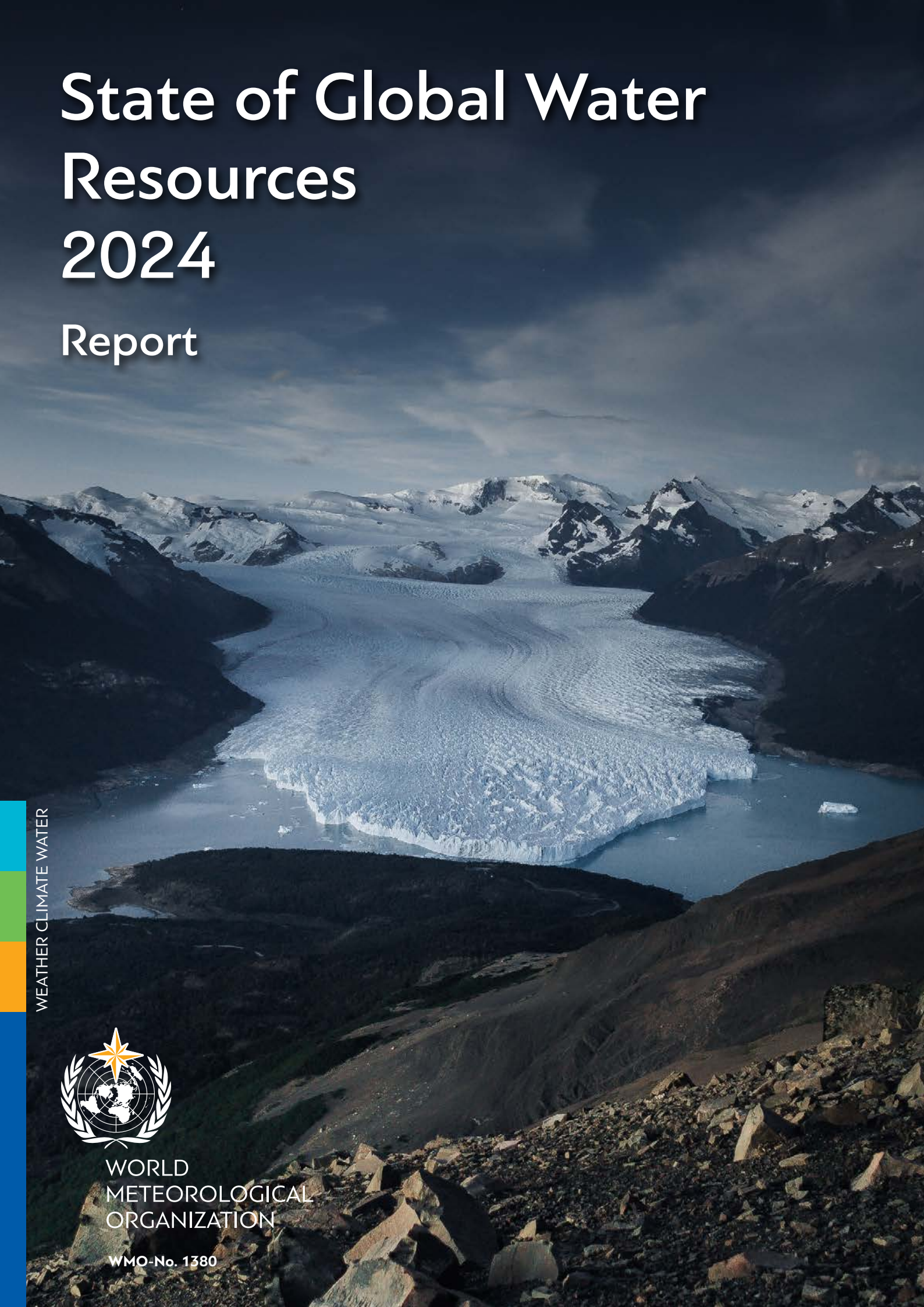

WEATHER CLIMATE WATER

WORLD METEOROLOGICAL ORGANIZATION

WMO-No. 1380

Give us your feedback!

https://forms.office.com/e/cvThhHNq8H

Interactive version of the report

https://storymaps.arcgis.com/stories/50803c1f47444637b8e2c4683c6c0689

WMO Publication page

https://wmo.int/publication-series/state-of-global-water-resources-2024

WMO-No. 1380

Chair, Publications Board
World Meteorological Organization (WMO)
7 bis, avenue de la Paix
P.O. Box 2300
CH-1211 Geneva 2, Switzerland

Tel.: +41 (0) 22 730 84 03
Email: publications@wmo.int

ISBN 978-92-63-11380-1

Cover photo: Ignacio Bruno, “A quiet night at the edge”, Santa Cruz Province, Argentina.

Contents

Scope ii

Foreword iii

Acknowledgements iv

List of abbreviations vii

Executive summary viii

Introduction 1
- Data sources 3
- Anomaly calculation 4
- The backdrop: Overview of climatic conditions in 2024 5

River discharge 8

Reservoirs 13
- Inflow into selected reservoirs 13
- Reservoir storage 14

Lakes 16
- Lake levels 16
- Lake water temperature 16

Groundwater levels 19

Soil moisture 22
- Observed soil moisture 22
- Modelled soil moisture 22

Evapotranspiration 24

Terrestrial water storage 26

Snow cover and glaciers 28
- Snow water equivalent and seasonal peak snow mass 28
- Glaciers 30
- Case study on glaciers in Colombia 32

High-impact hydrological events 33
- Floods in Morocco and Algeria 33
- Floods in Europe 35
- Floods in Viet Nam, China, Myanmar and the Philippines 36
- Floods in Afghanistan, the Islamic Republic of Iran and Pakistan 36
- Floods in Nepal and India 36
- Floods in the United Arab Emirates 37
- Floods and drought in Brazil 37
- Floods and drought in the United States 38
- Floods in Kazakhstan and the Russian Federation 38
- Floods in West and Central Africa 38
- Floods in East Africa 39
- Floods in Australia 39
- Glacier outburst flood in Canada 39

Outlook 40

References 41

Annex. Technical annex 45

References 80

Scope

About the report:

The State of Global Water Resources Report, published annually by WMO, provides a comprehensive quantitative overview of global water resources, with a focus on hydrological variability and trends. It supports countries, decision makers and stakeholders in understanding the current state of water resources, identifying hotspots and supporting effective water management strategies. The report is based on data contributed by WMO Members, as well as information from global hydrological modelling systems and satellite observations provided by various partners.

What the report contains:

- Assessment of global freshwater availability, including streamflow, lakes, groundwater, soil moisture, snow and ice, and combined terrestrial water storage.
- Map of key hydrological extreme events throughout the year such as floods and droughts.
- A case study highlighting regional and national water resource conditions.
- Global maps with easy-to-understand colour-coded indicators.
- Comparative analysis of the current state with long-term hydrological normals, and an evaluation of the impact of climate variability and change on water resources and the hydrological cycle.

What the report does not contain:

- Detailed national or subnational, or regional or trans-boundary water management strategies.
- Projections or future scenario modelling (the focus is retrospective, not predictive).
- Policy recommendations – it is a scientific and technical report that can be used as a basis for future strategy, policies and investment decisions.
- Full raw datasets – only indicators and highlights are included.

Who the report is for:

Government agencies, policymakers and investors working on water resources and climate adaptation.

Hydrologists, climatologists and environmental scientists, as well as members of the media and the general public interested in global water resources trends and climate impacts and seeking authoritative and recent global data.

International organizations involved in water security, development and disaster risk reduction.

How to cite the report:

World Meteorological Organization (WMO). *State of Global Water Resources 2024* (WMO-No. 1380). Geneva, 2025. DOI: https://doi.org/10.59327/WMO/WATER/2024

Foreword

Water is life. It sustains our societies, powers our economies and anchors our ecosystems. And yet the world's water resources are under growing pressure, and – at the same time – more extreme water-related hazards are having an increasing impact on lives and livelihoods. Reliable, science-based information is more important than ever before, because we cannot manage what we do not measure.

The WMO *State of Global Water Resources 2024* is part of WMO's commitment to provide that knowledge. It is an authoritative, independent and comprehensive assessment of the world's water resources and the hydrological cycle. Introduced in response to the growing global demand for reliable science-based evidence to inform policy and guide decisions, the report has gained widespread endorsement from WMO Members and international partners.

It offers a detailed overview of water resources across major basins by comparing recent observations and model results with long-term averages, reflecting the dynamic nature of the water cycle. Information on the state of the cryosphere – snow and ice – provides valuable insights and data for policymakers in the 2025 International Year of Glaciers' Preservation, which is co-implemented by WMO.

The 2024 edition builds upon the success of previous editions and expands its scope by incorporating new variables such as precipitation, lake water levels, lake surface temperature, peak snow cover and water quality. The report highlights the critical need for improved data sharing on streamflow, groundwater, soil moisture and water quality, which remain heavily under-monitored. Continued investment and enhanced collaboration in data sharing are vital to close these gaps, in line with the WMO Unified Data Policy and the WMO Hydrological Observing System (WHOS). Without data, we risk flying blind.

I extend my deepest gratitude to the National Meteorological and Hydrological Services, data centres, researchers and institutions that provided inputs on in situ observations, hydrological and land surface models as well as remote sensing data. All of these are essential for capturing the complex and evolving water cycle and making this information accessible and actionable.

I am confident that this report equips decision makers with the intelligence and insights needed to make informed, forward-looking decisions. It supports vital global initiatives, including the Early Warnings for All campaign and the Sustainable Development Goals.

WMO looks forward to continuing to work with WMO Members and many partners on this report series. We remain committed to a vision in which every country, community and citizen can access timely, reliable water data and information to safeguard lives, livelihoods and ecosystems.

(Prof. Celeste Saulo)
Secretary-General

Acknowledgements

WMO is grateful to the following contributors.

WMO MEMBER STATES AND TERRITORIES THROUGH HYDROLOGICAL ADVISERS AND ASSIGNED FOCAL POINTS FOR THE STATE OF THE GLOBAL WATER RESOURCES REPORT

Argentina; Armenia; Australia; Austria; Azerbaijan; Belgium; Belize; Benin; Bhutan; Botswana; Brazil; Bulgaria; Canada; Chile; China; Colombia; Costa Rica; Croatia; Cuba; Cyprus; Czechia; Denmark; Egypt, El Salvador; Estonia; Finland; France; Germany; Ghana; Guatemala; Guinea; Hong Kong, China; Hungary; Iceland; India; Islamic Republic of Iran; Iraq; Ireland; Israel; Italy; Jamaica; Japan; Jordan; Kazakhstan; Kenya; Republic of Korea; Kyrgyzstan; Latvia; Lesotho; Lithuania; Luxembourg; Malawi; Mali; Mauritius; Mexico; Republic of Moldova; Montenegro; Myanmar; Namibia; Nepal; Kingdom of the Netherlands; New Zealand; Nigeria; North Macedonia; Norway; Pakistan; Panama; Paraguay; Peru; Philippines; Poland; Portugal; Russian Federation; Serbia; Singapore; Slovakia; Slovenia; South Africa; Spain; Sri Lanka; Sweden; Switzerland; United Republic of Tanzania; Thailand; Turkmenistan; Ukraine; United Kingdom of Great Britain and Northern Ireland; United States of America; Uruguay; Uzbekistan; Viet Nam.

Hydrological Advisers and focal points contributed to and supported the preparation of the present report by providing observational data, information about major hydrological events that occurred in 2024 and other relevant information, and participated in the review and validation of the report.

WMO non-Member, State of Palestine, also supplied data.

STEERING COMMITTEE MEMBERS

Jan Danhelka (Czechia, Vice-President of WMO INFCOM); Harry Dixon (United Kingdom); Lucy Barker (United Kingdom, WMO HydroSOS Technical Team Lead); Albert Martis (Curaçao and Sint Maarten, Chair of WMO Hydrological Coordination Panel); Michel Jean (Canada, President WMO INFCOM); Harry Lins (United States); Ian Lisk (United Kingdom, President WMO SERCOM); Ilias Pechlivanidis (Sweden, WMO Research Board); Marcelo Uriburu Quirno (Argentina, Vice-Chair of the WMO Standing Committee on Hydrological Services); Yuri Simonov (Russian Federation, Chair of the WMO Standing Committee on Hydrological Services); Narendra Tuteja (Australia, Chair of the WMO Expert Team on Operational Hydrological Prediction Systems); Andy Wood (United States, WMO Expert Team on Operational Hydrological Prediction Systems).

REGIONAL HYDROLOGICAL ADVISERS

Angela Corina (WMO Regional Association VI), John Fenwick (WMO Regional Association V), Mohamed Housseini Ibrahim (WMO Regional Association I), Mamoru Miyamoto (WMO Regional Association II), Waldo Lavado (WMO Regional Association III), and Peter Clarke (WMO Regional Association IV), who contributed to the preparation and review of the report.

WMO EXPERTS

Experts from the Standing Committee on Climate Services, Standing Committee on Hydrological Services, Standing Committee on Services for Agriculture and Study Group on Renewable Energy Transition who participated in the preparation and review of the report.

MEMBERS OF THE GLOBAL HYDROLOGICAL MODELLING COMMUNITY

Diani Nimanthika Abeyrathne (University of Tokyo), Clement Mathieu Jacques Albergel (European Space Agency (ESA)), Alice Andral (CLS Group), Berit Arheimer (Swedish Meteorological and Hydrological Institute (SMHI)), Nishan Kumar Biswas (NASA), Eva Boergens (German Research Centre for Geosciences (GFZ) Potsdam), John D. Bolten (National Aeronautics and Space Administration (NASA)), Beatriz Calmettes (CLS Group), Laura Carrea (University of Reading), Cedric H. David (NASA), Bram Droppers (Utrecht University), Omid Elmi (University of Stuttgart), Mohamed Elshamy (Environment and Climate Change Canada (ECCC)), Riley Hales (Brigham Young University (BYU)), Shaun Harrigan (European Centre for Medium-range Weather Forecasts (ECMWF)), Yeshewatesfa Hundecha (SMHI), Ruben Imhoff (Deltares), Kristina Isberg (SMHI), Wayne Jenkinson (ECCC), Jeffrey Karn (ECCC), Rohini Kumar (Helmholtz Centre for Environmental Research – UFZ), Sujay Kumar (NASA), Wenchao Ma (University of Tokyo), Henrik Madsen (DHI), Fadji Zaouna Maina (NASA), Simon A. Mischel (Federal Institute of Hydrology (BfG)), Lawrence Mudryk (ECCC), Alexandra Murray (DHI), Jim Nelson (BYU), Wanshu Nie (NASA), Emmanuel Nyenah (Goethe University Frankfurt), Oldrich Rakovec (Czech University of Life Sciences Prague), Robert Reinecke (University of Mainz), Jörgen Rosberg (SMHI), Peyman Saemian (University of Stuttgart), Luis Samaniego (Helmholtz Centre for Environmental Research – UFZ), Pallav Kumar Shrestha (Helmholtz Centre for Environmental Research – UFZ), Nico Sneeuw (University of Stuttgart), Edwin H. Sutanudjaja (Utrecht University), Mohammad J. Tourian (University of Stuttgart), Athanasios Tsiokanos (Deltares), Niko Wanders (Utrecht University), Albrecht Weerts (Deltares), Richard Alpfjord Wylde (SMHI), Kosuke Yamamoto (Japan Aerospace Exploration Agency (JAXA)), Kei Yoshimura (University of Tokyo), Xing Yuan (Nanjing University of Information Science and Technology (NUIST)), Yongqiang Zhang (Institute of Geographic Sciences and Natural Resources Research (IGSNRR), China), Markus Ziese (Deutscher Wetterdienst (DWD)), who contributed to the initial discussions, report preparation, global modelling and remotely sensed data, feedback and review.

GLOBAL DATA CENTRES AND EXTERNAL EXPERTS

Feifei Cao (International Groundwater Resources Assessment Centre (IGRAC)), Stephan Dietrich (BfG), Elie Gerges (IGRAC), Elisabeth Lictevout (IGRAC), Simon A. Mischel (Global Runoff Data Centre (GRDC)), Philipp Saile (Global Environment Monitoring System for Freshwater (GEMS/Water)), Matthias Zink (International Soil Moisture Network (ISMN)), Markus Ziese (Global Precipitation Climatology Centre (GPCC)), who supported the preparation of the report. We thank Jan Polcher and Aaron A. Boone (Global Energy and Water Exchanges (GEWEX)) for contributing to the preparatory workshop for this report. We also thank the research group of Nico Sneeuw (University of Stuttgart) for datasets for the extension of in situ river discharge data through satellite observations.

CONTRIBUTORS AND CO-AUTHORS FOR SPECIFIC CHAPTERS

Groundwater levels: Feifei Cao (IGRAC), Elie Gerges (IGRAC), Elisabeth Lictevout (IGRAC), who led the preparation of the chapter and developed the methodology.

Soil moisture: Matthias Zink (ISMN), who contributed to the soil moisture chapter with in situ data and supported the drafting of the related section.

Terrestrial water storage: Eva Boergens and Andreas Güntner (GFZ), who provided the terrestrial water storage data which form an important part of the present report.

Snow cover and glaciers: Inés Dussaillant (World Glacier Monitoring Service (WGMS), University of Zurich), Lawrence Mudryk (ECCC) and Michael Zemp (WGMS, University of Zurich), who provided results on glacier mass changes and snow cover.

Water quality section in the annex: Philipp Saile (GEMS/Water), who provided results and drafted the text for the water quality analysis included in the annex to the report.

WMO SECRETARIAT LEAD AUTHORS

Sulagna Mishra (Scientific Officer) and Stefan Uhlenbrook (Director, Hydrology, Water and Cryosphere), who were also supported by hydrology colleagues within the Secretariat in producing and reviewing the report.

INDEPENDENT CONSULTANTS

Anastasia Lobanova and Iulii Didovets, who carried out the scientific analysis of the raw data to produce the results for the chapters on river discharge, soil moisture, evapotranspiration, reservoirs, lakes, snow cover and glaciers and high-impact hydrological events. They contributed significantly to writing of the report with support from the authors mentioned above. Nilay Dogulu, who reviewed the report and designed the conceptual illustrations and the infographic).

List of abbreviations

AET	Actual evapotranspiration
DJF	December–January–February
ESA	European Space Agency
GHMS	Global hydrological modelling system
GRACE	Gravity Recovery and Climate Experiment
GPCC	Global Precipitation Climatology Centre
GRDC	Global Runoff Data Centre
HydroSOS	Hydrological Status and Outlook System
IGRAC	International Groundwater Resources Assessment Centre
ISMN	International Soil Moisture Network
JJA	June–July–August
MAM	March–April–May
NMHSs	National Meteorological and Hydrological Services
SDGs	Sustainable Development Goals
SON	September–October–November
SWE	Snow water equivalent
TWS	Terrestrial water storage
WHOS	WMO Hydrological Observing System

Executive summary

HYDROLOGICAL CONDITIONS AND SIGNIFICANT EVENTS OF 2024

- **Climatic conditions:** The year 2024 was the hottest in the 175-year observational record, with the annual mean surface temperature reaching 1.55 °C (±0.13 °C) above the pre-industrial baseline (1850–1900). Early 2024 was dominated by pronounced El Niño conditions, which contributed to droughts in northern South America and southern Africa. The Amazon basin was hit by a severe drought: intensifying during April–June, it reached its peak in July–September, before easing partially in October–December. Below-normal precipitation conditions also spread across north-western Mexico, the northern part of North America – including the Fraser and Mackenzie river basins, as well as in southern and south-eastern Africa, including the Orange, Limpopo, Zambezi and Congo basins. Wetter-than-normal conditions prevailed over central-western Africa, the Lake Victoria basin in Africa, Kazakhstan and the southern Russian Federation, Central Europe, Pakistan and northern India, the southern Islamic Republic of Iran, and north-eastern China.

  In addition to an overview of the climatic conditions during the year, this report covers a wide range water cycle components (see the Figure), as explained below.

- **River discharge:**[1] In 2024, deviations of river discharge from normal conditions[2] occurred in approximately 60% of the global catchment area. In the past six years only about one-third of the global catchment area was under normal discharge conditions when compared to the 1991–2020 average. In 2024, above- to much-above-normal discharge conditions prevailed across Central and Northern Europe and parts of Asia, including Kazakhstan and the Russian Federation. Major basins such as the Danube, Ganges, Godavari and Indus

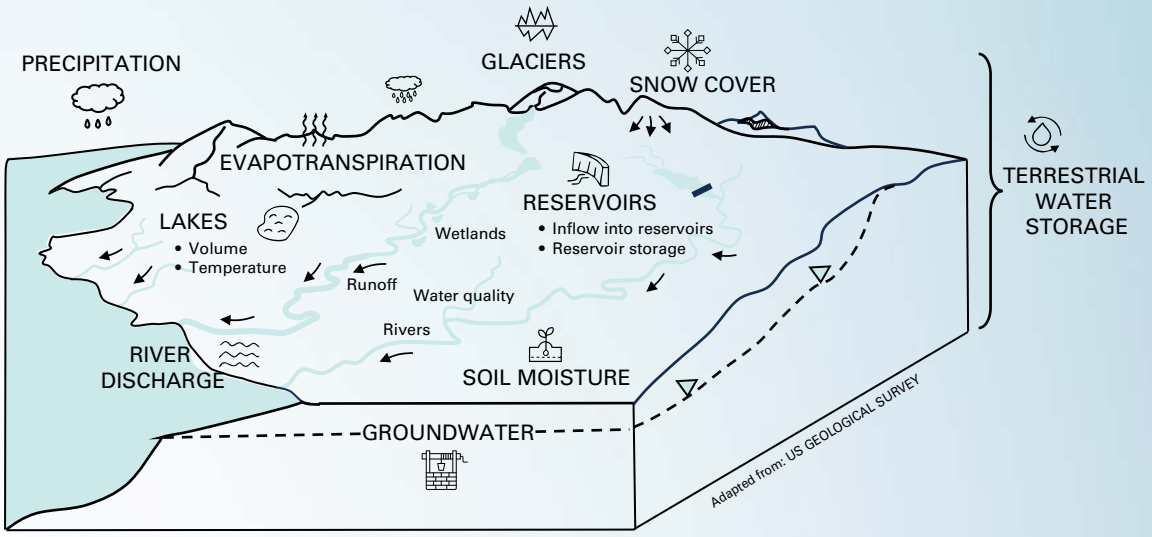

Figure. The components of the water cycle covered by the report

[1] Analysis based on observed and modelled results.

[2] Refer to Box 2 for definition of normal, above-normal and below-normal conditions

experienced above- to much-above-normal conditions. Severe drought, which had started at the end of 2023, persisted in South America, with much-below-normal discharge across key river basins, including the Amazon, São Francisco, Paraná and Orinoco. In Africa, above-normal discharge manifested in West African basins (Senegal, Niger, Lake Chad, Volta) affected by extensive flooding, while southern African basins (Zambezi, Limpopo, Okavango, Orange) recorded much-below-normal discharge conditions. Continuing from 2023, northern North American rivers (Mackenzie, Fraser, Nelson, Churchill) experienced below- to much-below-normal discharge, while Mississippi River discharge returned to the normal range in 2024 after a hydrological drought in 2023.

- **Reservoirs:** Inflows to reservoirs in southern Brazil within the La Plata basin remained below- to much-below-normal, consistent with the discharge conditions across almost the entire continent of South America. However, the reservoir storage was below-normal and normal in some parts of the basin. Above-normal inflows were observed in reservoirs across western and Northern Europe and South-east Asia, following above-normal discharge conditions in 2024. In Central and West Africa, reservoir storage was below normal despite above-normal inflows, hinting at the potential effect of reservoir regulation and/or water abstraction. The Aswan High Dam on the Nile experienced below-normal storage, while reservoirs along the East African coast (Greater Horn of Africa) recorded above- to much-above-normal storage, in line with above-normal inflows during 2024.

- **Lakes:** In Canada, lake levels within the Mackenzie, Fraser and Churchill River catchments remained consistently below- to much-below-normal. In Africa, most large lakes (Victoria, Turkana, Tanganyika and Chad) recorded much-above-normal levels, with the exception of Lake Kariba, which had much-below-normal levels. In the Middle East and Central Asia, lake levels were much below normal, and in Northern Europe and the European part of the Russian Federation, including Lake Ladoga, lake levels were above normal, as was the case for Lake Baikal in the Russian Far East. Lake surface temperatures were anomalously high globally in July. Nearly all out of 75 selected principal lakes across the globe saw above- to much-above-normal temperatures in July, with a few exceptions (for example, Lakes Nicaragua and Guri in Central and South America and lakes in Sweden, eastern China and across the northern United States).

- **Groundwater levels:** The analysis of groundwater levels includes data from a total of 37 406 groundwater monitoring stations across 47 countries. Groundwater levels vary locally due to aquifer heterogeneity and human influences like pumping; still, larger-scale regional trends were observed. In 2024, 38% of studied stations had normal groundwater levels; 25% were below- or much-below-normal and 37% were above- or much-above-normal. Above- and much- above-normal groundwater levels, shifting from below- and much-below-normal levels in 2023 and indicating recharge, were observed in parts of Europe, India, Florida and southern Brazil, linked to wetter-than-normal conditions and flooding. Continued or declining below-normal levels were observed in Southern Europe, parts of Africa, India, the United States, Mexico, Chile, Brazil and southern Australia. Declines in several regions (such as north-western India, the north-western and Midwestern United States, the Yucatán Peninsula and El Salvador) occurred without long-term drought conditions, pointing to over-abstraction as a key driver.

- **Soil moisture:** Widespread soil moisture deficits were observed across South America in 2024, especially over the Amazon and Paraná basins, and in most African basins; exceptions were the Chad, Niger (August) and Congo (December) basins, as well as the territory of the Horn of Africa, which remained consistently above normal. In Central Europe, soil moisture was much above normal, whereas in the Mediterranean basin and Eastern Europe (larger parts of the Danube basin) soil moisture was below to much

below normal. In almost all African basins (Orange, Zambezi, Limpopo, Nile and Congo) the soil moisture was below to much below normal almost throughout 2024, except for the Chad and Niger in August and the Congo in December. Soil moisture in the Horn of Africa remained above to much above normal throughout the year. The availability of observed data for this variable still remains challenging both for detection of regional trends and for model validation. Note that in 2024 there were 220 stations in total, and in situ observations for only two countries (the United States and Spain) were received for the analysis.

- **Evapotranspiration:** Much-above-normal actual evapotranspiration (AET) was observed during December 2023 and May 2024 across large parts of North America, China, the Murray–Darling basin and the Horn of Africa. Much-above-normal AET occurred in March–May across the Persian Gulf countries and eastern Asian basins (Yangtze, Yellow, Lena, Amur and Enisey). Persistent AET deficits developed in South America, with much-below-normal values across the La Plata and Amazon basins from March to November 2024. In the southern African Limpopo, Zambezi, Orange and Congo basins, AET was below to much below normal throughout the entire year, and this was especially pronounced during the March–April–May (MAM) and June–July–August (JJA) seasons.

- **Terrestrial water storage:** In 2024, terrestrial water storage (TWS) was positive across sub-Saharan Africa, northern Australia, and eastern and western Central Africa. TWS deficits were particularly pronounced in South America, where the La Plata and Amazon basins continued to exhibit significantly reduced TWS. This reflects the persistence of drought conditions that have affected the region since 2023. Recovery to near-normal TWS occurred in Central and western Europe, which were previously affected by deficits in 2023, likely due to excessive precipitation during 2024.

- **Snow cover:** The snow water equivalent (SWE) (a measure for the amount of water contained in the snow pack) in March 2024 was below to much below normal in the eastern and Central European Danube, Dniepr, Elbe and Oder basins, while the seasonal peak snow mass was within the normal range in 2024 in these basins, suggesting that the peaks for both snow accumulation and melt occurred earlier in the season than typical. North America experienced significant SWE deficits in March, especially in the St. Lawrence and Mississippi basins. In Central Asia, above-normal seasonal peak snow mass combined with rapid warming in late March triggered flooding in northern Kazakhstan and nearby Russian Federation regions.

- **Glaciers:** The year 2024 was the third consecutive year in which widespread ice loss was recorded across all glaciated regions, with 450 Gt lost – equivalent to 1.2 mm of sea-level rise. Record mass loss occurred in Scandinavia, Svalbard and North Asia, while some regions, such as the Canadian Arctic and Greenland periphery, saw more moderate losses. Most small-glacier regions have likely passed "peak water" (the threshold where the glacier reaches its maximum runoff due to melting), with reduced summer mass balances suggesting declining runoff contributions, whereas the southern Andes and Russian Arctic still show increasing melt rates. During the last decade, Colombian glaciers have shown area decrease rates between 3% and 5% annually. In 2024, Colombian glaciers lost 5%, impacted by El Nino, the absence of solid precipitation and higher-than-normal temperature.

- **Significant events:** European, African and Asian regions were the most heavily hit by unprecedented or notable extreme events. Most such events were a result of excess water (that is, flash floods, heavy rainfalls or associated landslides). Africa was hard hit: Africa's tropical zone experienced unusually heavy rainfall in 2024 compared to historical

norms, resulting in more than 2 500 fatalities, 4 million people displaced and significant loss of infrastructure. Europe experienced its most extensive flooding since 2013, with one-third of its river networks exceeding "high" flood thresholds,[3] and Asia and the Pacific were hit by record-breaking rainfall and tropical cyclones, resulting in over 1 000 deaths. Brazil experienced simultaneous extremes, with catastrophic flooding in the south of the country taking 183 lives and continuation of the 2023 drought in the Amazon basin, affecting 59% of the country's territory.

KEY ADVANCEMENTS OF THE 2024 REPORT

- **Observations**: Over the past four years, the number of observed data points received from WMO Members, GRDC and other partners for river discharge measurements increased dramatically: from just 14 stations in 7 countries in 2021 to 2 777 stations in 41 countries in 2024. However, despite improvements in observational data, Africa and Asia remain underrepresented in hydrological data collection, representing only 3% of the stations included, highlighting the need for improved monitoring and data sharing, particularly in these areas. Similarly, the coverage of groundwater observational stations improved compared to last year, with data from 37 406 stations across 47 countries available in 2024. In contrast, soil moisture observations remained scarce, with only 220 stations – each with limited historical records – reported from just 2 countries in the current edition.

- **Models and data sources:** There was a sharp rise in the number of groups participating in the 2024 edition of this report. Modelling, remote sensing and in situ observation-based data products all contributed to the 2024 report; among these, 12 global hydrological modelling systems (GHMSs) provided substantial input that strengthened the analysis of variables, especially river discharge, evapotranspiration, soil moisture, snow and ice and TWS.

- **Coverage:** The 2024 edition of this report was enhanced by the addition of a new chapter providing an overview of climatic conditions with sections covering precipitation and drought indices, as well as a new lakes chapter with sections covering lake levels and lake water temperature.

- **Model validation:** More than 64% of basins (where validation was possible) showed consistent results between observed data and the multi-model mean. Moreover, the intra-model agreement was also robust: over 50% of the models agreed on the anomaly trend for 98% of the assessed area. The highest agreement was observed in South America, North America and Western Europe. Conversely, notable discrepancies were identified in southern Africa, Southern Europe, and parts of Asia.

[3] "High" flood threshold is defined here as flooding with a five-year return period.

OUTLOOK

The focus for future editions of the report will be to enhance the accessibility and availability of observational data (through both better monitoring and improved data sharing), further integrate relevant variables into the report, further build the capacity of Members to develop status products at monthly scale to support water management at national scale and encourage country participation to better understand and report water-cycle dynamics at a global scale. Future reports are anticipated to be exported from WMO's Global Hydrological Status and Outlook System (HydroSOS), for both national status products and global modelling products, and future reports will include even more observational data, supported by initiatives like the WMO Hydrological Observing System (WHOS) and collaboration with global data centres such as the Global Precipitation Climatology Centre (GPCC), Global Runoff Data Centre (GRDC), International Soil Moisture Network (ISMN), International Groundwater Resources Assessment Centre (IGRAC), Global Environment Monitoring System for Freshwater (GEMS/Water) Data Centre and International Data Centre on Hydrology of Lakes and Reservoirs (HYDROLARE).

Introduction

The State of Global Water Resources, now in its fourth edition, is a unique, standardized, science-based report series and the most comprehensive annual assessment of water resources availability and variability at the global scale. Understanding and quantifying water resources and hydrological extremes at global, regional and local levels is critical for managing risks posed by droughts, floods, cryosphere loss and other threats, as well as for guiding sustainable development and adapting to a changing climate. By delivering accessible, consistent and actionable water-related data, this report supports integrated water, climate and land management, and strengthens resilience, sustainability and equity in the face of accelerating global change. By evaluating key hydrological components, including river discharge, groundwater, evapotranspiration, terrestrial water storage, snow and ice, and other elements of the hydrological cycle, as well as high-impact events for the year 2024, this report provides a solid scientific foundation for informed decision-making at all levels based on the latest hydrological data.

The report is the result of collaboration between scientists and practitioners, combining expertise from across disciplines. The scope and quality of the State of Global Water Resources report is ensured through the sustained engagement of WMO Members, represented by their National Meteorological and Hydrological Services (NMHSs), along with contributions from global data centres, the hydrological modelling community, Earth observation centres and international experts and scientists.

The 2024 edition of the report presents a more comprehensive overview of global water resources by introducing new sections on precipitation, lake water levels and lake water temperature. This edition of the report continues integrating both in situ observations and model-based data derived from Earth observations and modelling. While in situ observations are critical, they are point based and therefore subject to limitations in station density and spatial representativeness, and they can be enhanced by modelling and Earth-observation data. A notable improvement in this year's report is the considerable expansion in the number of stations and modelling systems contributing to the analyses – presented in Figure 1. Over the past four years, the number of observed data points received from WMO Members, GRDC and other partners for river discharge measurements increased significantly: from just 14 stations in 7 countries in the 2021 report to 2 777 stations in 41 countries in the 2024 report. Similarly, for groundwater, data from 37 406 wells in 47 countries were collected in 2024, compared to 8 246 wells in 10 countries in 2022 (Figure 1).

For the first time, in the 2024 report we have we have used remote-sensing-based discharge estimates to infill in situ observation records in streamflow. The soil moisture and water quality indicators (included in the annex) are based on observed data provided by Members of the International Soil Moisture Network (ISMN) and GEMS/Water Data Centre.

The global hydrological modelling and Earth observation communities have made substantial contributions to the sections on river discharge, reservoir inflows and storage, lake levels, soil moisture, evapotranspiration, terrestrial water storage, and snow cover and glaciers. These contributions have strengthened the analyses, particularly in ungauged or data-sparse regions.

The 2024 edition of the report contains this introductory chapter providing an overview of precipitation patterns and a global drought index, as well as chapters on River discharge, Reservoirs, Lakes, Groundwater levels, Soil moisture, Evapotranspiration, Terrestrial water storage and Snow cover and glaciers, each offering global and/or regional insights. The chapter on snow cover and glaciers focuses on snow water equivalent and the state of major glaciers worldwide. Finally, the chapter on High-impact hydrological events provides a global overview of extreme and impactful hydrological events from 2024.

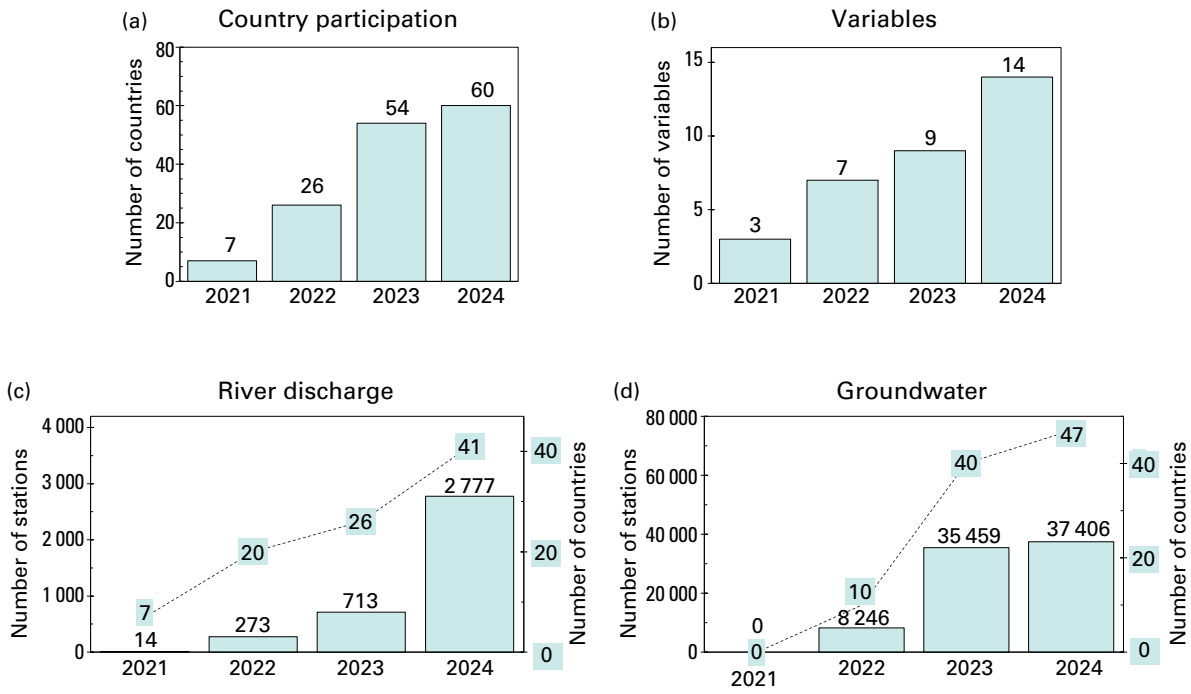

Figure 1. Growth in data sources for the State of Global Water Resources reports in the years 2021, 2022, 2023 and 2024: (a) number of countries contributing data, (b) number of variables, (c) number of stations with observed river discharge data (both quality-controlled and provisional data), (d) number of groundwater wells

There has been a continued effort to compile an extensive global dataset for the State of Global Water Resources report, combining observed and modelled hydrological data from diverse sources in order to play a key role in advancing international data sharing. Strengthening data sharing and engagement from WMO Members will remain central for future editions of the report. A comprehensive understanding of hydrological processes and their impacts on water resources based on observed data is essential for improving the validation of model outputs across global river basins. In turn, modelling and Earth observation products can provide data that are reliable in space and time and fill gaps in regions with scarce (or no) observations, thus improving understanding of the state of water resources. This strengthens reliable and informed decision-making by a wide range of stakeholders – from local water users and resource managers to national authorities.

These efforts are supporting progress towards achieving the objectives of the Early Warnings for All (EW4All) initiative, particularly by promoting capacity building for regular status calculations at national and regional scales, and by encouraging data sharing (which is key for improving forecasting systems) and accessibility for effective water-related hazard monitoring, moving towards the provision of universal early warning systems by 2027.

Additionally, the report complements the WMO Global Hydrological Status and Outlook System (HydroSOS) by contributing to the development of standardized indicators for assessing current hydrological conditions and forecasting sub-seasonal to seasonal outlooks.

DATA SOURCES

The data used in the report were gathered from various sources to ensure a robust, spatially consistent and comprehensive analysis (refer to Box 1 and Data sources in the annex), including NMHSs, the Earth observation community (which provided satellite-based observations) and the global modelling community. The River discharge and Soil moisture chapters are based on modelled and observed data, and the Water quality (included in the annex) and Groundwater levels chapters are based only on in situ observations. Where possible, in situ data were used to validate the modelled results. Global hydrological modelling systems (GHMSs) contributed to obtaining values for additional hydrological variables, in particular soil moisture, reservoir inflows, actual evapotranspiration and terrestrial water storage.

BOX 1. DATA SOURCES 2024

- *Precipitation and drought indices:* Global Precipitation Climatology Centre (Becker et al., 2013; GPCC, 2025; Schneider et al., 2014).
- *Observed river discharge data:* National Meteorological and Hydrological Services (NMHSs), the Global Runoff Database Centre (see GRDC Data Portal), extended river discharge estimates using remote sensing data (Elmi et al., 2024; Saemian et al., 2025).
- *Modelled river discharge data:* Twelve global hydrological modelling systems (GHMSs) – CaMa-Flood with Dam (Hanazaki et al., 2022; Yamazaki et al., 2011), Conjunctive Surface–Subsurface Process version 3 (CSSPv3) (Yuan et al., 2018), DHI-GHM (Murray et al., 2023), ecLand (Boussetta et al., 2021), Global Flood Awareness System (GloFAS) (Alfieri et al., 2013; Grimaldi et al., 2023), HBV-PML (Huang et al., 2022; Zhang et al., 2019), mesoscale Hydrologic Model (mHM) (Kumar et al., 2013; Samaniego et al., 2010, 2019), PCR-GLOBWB 2 (Sutanudjaja et al., 2018), GEOGLOWS (Hales et al. 2025), WaterGAP 2.2e (Müller Schmied et al., 2021, 2024), World-Wide HYPE v1.3.9 (Arheimer et al., 2020) and Wflow_sbm (Eilander et al., 2021; Imhoff et al., 2020; Verseveld et al., 2024).
- *Inflow into selected reservoirs globally:* Four GHMSs – CaMa-Flood with dams (Hanazaki et al., 2022; Yamazaki et al., 2011), World-Wide HYPE (Arheimer et al., 2020), CSSPv3 (Yuan et al., 2018) and Wflow_sbm (Eilander et al., 2021; Imhoff et al., 2020; Verseveld et al., 2024).
- *Reservoir volume anomalies:* Adapted from Biswas et al. (2021).
- *Lake levels and temperature:* European Space Agency (ESA) (Lake CCI project).
- *Groundwater level data:* International Groundwater Resources Assessment Centre (IGRAC) for 47 selected countries.
- *Soil moisture:* Two GHMSs – CSSPv3 (Yuan et al., 2018), mHM (Kumar et al., 2013; Samaniego et al., 2010, 2019) and observed data from the International Soil Moisture Network (ISMN).
- *Evapotranspiration:* Six GHMSs – CSSPv3 (Yuan et al., 2018), mHM (Kumar et al., 2013; Samaniego et al., 2010, 2019), WaterGAP 2.2e (Müller Schmied et al., 2021, 2024), World-Wide HYPE v1.3.9 (Arheimer et al., 2020), HBV-PML (Huang et al., 2022; Zhang et al., 2019) and Wflow_sbm (Eilander et al., 2021; Imhoff et al., 2020; Verseveld et al., 2024).
- *Terrestrial water storage (TWS):* GRACE/GRACE Follow-On satellites (Landerer et al., 2020) and three GHMSs – CSSPv3 (Yuan et al., 2018), mHM (Kumar et al., 2013; Samaniego et al., 2010, 2019) and HBV-PML (Huang et al., 2022; Zhang et al., 2019).
- *Glaciers:* WMO Member States and Territories, WGMS.
- Snow water equivalent: Environment and Climate Change Canada (Mudryk et al., 2024, 2025), from two GHMSs: Today's Earth – Global (TEJRA55) (Ma et al., 2021; Yoshimura et al., 2008) and mesoscale Hydrologic Model (mHM).
- *Water quality (in the annex):* The Global Freshwater Quality Database (GEMStat – The global water quality database).
- *High-impact events:* Communication from WMO Members for WMO State of the Climate report, open data sources, such as the EM-DAT database (CRED, 2025), ReliefWeb and others.

Note: See Table A1 in the annex for a list of GHMSs contributing to each variable.

ANOMALY CALCULATION

For each of the variables presented, the anomaly was calculated by comparing the annual, seasonal or monthly mean value in 2024 to the distribution of the mean obtained from the historical period as described in Box 2 and presented in Figure 2. Note that in the present report, the term "anomaly" is used to describe the status of water resources in each basin in comparison with the long-term historical near-normal conditions for that basin, and that historical periods differ from variable to variable, as well as spatially for observed discharge data (refer to Table A2 in the annex). Further details on the methods (including an overview of all data sources), the GHMSs used in the analysis, the definitions of the indicators used in the report, and additional results are documented in the annex.

BOX 2. ANOMALY CALCULATION

The annual mean of each hydrological variable (for example, river discharge) for a defined reference period of data (modelled or observed) was calculated for each year. Each respective variable in 2024 falls under categories based on the following definitions:

much below normal:	$Q_{2024} \leq$ 10th percentile (referring to exceptionally dry conditions)
below normal:	10th < Q_{2024} < 25th percentile
normal:	25th ≤ Q_{2024} ≤ 75th percentile
above normal:	75th < Q_{2024} < 90th percentile
much above normal:	$Q_{2024} \geq$ 90th percentile (referring to exceptionally wet conditions)

Where results are obtained from several models, the above-specified categories were assigned an integer ("much below normal" = 1, "below normal" = 2, "normal" = 3, "above normal" = 4, "much above normal" = 5), then an average was calculated across the outputs of the ensemble of models for each of the basins. The resulting number was rounded and translated back into one of the categories listed above.

Note that the reference period varies for the different variables based on data availability. For example, 30 years (1991–2020) is the reference period for river discharge, whereas 20 years (2005–2024) is used for groundwater.

While historical periods differ from variable to variable, as well as spatially for observed discharge data (refer to Table A2 in the annex), the classification of the anomaly ranking remains the same.

For further information on the reference period used for each variable, refer to Table 2 in the annex. Note that the selection of different reference periods may influence the calculated results.

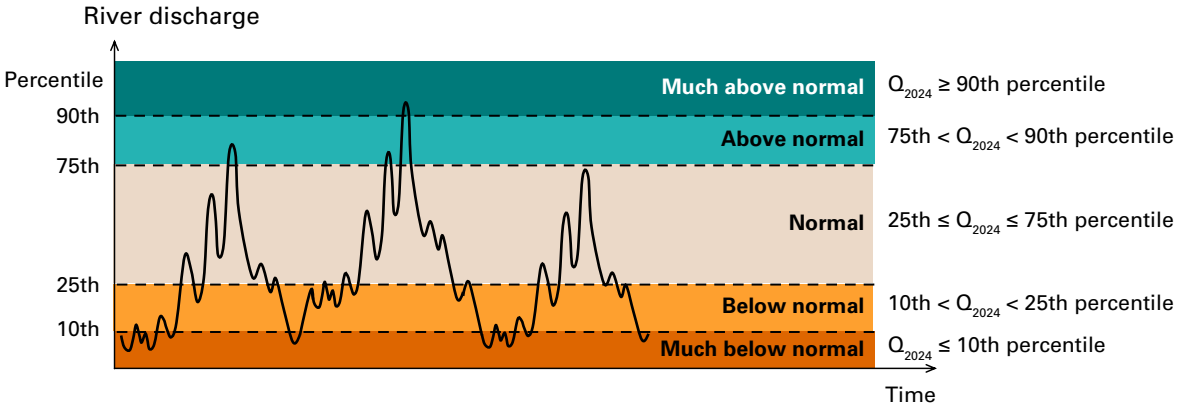

Figure 2. Conceptual diagram illustrating the classification of variable conditions (for example, river discharge) in 2024 relative to the historical reference period. Percentile thresholds define five categories: much above normal (≥90th percentile), above normal (75th–90th percentile), normal (25th–75th percentile), below normal (10th–25th percentile), and much below normal (≤10th percentile).

THE BACKDROP: OVERVIEW OF CLIMATIC CONDITIONS IN 2024

This section is based on the key findings from the WMO flagship report *State of the Global Climate 2024* (WMO-No. 1368), as well as Global Precipitation Climatology Centre (GPCC) precipitation and drought data products.

- El Niño conditions dominated early 2024, causing drought conditions in northern South America and southern Africa.
- Severe drought conditions hit the Amazon basin, intensifying during April–June and reaching a peak in July–September, before easing partially in October–December.
- Below-normal precipitation conditions were spread across north-western Mexico, northern North America – including the Fraser and Mackenzie river basins, and southern and south-eastern Africa – including the Orange, Limpopo, Zambezi and Congo basins.
- Wetter-than-normal conditions prevailed over central-western Africa, the Lake Victoria basin in Africa, Kazakhstan and the southern Russian Federation, Central Europe, Pakistan and northern India, the southern Islamic Republic of Iran, and north-eastern China.

The first quarter of 2024 was characterized by strong El Niño conditions, which had been developing since mid-2023. ENSO-neutral conditions were established by June 2024. As is typical for El Niño phases, the early part of the year brought pronounced dry anomalies to northern South America and southern Africa. Additionally, the year 2024 was marked by record-breaking global temperatures, with the annual mean surface temperature reaching 1.55 °C (±0.13 °C) above the pre-industrial baseline (1850–1900), making it the hottest year in the 175-year observational record. In fact, nearly every month of the year broke the previous heat record. The global mean sea level and ocean heat content also reached record highs in 2024. For ocean heat content, the rate of temperature increase over the past two decades is more than double the rate observed during the period from 1960 to 2005.

PRECIPITATION

Figure 3 presents the annual precipitation anomalies for 2024, and Figure 4 shows the seasonal anomalies in precipitation, both expressed as percentiles and derived from the Global Precipitation Climatology Centre (GPCC) product (GPCC, 2025), which provides gridded (1° resolution, ~111 km at the Equator), monthly near-real-time precipitation data.

Precipitation was significantly below normal across several regions in 2024, as presented in Figure 3, most notably over the Amazon basin, where rainfall remained below to much below normal until approximately October (Figure 4). Similarly, dry conditions were observed in north-western Mexico, across northern North America – including the Fraser and Mackenzie river basins – and along the north-eastern coast of North America. In southern and south-eastern Africa, including the Orange, Limpopo, Zambezi and Congo basins, precipitation deficits were particularly pronounced during January–March and again in October–December. Above-normal annual precipitation prevailed over central-western Africa, in the Niger and White Nile basins during July–September, and in the Lake Victoria basin in central-eastern Africa.

In Europe, precipitation was much above normal in MAM in Central and Northern Europe, and in DJF across Eastern Europe, extending to Kazakhstan and southern parts of the Russian Federation, and north-eastern China. Above-normal precipitation also affected South-east Asia and central-northern Australia during the MAM and SON seasons, as well as countries of the Persian Gulf in MAM.

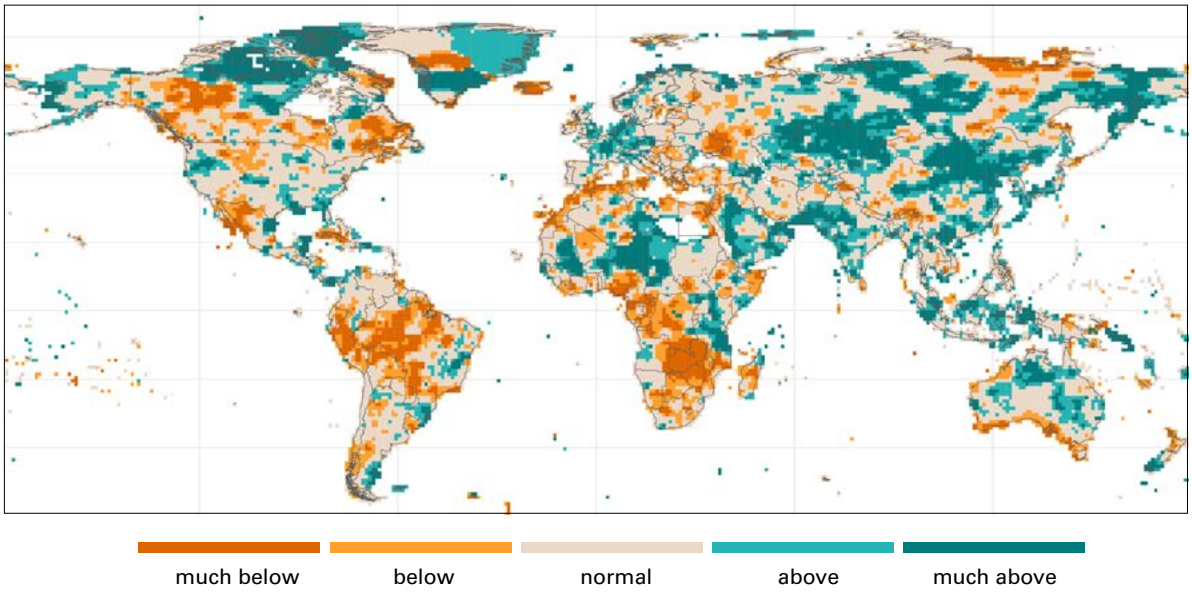

Figure 3. Total annual precipitation in 2024 expressed as anomalies compared with the 1991–2020 reference period

Note: The boundaries and names shown and the designations used do not imply official endorsement or acceptance by WMO or the United Nations.

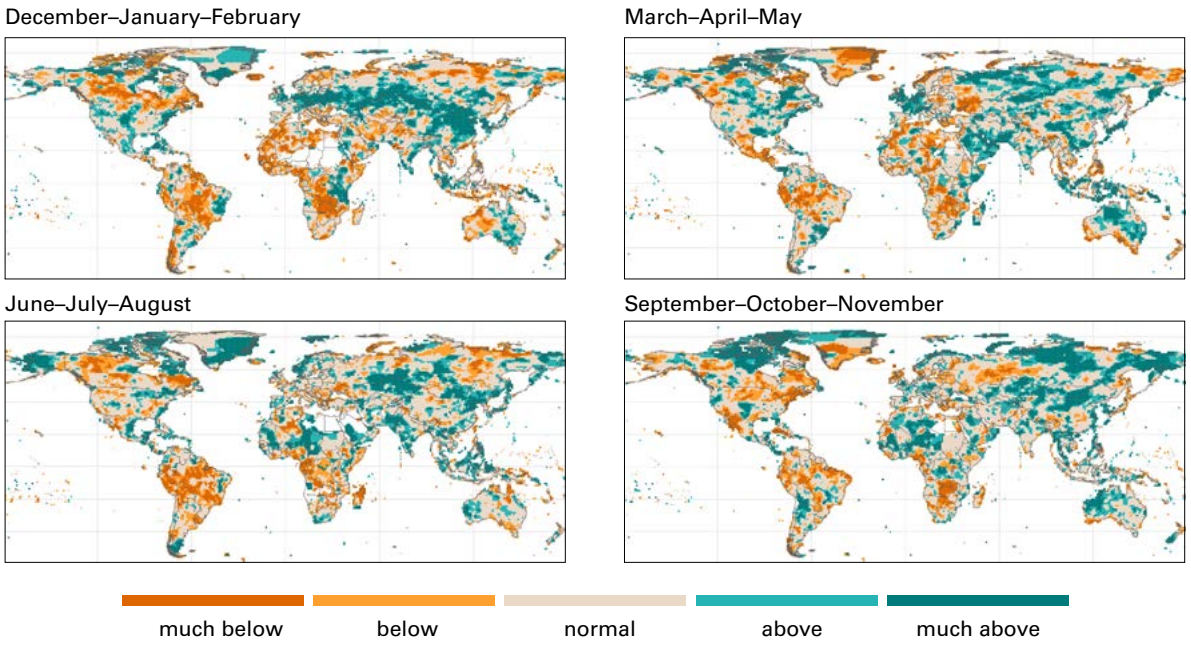

Figure 4. Seasonal precipitation in 2024 expressed as anomalies compared with the 1991–2020 reference period. DJF = December–January–February (includes December 2023), JJA = June–July–August, MAM = March–April–May; SON = September–October–November.

Note: The boundaries and names shown and the designations used do not imply official endorsement or acceptance by WMO or the United Nations.

DROUGHT INDEX

The Global Precipitation Climatology Centre Drought Index (GPCC-DI), as presented in Figure 5, (Schneider et al., 2014) is a combination of two drought indices: the Standardized Precipitation Index (SPI) and the Standardized Precipitation Evapotranspiration Index (SPEI). The SPI gives an indication of the severity of precipitation deficits, with more negative values indicating deficits that are more severe and less likely to occur. The inclusion of evapotranspiration (derived using temperature data) in the SPEI provides a better consideration of the climatic water balance, and in general this index can be considered to perform better in more arid environments and hotter climates. The SPI and the SPEI are combined such that the resulting indicator enables an unbiased global assessment of drought conditions. The SPI and SPEI cannot be calculated for dry and cold regions like the Tibetan Plateau and southern Andes, these regions and are therefore left blank.

Drought conditions in the Amazon basin developed during the March–June period, reaching their full intensity in July–September, and then weakened in the final quarter of the year. In Northern Africa, which experienced multi-year drought, drought conditions persisted from June through September. In East Africa, drought conditions persisted over the entire year, except for DJF. In contrast, drought indices indicated wetter-than-normal conditions in northern Australia during January–March, and in northern China and the Asian part of the Russian Federation during July–September.

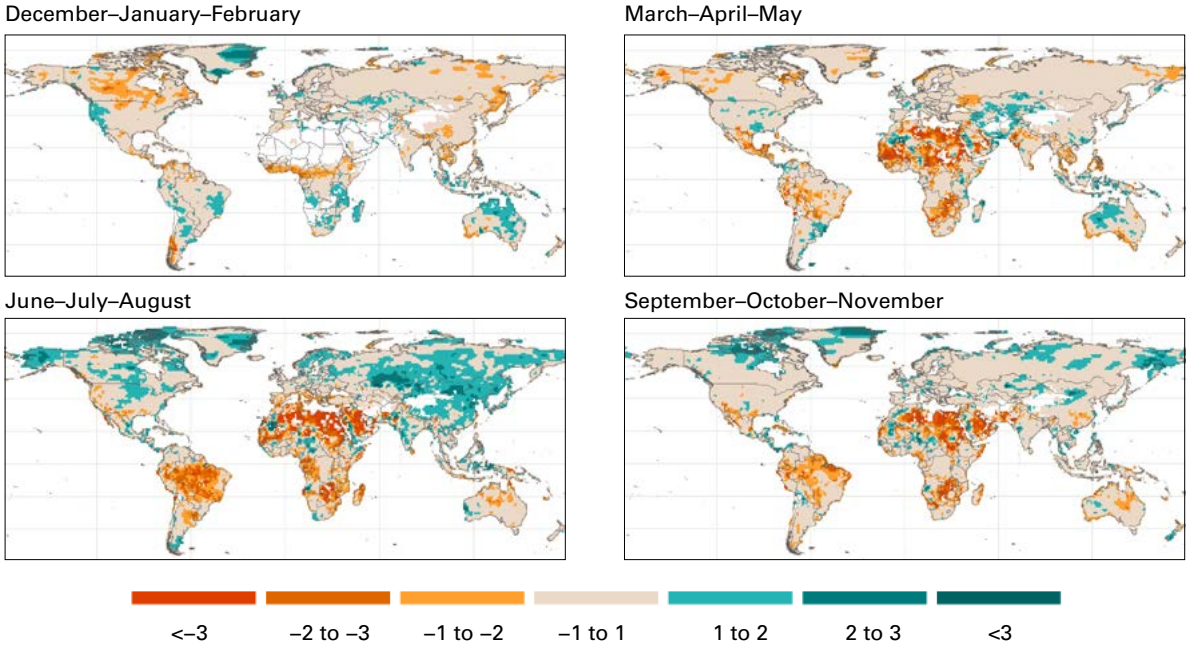

Figure 5. Global Precipitation Climatology Centre Drought Index (GPCC-DI) in 2024 over four seasons. Beige indicates normal precipitation, green shades indicate wetter-than-normal conditions and orange–red shades indicate drier than normal conditions. DJF = December–January–February (includes December 2023), JJA = June–July–August, MAM = March–April–May; SON = September–October–November.

Note: The boundaries and names shown and the designations used do not imply official endorsement or acceptance by WMO or the United Nations.

River discharge

- There was a significant increase in the number of stations providing observational data for the report: daily river discharge data (corresponding to the selection criteria, as described) were available from 2 777 stations in 41 countries.
- For 64% of gauges validated, observed and modelled multi-model mean trends showed agreement, specifically in South America, North America and Western Europe. However, modelled anomalies disagreed with observations in South Africa, Southern Europe and Asia.
- Similarly to 2023 and 2021, river discharge in 2024 exhibited deviations from normal conditions in approximately 60% of the global catchment area. Only about one-third of the global catchment area was within normal discharge conditions during each of the past six years with respect to the 1991–2020 period.
- Much-above-normal discharge conditions were observed across Central and Northern Europe and parts of Asia. Major basins, such as the Danube, Ganges, Godavari and Indus saw above- to much-above-normal conditions.
- Severe drought, which had started at the end of 2023, persisted in South America, with much below-normal discharge across key river basins, including the Amazon, São Francisco, Paraná and Orinoco.
- Discharge conditions in Africa were above normal in West African basins (Senegal, Niger, Lake Chad, Volta) which were affected by extensive flooding, while southern African basins (Zambezi, Limpopo, Okavango, Orange) saw much-below-normal discharge conditions.
- As in 2023, northern North American rivers (Mackenzie, Fraser, Nelson, Churchill) experienced below-to much-below-normal conditions, while Mississippi discharge was normal in 2024, following a drought in 2023.

This 2024 edition of the State of Global Water Resources report uses the same HydroBASINS level 4 spatial delineation adopted by the previous report (Lehner et al., 2008). The proposed delineation represents approximately 986 river basins (with a minimum upstream area of 10 000 km^2) around the globe (Figure A1 in the annex).

The river discharge analysis in the 2024 edition of the report, similarly to the previous editions, is based on in situ data received from WMO Members represented by NMHSs, mainly obtained via the GRDC database (see GRDC Data Portal). These data were supplemented with substantial contributions from GHMSs and the Remote Sensing-based Extension of GRDC (RSEG) dataset, which provides extended time series of river discharge observations using Earth system-based products (Elmi et al., 2024). The 12 GHMSs listed in the annex, Table A3 were used for this year's report. For more information about the models, the input data used and other details, please refer to the Global hydrological modelling systems section in the annex.[1]

[1] Simulations from GHMSs may contain uncertainties arising from model structure, input data or configuration. To capture a broader range of these uncertainties, an ensemble of GHMSs was used. Intercomparison of the models and validation against in situ data is provided in the annex.

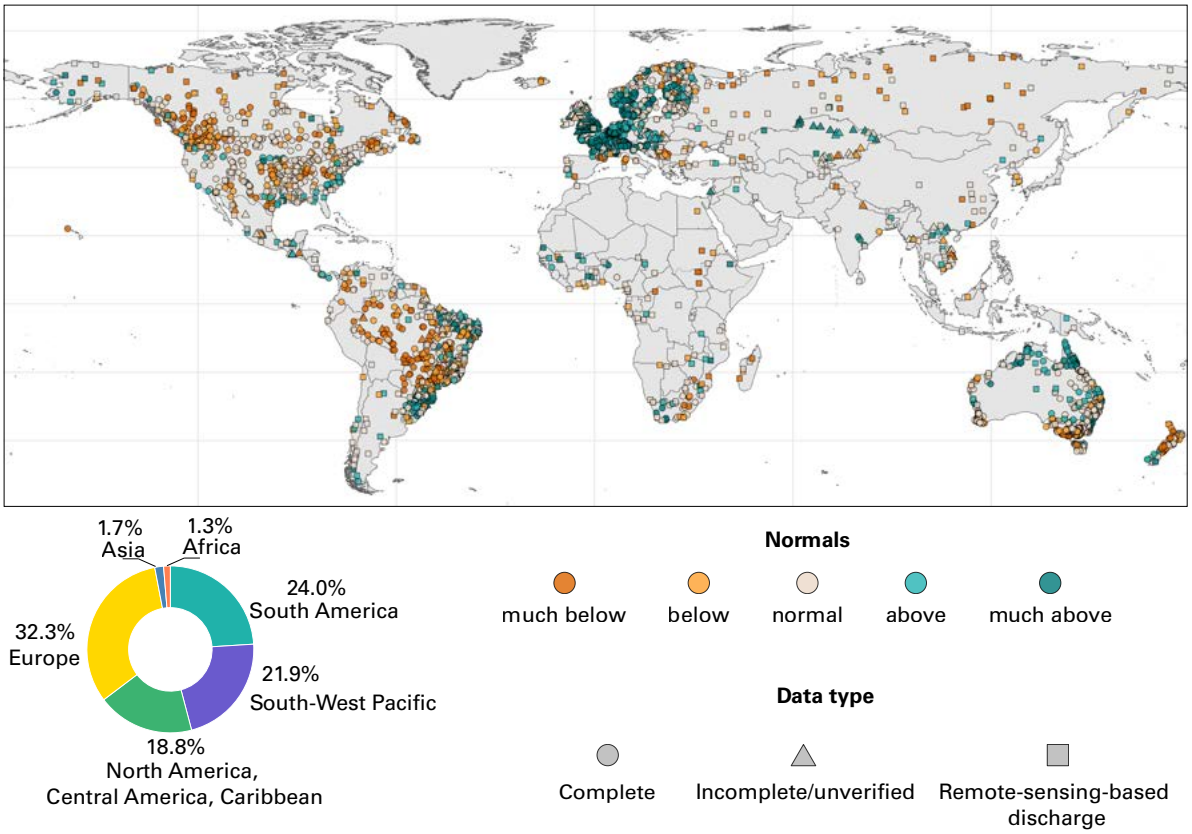

Figure 6. Observed mean river discharge for the year 2024 compared to the period 1991–2020 or 2001–2020. The results are based on observed river discharge data: circles indicate stations with 30 years of observations, triangles indicate stations with at least 20 years of observations, and squares represent extended time series of river discharge data derived from satellite-based infilling (RSEG dataset). Observations were obtained from National Meteorological and Hydrological Services (NMHSs) and the Global Runoff Data Centre (GRDC). The inset chart (bottom left) shows the data distribution excluding the 473 extended data points. The observed data were used to validate the GHMS simulations shown in Figure 7, where the reference period was adjusted to match the available in situ records (see Figure A8 in the annex). Regions shown on the map correspond to the official WMO regions.

Note: The boundaries and names shown and the designations used do not imply official endorsement or acceptance by WMO or the United Nations.

The volume of observational data for the year 2024 has substantially increased (Figure 1). This is partially due to selection criteria within the GRDC database being relaxed, as well as increased engagement from countries and the addition of the infilled data from Earth system-based products.

Only in situ stations with no more than 10% missing values for the period covering at least the first 10 months of 2024 (until 31 October 2024) and the historical period of at least 20 years (2001–2020) were selected for the analysis (Figure 6 provides a breakdown by the type of data received). Non-verified data were accepted. At the time of preparation of this report, observed daily river discharge data (corresponding to the selection criteria, as described) were available for 3 250 stations in total – 2 777 stations providing in situ observations and 473 stations from the Earth system-based infilled product.[2] Most of these stations are located in Europe (32.3%), South America (24.0%), the South-west Pacific (21.9%), and North America,

[2] More data will likely be available and accessible for all regions in the future, but additional data were not available in time to be considered in this report.

Central America and the Caribbean (18.8%). The smallest proportion of available stations are found in Africa and Asia (3.0% in total). Overall, this represents a substantial increase, with the number of stations multiplied by 4.5 compared with the previous (2023) edition of this report, which included data from 713 stations. By comparison, the 2022 edition included data from only 273 stations, and the 2021 edition from just 14 stations.

For the data obtained from GHMSs, the annual mean river discharge for 2024 was compared with historical values from 1991 to 2020, while in the case of the observed river discharge stations the 2024 mean was compared with available data (that is, at least 20 years of data – 2001–2020). The annual discharge was then classified as normal, above normal, below normal, much above normal or much below normal relative to these historical values (refer to Table A2 in the annex for more details). The annex provides details on each of the GHMSs used, together with information on their set-up and calibration with historical data, and on how simulations for 2024 were produced. In basins where observed river discharge data were available and covered a 30-year historical period, the trends simulated by the GHMSs were validated.

Figure 6 presents the observed mean river discharge for the year 2024 against the selected historical period (1991–2020 or 2001–2020) derived from three data sources (in situ observations from Members, GRDC data and infilled data), and Figure 7 presents the modelled mean river discharge for the year 2024 against the selected historical period (1991–2020). The calculation is based on ensemble results from the GHMSs (see the annex for details on the method of calculations). In cases where observational data were available, they were used to validate the model results shown in Figure 7. A detailed presentation of the validation showing basins where the GHMS simulations agreed with the observed data is provided in the annex, Figure A7.

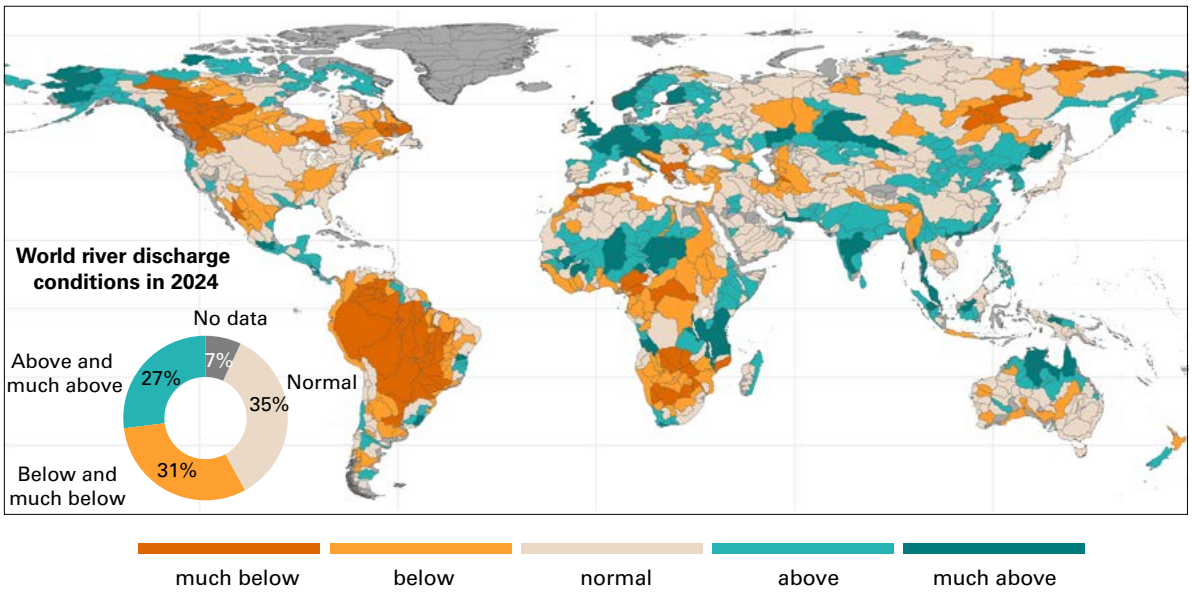

Figure 7. Mean river discharge in 2024 expressed as anomalies compared with the 1991–2020 reference period (for basins larger than 10 000 km^2). The results presented here are derived from the modelled river discharge data obtained from an ensemble of 12 GHMS simulations (see Methods in the annex). Inset (bottom left) shows the percentage distribution of the modelled catchment area under the given conditions. Dark grey areas indicate no modelling data. The results were validated against hydrological observations wherever available (see Figure A7 in the annex).

Note: The boundaries and names shown and the designations used do not imply official endorsement or acceptance by WMO or the United Nations.

Validation of modelled results showed good overall agreement[3] (>64% of basins) between observed and simulated anomalies (based on multi-model mean) for the year 2024, particularly in South America, North America and Western Europe. At the same time, modelled anomalies disagreed with observations in South Africa, parts of Europe and Asia. Note that discrepancies between modelled and observed hydrological flows may arise from complex topography, such as high mountains that create localized discharge anomalies unrepresentative of wider regional conditions (as seen in parts of Norway). The locations of the gauges used to validate the modelled results are presented in Figure A3 in the annex (for full validation results refer to Figure A7). The location of the gauges with observed river discharge data is critical for reliable model validation, as presented in the annex, Figure A6.

In 2024 river discharge exhibited deviations from normal conditions in approximately 60% of the global catchment area (Figure 8). With respect to the historical period, the year 2024 was characterized by drier-than-normal conditions in approximately 30% of the area globally, while conditions in approximately 30% were normal and in another 30% they were above normal (Figure 8). In 2024, at the global scale, a smaller basin area was under dry conditions than in 2023, while the basin area under wetter-than-normal conditions almost doubled. A comparison of the areas under different river discharge conditions for every year from 1991 to 2024 using a constant historical normal (1991–2020), showed that only about one-third of the global catchment area (though not the same basins year to year) was under normal discharge conditions during each of the past six years, showing the increasing variance in river flow conditions due to several factors, including climate change.

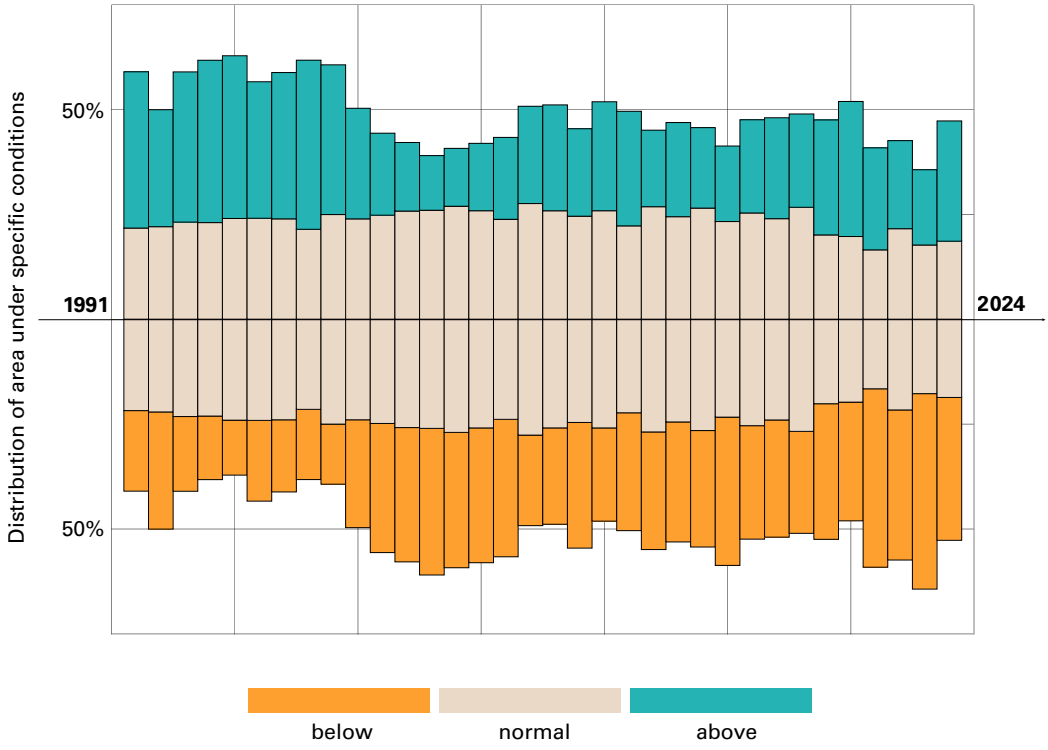

Figure 8. The distribution of the global basin area under different river discharge conditions for the years 1991–2024.[4] Note that the percentage distribution excludes the 7% of the global basin for which no data were available.

[3] More than 50% of models agreed on the trend for 98% of the area.

[4] A change in basin delineation was adopted in 2022; also, the number of models was different from year to year.

In 2024, above- to much-above-normal discharge conditions prevailed across Central and Northern Europe, including the upstream Danube basin and nearly the entire territories of France, Germany, Norway, Sweden, Finland and the United Kingdom. In Asia, basins in India, such as the Godavari, Krishna, Ganges, and parts of the upstream Indus showed similar above-normal discharge conditions. In Kazakhstan and the Russian Federation, the Lake Balkhash basin recorded much-above-normal flows, as did the Ural and Ob rivers, which experienced major flooding, largely driven by snowmelt.

South America was gripped by an extended drought event in 2024, intensifying the conditions already established in 2023; much-below-normal discharge conditions were found across the Amazon, São Francisco, La Plata (including the Paraná) and Orinoco river basins, and others. The La Plata river basin has been affected by drought since 2020.

In North America, northern basins such as the Mackenzie, Fraser, Nelson and Churchill, as well as the upstream Colorado River again experienced below- to much-below-normal discharge, mirroring 2023. The Mississippi River, however, returned to normal conditions following the extended drought of 2022–2023.

In Africa, the Senegal, Niger and Volta river basins as well as the Lake Chad basin had above- to much-above-normal discharge conditions. On the other hand, the Zambezi, Limpopo, Okavango and Orange river basins in southern Africa had below- to much-below-normal discharge conditions.

In 2024, most of Australia saw normal or below-normal discharge conditions, while catchments in northern Australia saw much-above-normal discharge conditions. The declining trend in annual average streamflow in many parts of Australia can be attributed to the impacts of climate change on unregulated catchment inflows (see Australia's changing climate).

New Zealand's North Island had below normal discharge conditions, while its South Island had above-normal discharge conditions.

Reservoirs

- Above-normal inflows were observed in reservoirs across Western and Northern Europe and South-east Asia, following above-normal discharge conditions in 2024.
- In the Amazon and Paraná basins, affected by extensive drought in 2024, reservoir inflows were below to much below normal; however, storage remained normal in some parts of the catchments.
- In Central and West Africa, reservoir storage was below normal despite above-normal inflows. The Aswan High Dam on the Nile experienced below-normal storage, while reservoirs in the Greater Horn of Africa recorded above- to much-above-normal storage, in line with surplus inflows during 2024.

This chapter presents the state of reservoirs in 2024. It includes modelled inflow into selected reservoirs across the globe by GHMSs and anomalies in reservoir volume obtained from NASA, adapted from Biswas et al. (2021).

INFLOW INTO SELECTED RESERVOIRS

The inflow data were obtained from three sources that comprise one satellite-based and three GHMS products, namely, the Wflow_sbm (Eilander et al., 2021; Imhoff et al., 2020; Verseveld et al., 2024), CaMa-Flood with Dam (Hanazaki et al., 2022; Yamazaki et al., 2011), World-Wide HYPE (Arheimer et al., 2020) and CSSPv3 (Yuan et al., 2018) models (more details listed in Table A1 in the annex). All available reservoirs from the above sources were included for analysis (the superset of all reservoirs included in the model set-up) and were identified by their Global Reservoir and Dam (GRanD) ID (Lehner et al. 2021).

Daily inflow data for the reservoirs were computed for the historical period between 1991 and 2020 and for the year 2024. Inflow anomalies were then calculated following the same method as for the river discharge anomalies (see Box 2). The results are presented in Figure 9. Water inflow into the reservoirs was selected as an indicator due to its lower dependency from water resources management strategies, such as reservoir operations.

Inflow into reservoirs in southern Brazil, within the La Plata basin, remained below to much below normal in 2024, consistent with the widespread much-below-normal river discharge conditions observed across nearly all of South America. A similar situation was observed in northern Mexico, particularly in the Sonora River basin. In south-eastern Europe, reservoir inflows were also below normal, especially in Greece, Türkiye and the Balkans. In southern Africa, reservoirs within the Limpopo River basin received lower-than-normal inflows, following lower-than-normal precipitation and discharge conditions. Reservoirs across Western and Northern Europe recorded above-normal inflows, following above normal discharge conditions. Higher-than-normal reservoir inflows were also recorded in South and South-east Asia, reflecting the excess precipitation observed in 2024.

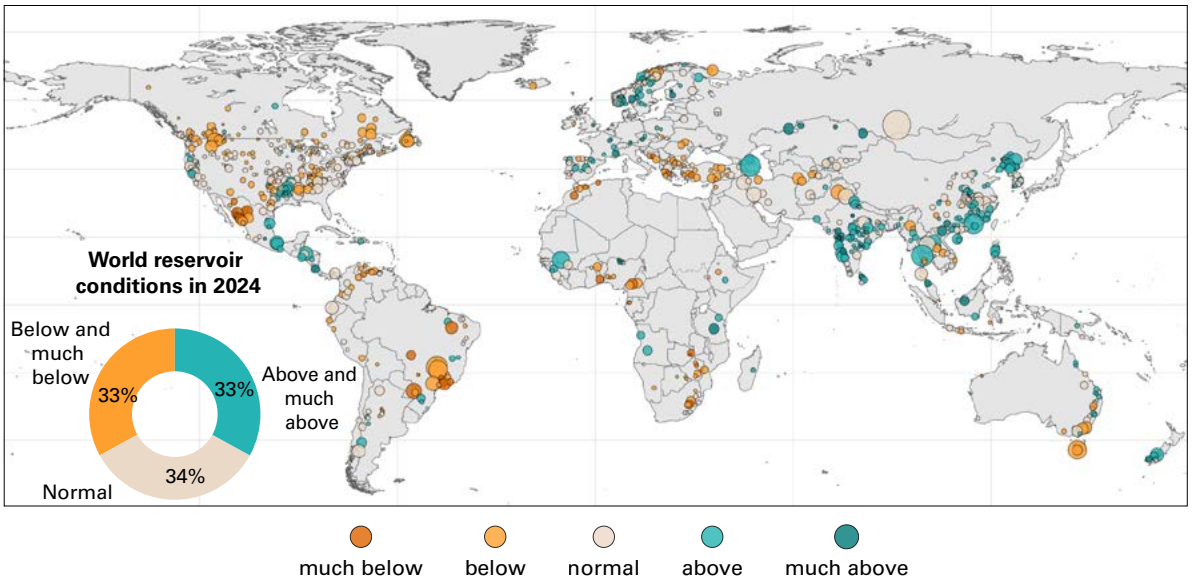

Figure 9. Annual mean inflow into selected reservoirs in 2024 expressed as anomalies compared with the 1991–2020 reference period. The size of the dots corresponds to the maximum storage volume of the reservoirs. The inset (bottom left) shows the percentages of reservoir volumes under the given conditions.

Note: The boundaries and names shown and the designations used do not imply official endorsement or acceptance by WMO or the United Nations.

RESERVOIR STORAGE

This section presents the results on reservoir storage anomalies in 2024. The approach used involves merging several satellite-based datasets, as described in Biswas et al. (2021). In total, reservoir storage anomalies for the year 2024 were assessed for 2 868 reservoirs (only reservoirs with a maximum capacity of 100 million m^3 and above were included). The results are shown in Figure 10.

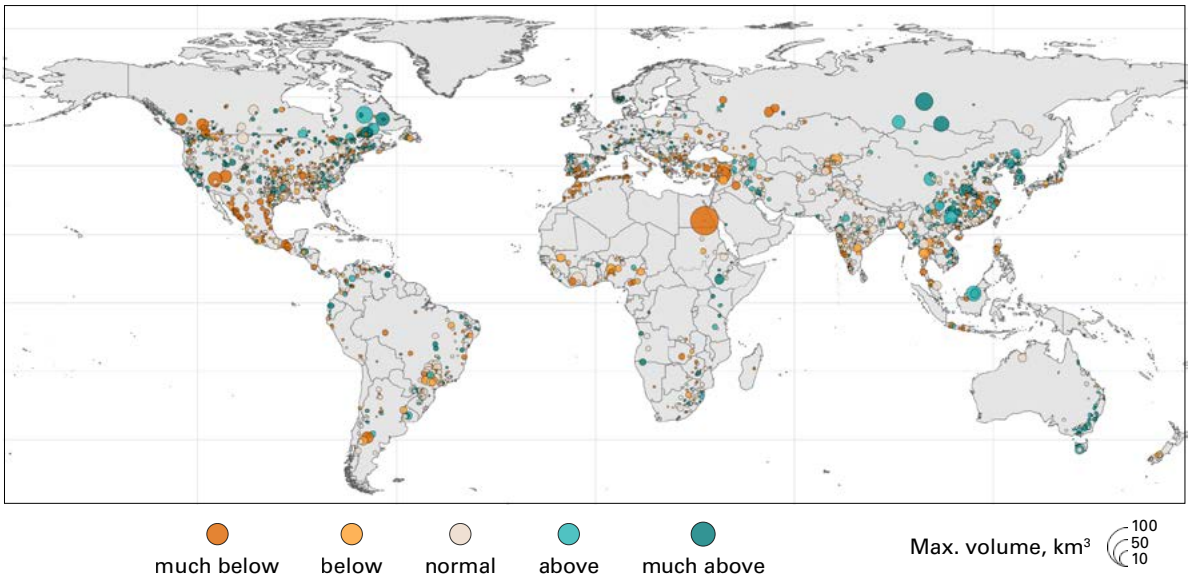

Figure 10. Reservoir storage in 2024 expressed as the annual mean of monthly anomalies compared with the 2003–2020 reference period

Note: The boundaries and names shown and the designations used do not imply official endorsement or acceptance by WMO or the United Nations.

Reservoir storage depends on the balance between the inflows and outflows. While inflows are primarily driven by hydrometeorological conditions, storage is also significantly influenced by human management. Dam operators can regulate outflows to keep or release water as needed. As a result, storage dynamics may not directly reflect reservoir inflow patterns. For example, during periods of low inflow, operators may still retain water, increasing reservoir volume while reducing outflows.

Reservoir storage in the Mediterranean basin – including Greece, southern Spain, the North African coast and Türkiye – was predominantly below to much below normal in 2024.

The Aswan High Dam on the Nile recorded below-normal storage levels, while reservoirs along the Eastern African coast (Greater Horn of Africa) experienced above- to much-above-normal storage, consistent with above-normal inflows.

In South America, reservoir storage in the Amazon and Paraná basins remained predominantly normal to below normal, reflecting consistently below- to much-below-normal inflows. Reservoir volumes in British Columbia, Canada, were above normal despite the below normal inflows; on the other hand, in India and South-east Asia the inflows into reservoirs were above to much above normal, while the volumes remained normal or below normal. The maintenance of near-normal storage in some areas may indicate reliance on carry-over storage from previous years or the implementation of water conservation measures in response to ongoing drought conditions. On the other hand, below-normal reservoir storage despite above-normal inflows may indicate that reservoirs were at low capacity prior to 2024 or that there were increased discharges from reservoirs in 2024. In 2024, total reservoir storage in Australia was at 74% of the total accessible reservoir storage (see the Australian Bureau of Meteorology Water Storage Dashboard).

Lakes

- Lake levels were consistently below to much below normal across the Mackenzie, Fraser and Churchill river catchments in Canada's Northwest Territories.
- In Africa, most lakes (Victoria, Turkana, Tanganyika and Chad) recorded much-above-normal levels, with the exception of Lake Kariba, which had much-below-normal levels. July temperature was much above normal for these lakes.
- In the Middle East and Central Asia, lake levels were much below normal.
- In Northern Europe and the European part of the Russian Federation (Lake Ladoga), lake levels were above normal. Lake Baikal also recorded above-normal levels.
- Nearly all out of 75 selected principal lakes across the globe saw above- to much-above-normal temperatures in July, with a few exceptions of (for example, Lakes Nicaragua and Guri in Central and South America and lakes in Sweden, eastern China and across the northern United States).

This chapter provides anomalies in lake levels and water temperatures in July 2024 for 75 selected lakes with respect to the historical period of 1995–2020. The 75 selected lakes consisted of 55% near natural-lakes, 12% regulated lakes and 33% reservoirs. The data were derived from the ESA's Lake CCI project, which aims to provide consistent essential climate variables. Two such climate variables are lake water level, which is critical to understanding the balance between water inputs and water loss and their connection with regional and global climate changes, and lake surface water temperature, which reflects regional air temperatures, and hence mixing regimes, driving biogeochemical cycling and seasonality.

LAKE LEVELS

Lake levels (Figure 11) were consistently below to much below normal across Canada's Northwest Territories, in the basins of the MacKenzie, Faser and Churchill rivers. Lakes across Africa, including Lakes Victoria, Turkana, Tanganyika and Chad, had much-above-normal levels. Only Lake Kariba in the Zambezi river basin had much-below-normal levels.

Across the Middle East and Central Asia, lake levels were much below normal. In Sorthern Europe, and in the European part (Lake Ladoga) and Far East of the Russian Federation (Lake Baikal) the levels were above normal.

LAKE WATER TEMPERATURE

The January and July lake surface water temperatures were assessed for the same 75 lakes to cover the summer anomalies in both the hemispheres. (Figure 12). July lake water temperatures were much above normal across all of Africa, with the exception of Lakes Volta and Kainji in West Africa.

Lakes across the European part of the Russian Federation, the Russian Far East, the Middle East, China and Canada's Northern Territories all saw above- to much-above-normal temperature

in July, although there were a few exceptions with normal temperatures in the northern United States, Sweden (Lake Vänern), southern Chile (Todos Los Santos and Argentino lakes) and Central Asia (Lakes Sarikamish and Garabogazköl). In Central and South America, lakes Nicaragua and Guri saw much-below-normal July temperatures.

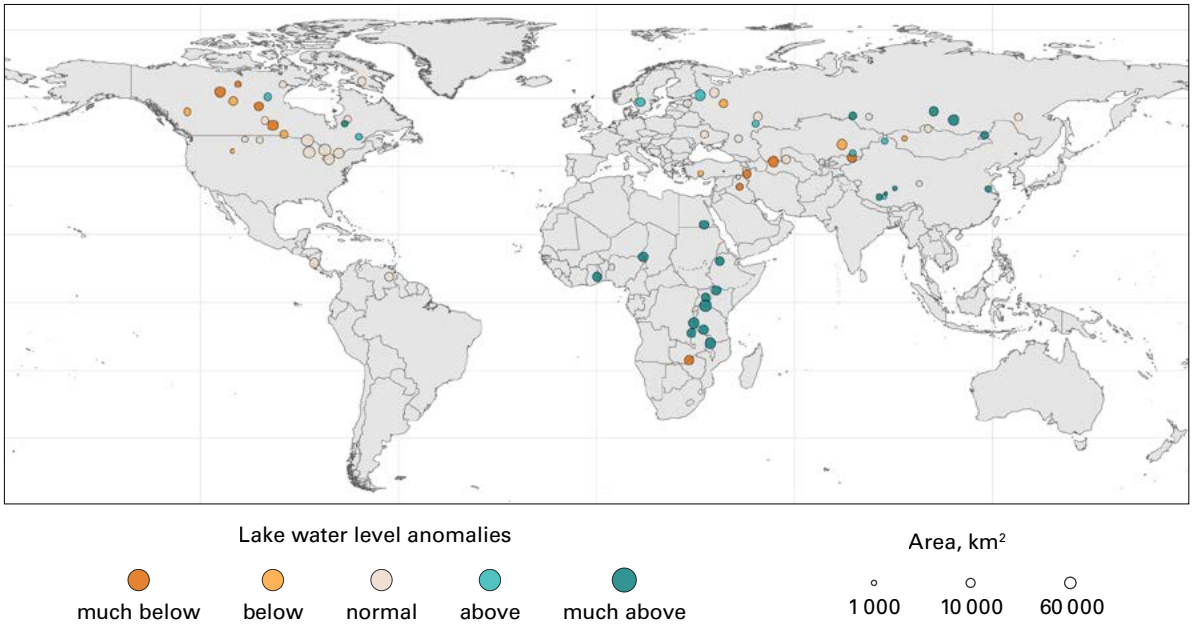

Figure 11. Lake water levels in 2024 expressed as anomalies compared with the 1995–2020 reference period. The selected 75 water bodies consist of 55% near-natural lakes, 12% regulated lakes and 33% reservoirs.

Note: The boundaries and names shown and the designations used do not imply official endorsement or acceptance by WMO or the United Nations.

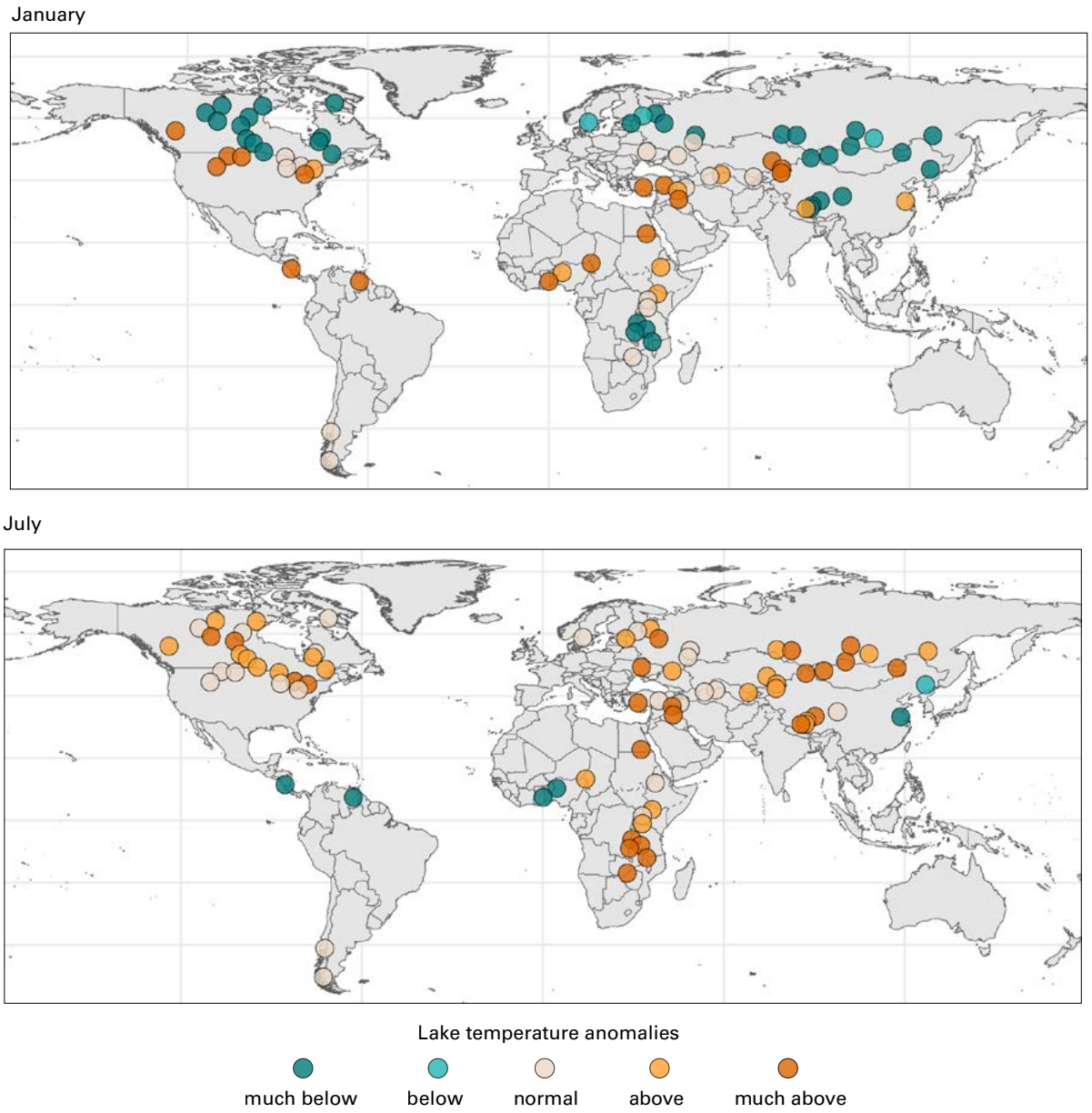

Figure 12. Lake surface water temperature in January and July 2024 expressed as anomalies compared with the 1995–2020 reference period.

Note: The boundaries and names shown and the designations used do not imply official endorsement or acceptance by WMO or the United Nations.

Groundwater levels

- In 2024, 38% of wells had normal groundwater levels; 25% were below/much below normal and 37% were above/much above normal.
- Groundwater levels vary locally due to aquifer heterogeneity and human influences like pumping, despite regional trends. Nevertheless, regional patterns are observed, indicating that groundwater is subject to broader regional influences.
- Groundwater-level rise was observed in parts of Europe, India, Florida and southern Brazil, linked to wetter-than-normal conditions and flooding.
- Continued or worsening low levels were seen in Southern Europe, parts of Africa, India, the United States, Mexico, Chile, Brazil and Australia.
- Declines in several regions occurred without drought, pointing to over-abstraction as a key driver.

This chapter presents the status of groundwater levels in 2024 compared to the 20-year reference period 2005–2024, based on in situ monitoring data shared by national and subnational institutions in charge of groundwater monitoring. Where 20 years of data were not available, a 10-year reference period (2015–2024) was used, which is the case for Brazil, Costa Rica, Iraq, Kenya and the State of Palestine. As in 2023, several countries shared groundwater level monitoring data but were not included in this report because less than 10 years of data were available (the Gambia, Rwanda, Somalia, Nigeria) or because data from 2024 were not yet available at the time of reporting.

After data filtering to ensure data consistency and completeness, the analysis includes data from a total of 37 406 wells across 47 countries (see the annex for data source and filtering details). To improve visualization on the global map and to better highlight regional patterns, the ranking of groundwater levels in wells was averaged over 0.5° grid cells, resulting in 4592 grids in total. Note that the spatial representativeness (number and distribution of wells) within each grid is not represented, which may introduce minor biases (for example, cells with only one or a few stations may not represent overall conditions). For more detailed local insights, station-level maps are provided in the annex.

As in 2023, normal groundwater levels were observed in 38% of wells in 2024, with below- and much-below-normal levels in 25% of wells (30% in 2023) and above- and much-above-normal levels in 37% of the wells (30% in 2023) (Figure 13a).

The results show that groundwater level status is rarely uniform over a given area, due to the heterogeneous nature of aquifers and the influence of local factors (such as a pumping well or vicinity to rivers) on groundwater levels. Nevertheless, regional patterns are observed, indicating that groundwater is subject to broader regional influences.

Signs of groundwater-level rise have been observed in several regions, with a shift from below and much below normal in 2023 to above and much above normal in 2024. These areas include large parts of Western and Northern Europe, parts of western and north-eastern India, the south-eastern United States (Florida) and southern Brazil. These regions correspond with very wet climate conditions in 2024 (see Precipitation and River discharge), including

record-breaking floods (such as in Europe and southern Brazil). This shift is observed when wetter-than-normal conditions are combined with shallow groundwater tables and relatively rapid responses to precipitation, leading to increased recharge and reduced pumping.

In contrast, persistent or worsening below-normal groundwater levels, continuing from 2023, affected key regions, including Southern Europe (southern Portugal, southern and eastern Spain, southern France) and parts of Central/Eastern Europe (Hungary and north of Poland), northern and south-western South Africa, north-western India, the western and Midwestern United States, parts of Mexico, northern and central Chile, western Brazil, and parts of southern Australia.

While most of these areas also experienced dry climatic conditions or drought in 2024 (see Precipitation and River discharge), which may have exaggerated the below normal conditions in groundwater levels, these declines are likely driven by a combination of climate impacts and human activities rather than by climate alone. Notably, there are exceptions where declines are observed despite the absence of significant drought. This highlights the strong impact of human factors, such as over-abstraction, as observed for example in the north-western United States, the High Plains aquifer, the Yucatán Peninsula, El Salvador and north-western India (Jasechko et al. 2024; Kuang et al., 2024).

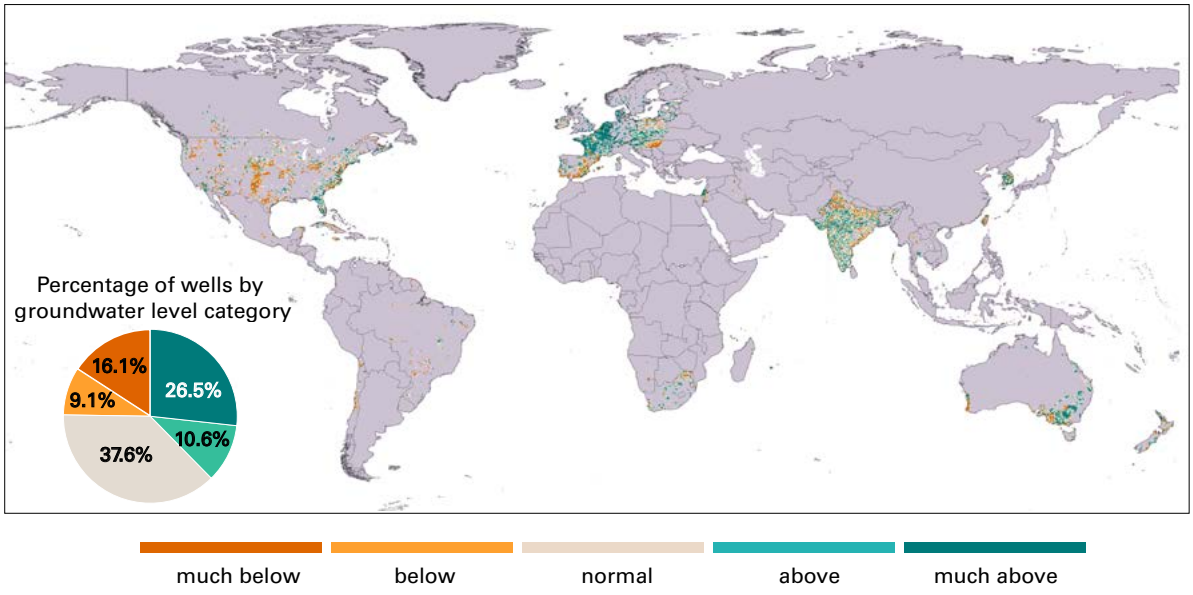

Figure 13a. Mean groundwater levels in 2024 expressed as anomalies (averaged over 0.5° grid cells) as compared to the 2005–2024 reference period (2015–2024 for Brazil, Costa Rica, Iraq, Kenya, State of Palestine). Inset (bottom left) shows groundwater levels in 2024 expressed as anomalies compared with the 2005–2024 (or 2015–2024) reference period.

Note: The boundaries and names shown and the designations used do not imply official endorsement or acceptance by WMO or the United Nations.

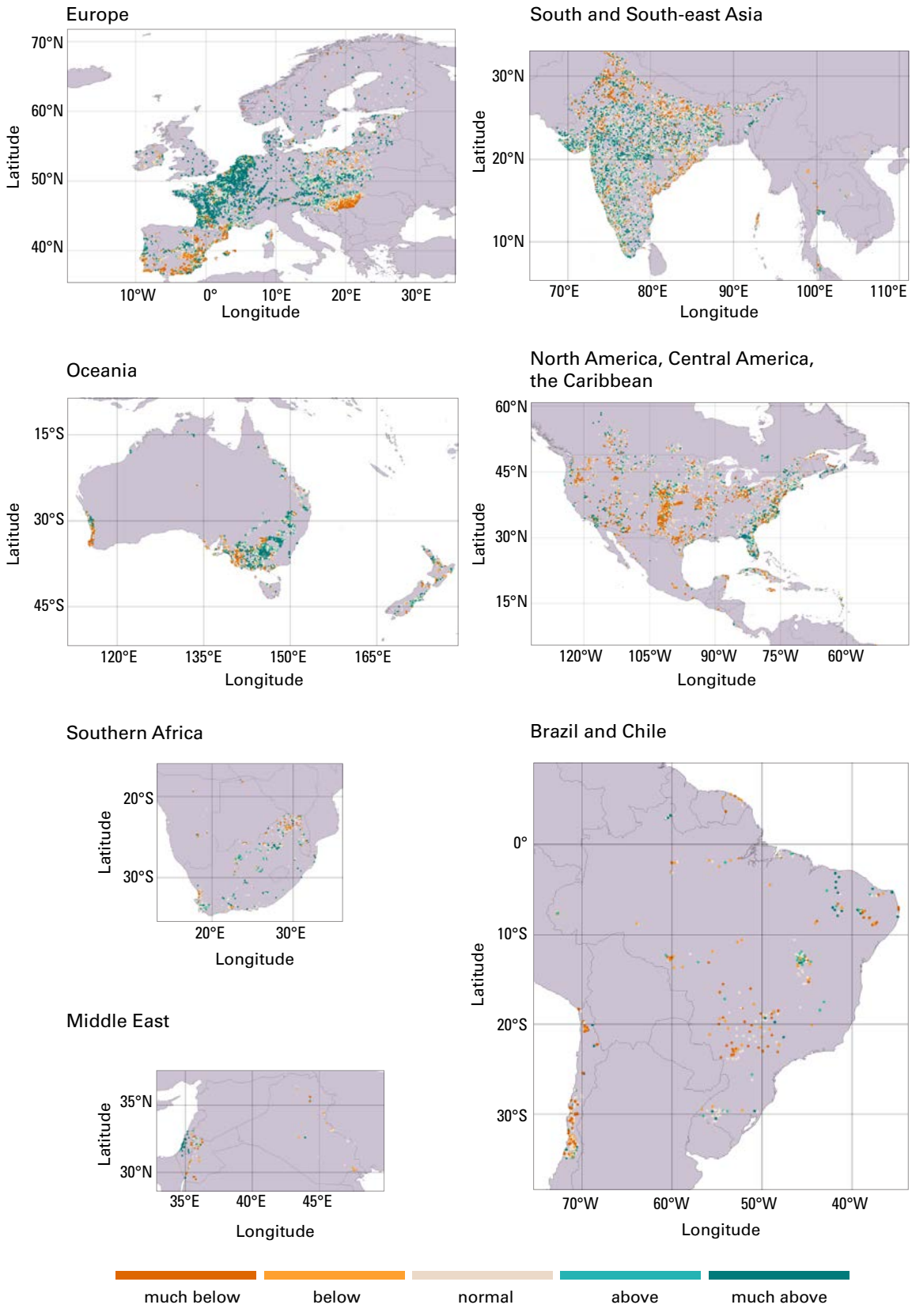

Figure 13b. Snapshots for selected countries showing mean groundwater levels in 2024 expressed as anomalies (as in Figure 13a).

Note: The boundaries and names shown and the designations used do not imply official endorsement or acceptance by WMO or the United Nations.

Soil moisture

- This year's report features an increase in coverage, with observed data received for analysis from about 220 in situ stations.
- Below-normal soil moisture was spread across South America in 2024, especially over the Amazon and Paraná basins.
- Persistent below-normal soil moisture was observed in most African basins; exceptions were the Chad, Niger (August) and Congo (December) basins. Only the Horn of Africa remained consistently above normal.
- In Central Europe the soil moisture was much above normal, whereas in the Mediterranean and Eastern Europe (large parts of Danube basin) it was below to much below normal.
- Regional data gaps limit the detection of broader dryness in the United States from October on, but a drying trend is still apparent, particularly in the deeper soil layer (down to 51 cm, right panel of Figure A12 in the annex), where many stations shifted from above-normal to normal or below-normal moisture levels

Surface soil moisture is one of the crucial variables driving hydrological processes. It influences the exchange of water and energy fluxes at the land surface/atmosphere interface, impacts river discharge generation, is important for biogeochemical cycles and co-controls vegetation development. Understanding soil moisture patterns is essential for sustainable water resources management and for the assessment and understanding of food production (see Soil moisture deficit and Essential Climate Variables).

OBSERVED SOIL MOISTURE

The International Soil Moisture network (ISMN) (Dorigo et al., 2013, 2021), the most comprehensive archive of in situ soil moisture data, includes approximately 3 100 monitoring stations worldwide. For the 2024 report, a subset of 400 stations, primarily located in the United States (Leavesley et al., 2008, 2010; Schaefer et al., 2007) and Spain (Gonzalez-Zamora et al., 2019), were initially selected as they had accumulated 15 years of data (2009 to 2024). After filtering for suitable data quality and acceptable data gaps, a final set of about 220 stations was retained for the analysis. It is important to note that these in situ soil moisture observations do not account for irrigation and may be influenced by local human activities. Maps showing results from Spain and the United States, details on the methodology and its limitations, and general limitations of in situ observations can be found in the annex.

MODELLED SOIL MOISTURE

The anomaly in surface soil moisture in 2024 has been obtained from two GHMSs – Conjunctive Surface–Subsurface Process version 3 (CSSPv3) (Yuan et al., 2018) and mesoscale Hydrologic Model (mHM) (Kumar et al., 2013; Samaniego et al., 2010, 2019) and compared with the modelled historical period 1991–2020 on a monthly basis to understand root zone soil moisture patterns (at 1 m depth). The anomaly calculation used was the same as for river discharge and reservoir inflow (as per Box 1).

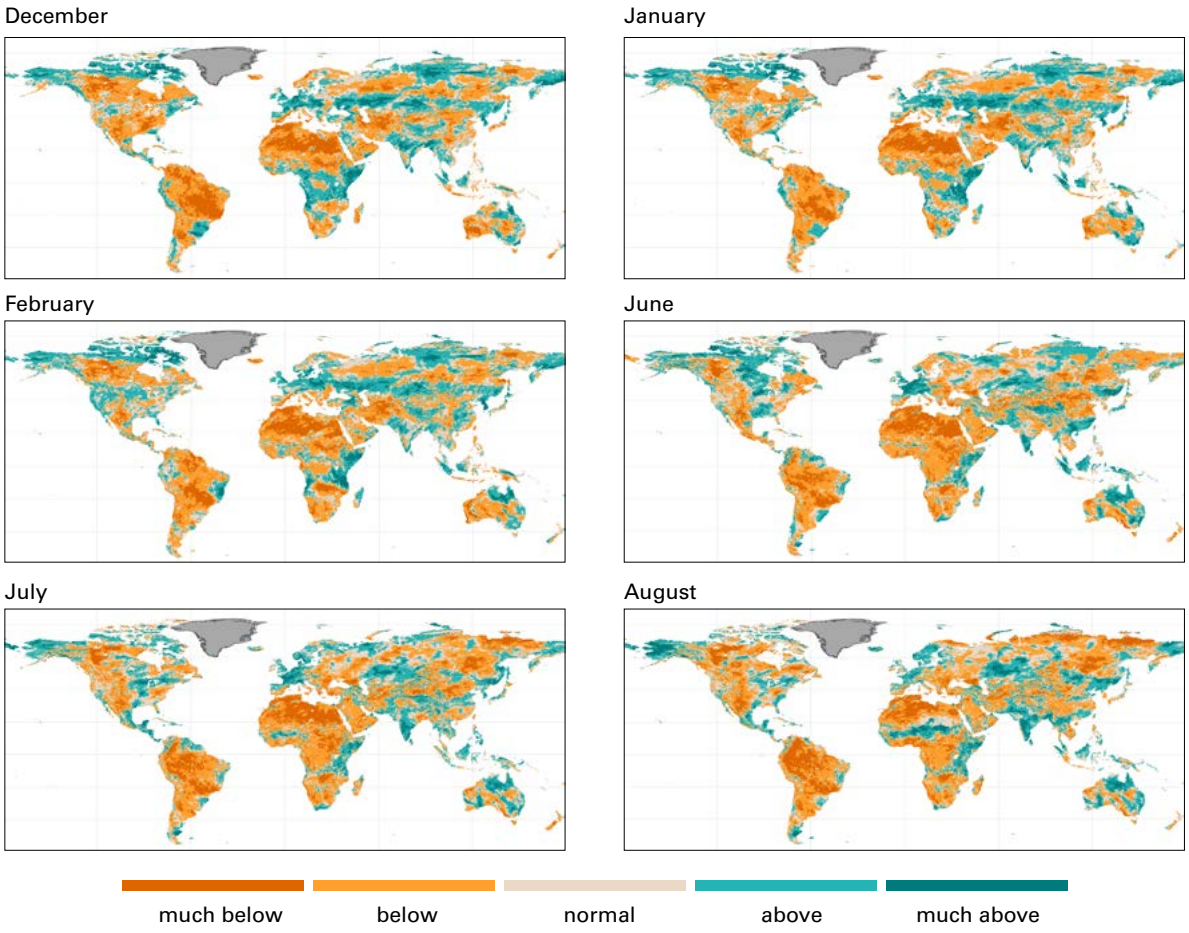

Figure 14. Monthly root zone soil moisture in 2024 (Dec. 2023–Feb. 2024 and Jun.–Aug. 2024) expressed as anomalies compared with the 1991–2020 reference period. Greenland is masked in accordance with Global Land Ice Measurements from Space (GLIMS).

Soil moisture was below to much below normal over almost the whole of South America throughout the year 2024 (Figure 14). The situation affected the entire basins of the Amazon and Paraná, which were hard hit by much-below-normal discharge conditions and drought.

In the Mackenzie river basin in North America, soil moisture levels remained largely much below normal throughout the year, while in the northern catchment of the Yukon River, soil moisture remained largely above to much above normal.

Throughout the year in Central Europe the soil moisture was much above normal, especially during JJA. On the other hand, during the summer period in Eastern Europe (large parts of the Danube basin), the soil moisture remained below to much below normal, and in the Mediterranean basin, the soil moisture remained below to much below normal throughout the entire year.

In almost all large African basins (Orange, Zambezi, Congo, Limpopo, Nile, Congo) the soil moisture was below to much below normal almost throughout 2024, except for August for the Chad and Niger and December for the Congo. Soil moisture in the Horn of Africa remained above to much above normal throughout the year.

The Murray–Darling river basin experienced above- to much-above-normal soil moisture throughout 2024, and in China the Yangtze and Yellow river basins saw below- to much-below-normal soil moisture in JJA.

Evapotranspiration

- Much-above-normal actual evapotranspiration (AET) was observed in early 2024 (DJF, MAM) across large parts of North America, the Murray–Darling basin, a region covering catchments in China and the Far East of the Russian Federation, and the Horn of Africa.
- Above-normal AET occurred in MAM across Persian Gulf countries and eastern Asian basins (Yangtze, Yellow, Lena, Amur, Enisey).
- Persistent AET deficits developed in southern Africa and South America, with much-below-normal values across the La Plata and Amazon basins from MAM through JJA and SON.

Actual evapotranspiration (AET), one of the key elements in the hydrological cycle, refers to the process by which water is evaporated, encompassing evaporation from the soil and from vegetation surfaces (including interception evaporation), and transpiration from plants. Elements influencing the rate of evapotranspiration include the level of solar radiation, atmospheric vapour pressure, humidity, air temperature, wind speed, soil moisture content (water availability) and vegetation type and cover. This process is responsible for a large part of the water loss from the soil during a crop's growth cycle and is critical for understanding the state of water resources. The rates of AET are controlled by the amount of water that is available (which is dependent on the existing hydrological conditions) in addition to the present weather conditions.

This chapter presents AET anomalies at the global scale for four seasons in 2024 with respect to the 1991–2020 historical period (Figure 15), derived from six GHMSs (listed in the annex, Table A1) and averaged over the river basins derived from the HydroBASINS level 4 delineation.

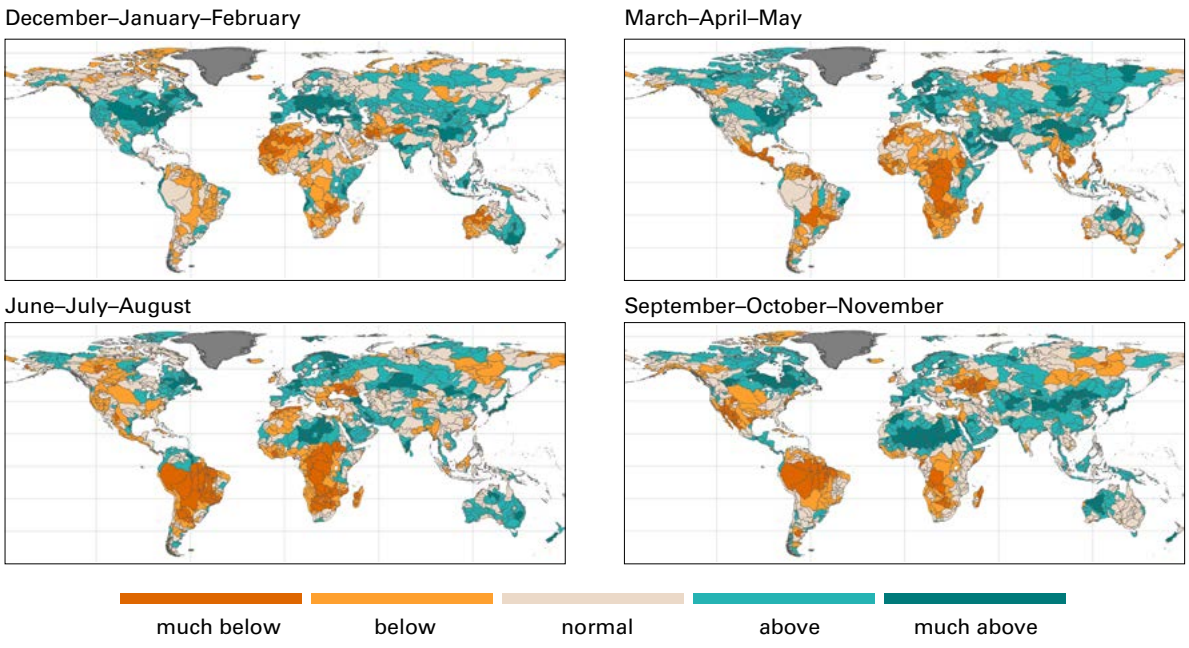

Figure 15. Seasonal actual evapotranspiration (AET) in 2024 expressed as anomalies compared with the 1991–2020 reference period based on an ensemble of six GHMSs

During the DJF and MAM seasons, AET was much above normal across large parts of North America, notably in the Mississippi, St. Lawrence and Colorado river basins. In Europe, during the same seasons much-above-normal AET values manifested across almost the entire region. In SON, the AET in Eastern Europe fell to much below normal, while it remained above normal in Central Europe.

Starting from March, over Persian Gulf countries the AET was above and much above normal, especially in the MAM season, when the AET was much above normal in the southern Islamic Republic of Iran and the United Arab Emirates, which were affected by heavy rainfalls.

The AET was much above normal in DJF and MAM across the Yangtze and Yellow river basins, as well as the basins of major rivers in the southern Russian Federation, such as the Don, Volga, Amur and Ob, and in northern Kazakhstan (Lake Balkhash). In JJA and SON, AET in the Don, Volga, Ural and Dniepr basins turned to below to much below normal, while the basins of major rivers and lakes across Asia (Tarim, Balkhash, Aral, Yangtze, Ganges, Yellow, Amur and others) exhibited above- to much-above-normal AET.

The La Plata River basin saw below-normal AET in DFJ and MAM, and in JJA and SON much-below-normal AET values spread over the entire La Plata and Amazon basins, conditioned by water deficit due to drought conditions in the region.

In the southern African Limpopo, Zambezi, Orange and Congo basins, AET was below to much below normal throughout the entire year, and this was especially pronounced during the MAM and JJA seasons. Only the Niger and Lake Chad basins saw above- and much-above-normal AET during JJA and SON.

Terrestrial water storage

- Positive terrestrial water storage (TWS) anomalies were observed in 2024 across sub-Saharan Africa, northern Australia, and eastern and western Central Africa.
- TWS deficits were particularly pronounced in South America, where the La Plata and Amazon basins continued to exhibit significantly reduced TWS, reflecting the persistence of drought conditions that have affected the region since 2020.
- Recovery to near-normal TWS occurred in Central and Western Europe (which was previously affected by deficits in 2023), likely due to excessive precipitation during 2024.

Satellite gravimetry is a remote-sensing-based method (used by GRACE and GRACE Follow-On (GRACE-FO) satellites (Landerer et al., 2020; Tapley et al. 2019)) that is capable of observing all large-scale mass changes on and below the Earth's surface. This includes, in particular, those caused by water storage changes, including in surface water, soil moisture, groundwater, as well as snow and ice. Terrestrial water storage (TWS), defined as the sum of all these storage compartments, is expressed as an anomaly relative to its long-term mean in equivalent water heights in centimetres as an area-averaged height of the water column over the area being considered. This chapter provides results of the TWS anomaly in the year 2024 obtained from the GRACE/GRACE-FO-based product.

The section on Terrestrial water storage in the annex provides more details on TWS and how TWS anomalies were calculated.

Global TWS patterns in 2024 (Figure 16) were very similar to those in 2023. TWS was above normal across eastern and western Central Africa and northern Australia, as well as in

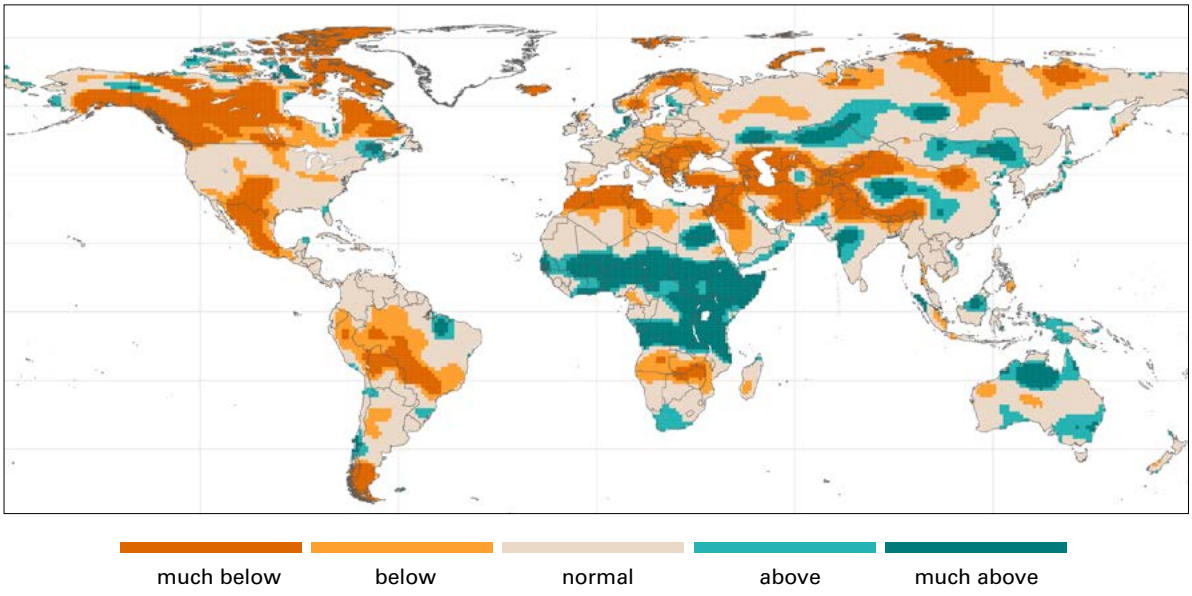

Figure 16. Terrestrial water storage (TWS) in 2024 expressed as anomalies compared with the 2002–2020 reference period. Note that Greenland and Antarctica are not included, as their negative ice mass balance trends over 2002–2020 period are large and therefore hide the other TWS anomalies when plotted on the same scale.

Note: The boundaries and names shown and the designations used do not imply official endorsement or acceptance by WMO or the United Nations.

the Tibetan Plateau region. At the same time, across several regions, including the entire territories of the Islamic Republic of Iran and Afghanistan, Eastern Europe, northern parts of North America and Mexico, TWS was much below normal, as in 2023.

The TWS conditions returned to near-normal levels in 2024 in Central Europe, following below- to much-below-normal levels in 2023.

In 2024, TWS deficits were particularly pronounced in South America, where the La Plata and Amazon basins continued to exhibit significantly reduced TWS, reflecting the persistence of drought conditions that have affected the region since 2023.

In Africa, the entire area of sub-Saharan Africa, including the Greater Horn of Africa, exhibited much-above-normal TWS in 2024. These positive TWS anomalies reflect the strong overall and longer-term water storage increase that has been seen in these areas since 2019 in particular (that is, a signal with longer persistence).

Snow cover and glaciers

- In 2024, Eastern and Central Europe saw below- to much-below-normal March snow water equivalent (SWE) with normal seasonal peak snow mass – indicating early accumulation and melt.
- North America experienced significant SWE deficits in March, especially in the St. Lawrence and Mississippi basins.
- In Central Asia, above-normal seasonal peak snow mass combined with rapid warming in late March triggered flooding in northern Kazakhstan and nearby regions of the Russian Federation.
- The year 2024 was the third consecutive year of widespread ice loss across all 19 glaciated regions, with 450 Gt of global glacier mass loss in 2024 – equivalent to 1.2 mm of sea-level rise.
- Record mass loss occurred in Scandinavia, Svalbard, and North Asia, while some regions like the Canadian Arctic and Greenland periphery saw more moderate losses.
- Most small-glacier regions have likely passed peak water, with reduced summer mass balances suggesting declining runoff contributions, whereas the southern Andes and Russian Arctic still show increasing melt rates.

This chapter presents the state of the snow cover and glaciers in 2024, focusing on snow water equivalent (SWE) in March, peak snow mass over the northern hemisphere (due to data availability) and glacier mass balance, as well as highlighting a case study on glaciers in Colombia.

SNOW WATER EQUIVALENT AND SEASONAL PEAK SNOW MASS

The March SWE in the northern hemisphere was obtained as an ensemble mean over the 1991–2024 period from four individual gridded products:

- The European Space Agency Snow CCI SWE version 2 product derived through a combination of satellite passive microwave brightness temperatures and climate station snow depth observations (Luojus et al., 2022);
- The Modern-Era Retrospective Analysis for Research and Applications version 2 (MERRA-2) (GMAO, 2015) daily SWE fields;
- SWE output from the ERA5-Land analysis (Muñoz Sabater, 2019);
- The physical snowpack model Crocus (Decharme and Barbu, 2024) driven by ERA5 meteorological forcing.

March mean SWE data from each product were regridded to a common 0.5° × 0.5° regular grid and averaged together (Figure 17). This is the same suite of products currently used to produce annually updated SWE data for the Arctic Report Card (Mudryk et al., 2024) and the Bulletin of the American Meteorological Society (BAMS) State of the Climate Report (Mudryk et al., 2025). March 2024 SWE values were converted to anomalies using the 1991–2020 reference period on a pixel-wise basis, as per Box 1.

To produce a daily snow mass time series, total daily SWE output from the Crocus-ERA5 snow model (Decharme and Barbu, 2024) was aggregated over a given land region. Peak snow mass values were then calculated for each water year, and the resulting series of values were used to calculate 2024 percentiles relative to the 1991–2020 reference period (Figure 18).

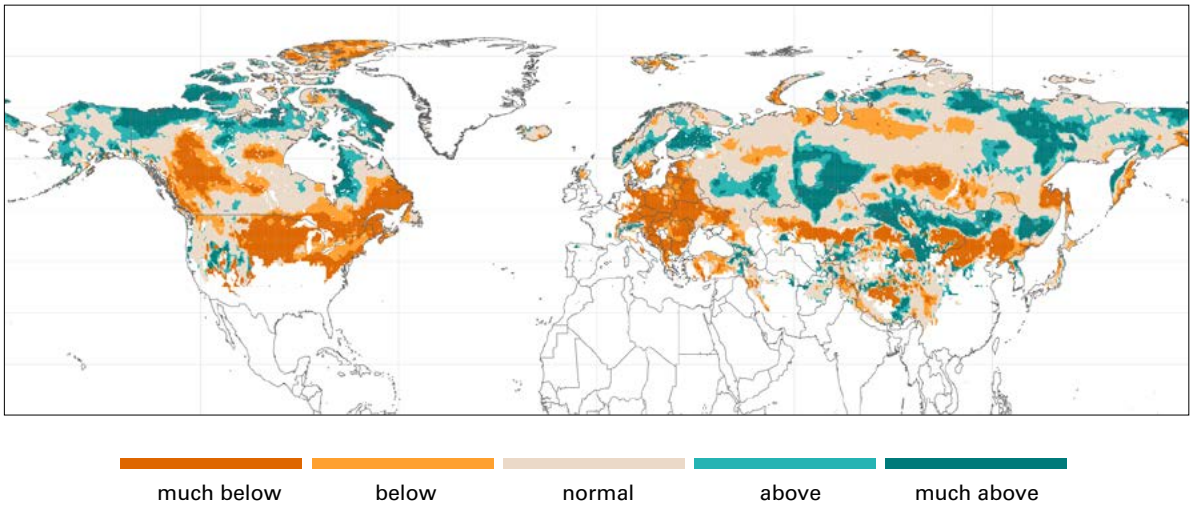

Figure 17. Snow water equivalent in March 2024 expressed as anomalies compared with the 1991–2020 reference period. Results are based on four gridded products (see the Snow water equivalent section in the annex for more details).

Note: The boundaries and names shown and the designations used do not imply official endorsement or acceptance by WMO or the United Nations.

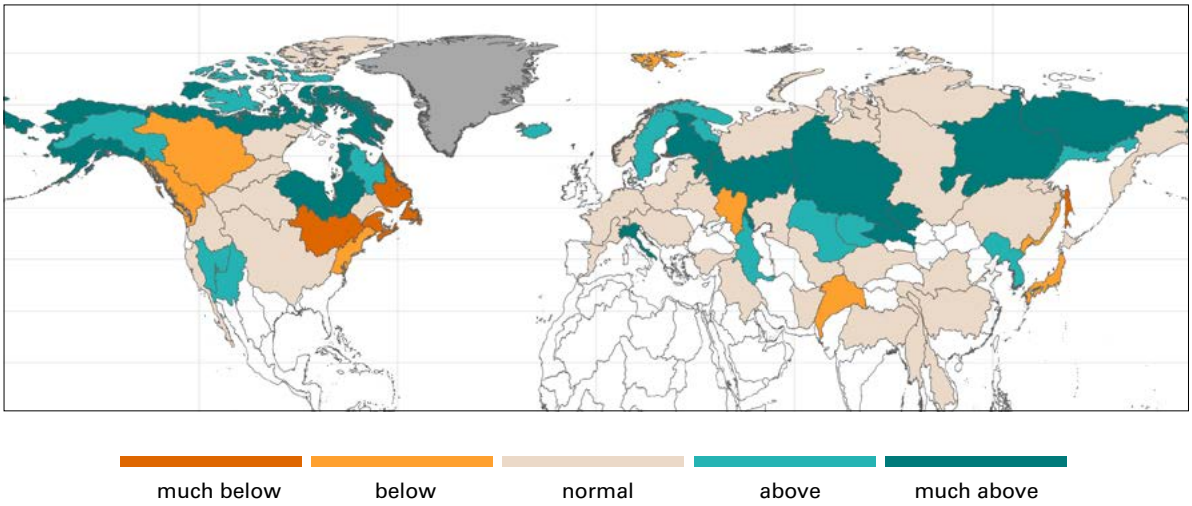

Figure 18. Seasonal peak snow mass over the entire northern hemisphere in 2024 expressed as anomalies compared to the 1991–2020 reference period

Note: The boundaries and names shown and the designations used do not imply official endorsement or acceptance by WMO or the United Nations.

In the Danube, Dniepr, Elbe and Oder basins in Eastern and Central Europe, March SWE was below to much below normal in 2024, while the seasonal peak snow mass was within the normal range in 2024, suggesting that both peak snow accumulation and melt occurred earlier in the season than typical. Only in the Alps was March SWE above to much above normal, as was the seasonal peak snow mass. In Northern Europe the peak snow mass was above to much above normal, except in Norway.

In North America, SWE conditions in March 2024 were much below normal across several major river basins. The St. Lawrence and Mississippi river basins had much-below-normal SWE in March, and the St. Lawrence also had below normal-peak snow mass, whereas the Mississippi basin saw normal conditions. The snowpack deficits may have had implications in the St. Lawrence basin for spring and summer runoff volumes and water availability downstream depending on further precipitation. The MacKenzie basin, and basins near the Pacific coast of Canada (including the Fraser river basin) also had below-normal peak snow mass.

Seasonal peak snow mass in the Ob, Lena, Volga and Kolyma basins in the Russian Federation, the Yukon basin in Alaska, and basins near the entire North American Arctic seaboard was much above normal for 2024; the March SWE was normal to above and much above normal in these basins.

GLACIERS

The present assessment of global glacier mass loss is based on a combination of glaciological field measurements (~500 glaciers or 1% of global glaciers) and geodetic satellite measurements (>200 000 glaciers or 96% of global glaciers) derived from the Fluctuations of Glaciers (FoG) database compiled by the World Glacier Monitoring Service (Dussaillant et al., 2025; WGMS, 2023). Winter and summer regional balances are calculated by downscaling the annual values using seasonal observations from FoG and the sine function analytical model proposed by Zemp and Welty (2023) (Figure 19).

Since, the 1990s, ice loss has been increasing in almost all regions, and it has considerably accelerated since 2000 (Hugonnet et al., 2021). This is mostly due to regions consistently presenting larger summer melt than winter accumulation after the 1990s (Figure 19).

In 2024, glaciers lost 450 Gt of water, which is equivalent to 1.2 mm of contribution to global mean sea-level rise. In 2024, for the third consecutive year, all glaciated regions in the world reported ice loss. While the mass loss was relatively moderate in some regions, such as the Canadian Arctic or the Greenland periphery, the glaciers in Scandinavia, Svalbard and North Asia experienced their largest annual mass loss on record.

Most of the regions dominated by small glaciers have already reached peak water[5] or are expected to reach it in the coming decades (Huss and Hock, 2018; Wimberly et al., 2025). The slightly reduced summer balance trends observed in Figure 19 for Europe, Scandinavia, the Caucasus, Western Canada North, South Asia West and New Zealand in recent years might indicate that these regions are past peak water conditions. On the other hand, the southern Andes (dominated by the Patagonian region), the Russian Arctic, and Svalbard continue to record increasing melt rates (albeit with small increases).

[5] "Peak water" refers to the point when a glacier's melting reaches its maximum annual runoff, after which the runoff decreases due to glacier shrinkage. See the annex for more details.

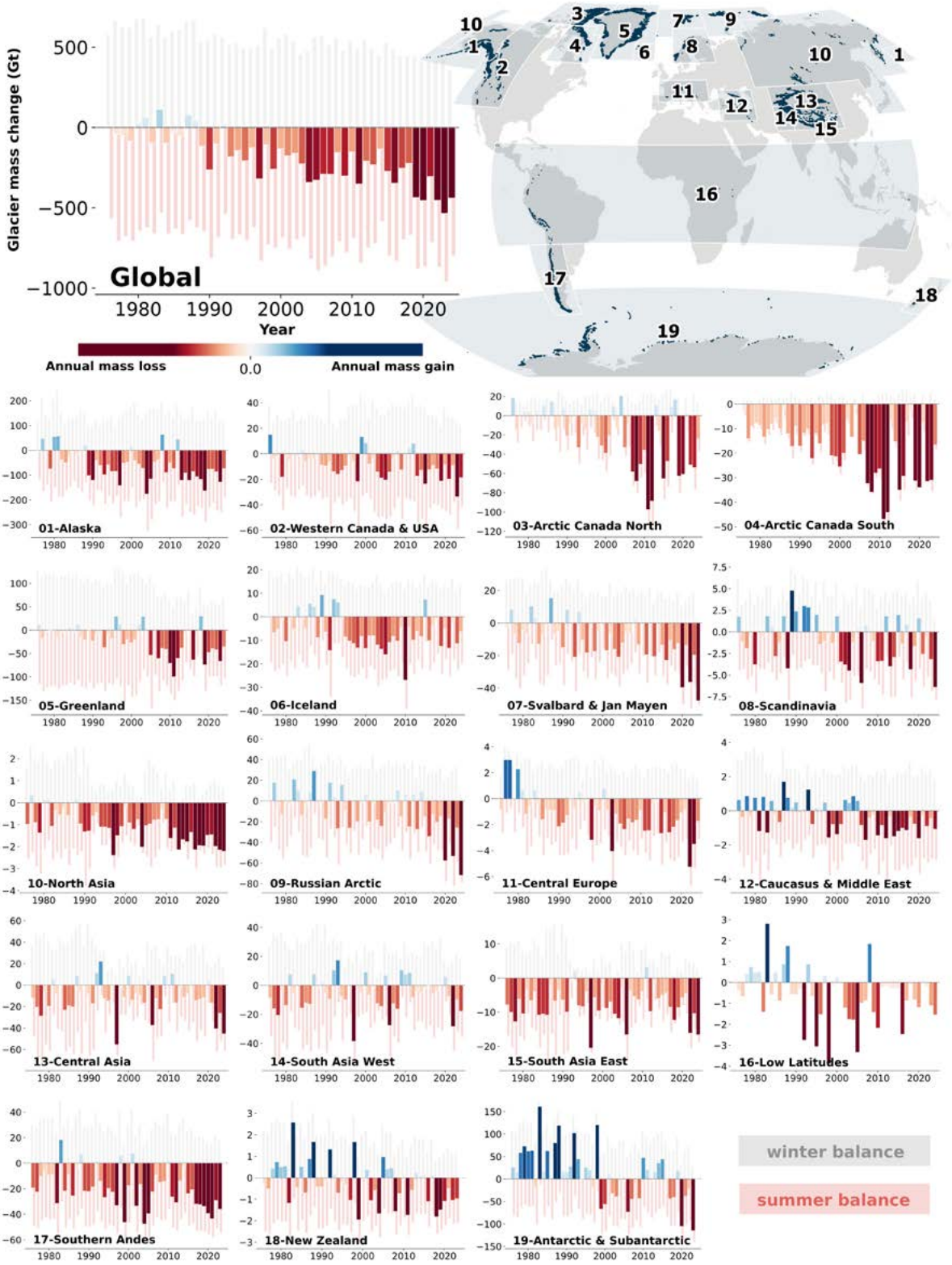

Figure 19. Annual and seasonal mass changes in gigatonnes (Gt) from 1976 to 2024 for the 19 GTN-G glacier regions. Annual net mass loss is represented in red and net mass gain in blue, with white corresponding to balanced years. The colour scale is set to the regional annual net mass change range, with darker colours representing the most negative and positive years, respectively. Note that seasonal and annual mass changes follow the hydrological year (see the annex).

Global estimates of annual glacier mass loss are good indicators of annual glacier contribution to global sea-level rise. However, because winters and summers occur at different times of the calendar year in the two hemispheres, global winter and summer estimates are not a good a proxy to understand the impact of glacier annual loss on the hydrological cycle. Regional winter and summer mass balances provide a better understanding of the evolution and impact of glacier contribution to runoff.

CASE STUDY ON GLACIERS IN COLOMBIA

Colombian glaciers, classified as tropical and equatorial glaciers due to their latitudinal location very close to the Equator, significantly increased their melting rates in 2023 and 2024 due to an extreme El Niño event. The total glacier area in Colombia, which was estimated at 33.09 ± 0.63 km^2 (accounting for 0.1% of Andean glaciers and 2.2% of tropical glaciers) at the beginning of 2022 (Ceballos et al., 2024), has declined by 5%, reaching 31.4 ± 0.5 km^2 at the beginning of 2024.[6]

During the last decade, Colombian glacier area has declined at 3% to 5% annually. Likewise, the mass balance (an environmental indicator), calculated for two glaciers in different geographic and local climatic conditions, continues to be negative, with a notable increase in mass loss in 2024 caused by El Niño, which led to the absence of solid precipitation and high solar radiation. The extinction of the Conejeras Glacier (located in central Colombia in a zone where coffee is grown), part of the Nevado Santa Isabel Glacier, was reported in 2024 after 18 years of observation.

[6] Glacier mass balance for 2024 is based on preliminary observations, but no large differences are anticipated after data verification.

High-impact hydrological events

- Africa faced severe and widespread flood impacts, with several countries in the tropical zone experiencing unusually heavy rainfall, leading to more than 2 500 deaths, 4 million people being displaced, and large-scale damage to infrastructure, agriculture and education systems.
- Europe experienced its most extensive flooding since 2013, with one-third of the river network exceeding "high" flood thresholds, causing over 335 deaths and 18 billion euros (€) in economic losses from multiple extreme events.
- Asia and the Pacific were hit by record-breaking rainfall and tropical cyclones, including Typhoon *Yagi* and spring floods in Afghanistan, resulting in over 1 000 deaths, severe economic damage and widespread humanitarian crises across multiple countries.
- Brazil experienced simultaneous extremes, with catastrophic flooding in the south of the country taking 183 lives and affecting almost 2.4 million people, combined with continued drought from 2023, which severely impacted the Amazon basin and 59% of the territory of the country.

This chapter presents a non-exhaustive review of selected major extreme hydrological and weather events that occurred in 2024 (Figure 20). The events were selected from several sources, including the EM-DAT database (CRED, 2025), the WMO *State of the Global Climate 2024* (WMO-No. 1368), direct communication from WMO Members to the WMO Secretariat (presented via the WMO Extremes Dashboard) and other public sources such as ReliefWeb. Events selected from the EM-DAT database were in the top 10th percentile either for number of casualties or for economic losses. From the WMO Extremes Dashboard, only events marked by respective NHMS as "unprecedented" were considered.

Most of the unprecedented or notable extreme hydrological and weather events in 2024 were in Europe, Africa and Asia. Most such events related to excess water (that is, flash floods, heavy rainfalls and associated landslides).

Africa was severely affected for the second year in a row: several countries in Africa's tropical zone experienced unusually heavy rainfall in 2024 compared to their historical norms, resulting in 2 500 fatalities and 4 million people being displaced. Millions of hectares of croplands were inundated. Hundreds of thousands of farm animals were lost, hundreds of healthcare facilities were destroyed or damaged, and 10 million children in Niger, Nigeria, the Democratic Republic of the Congo (DRC) and Mali were unable to attend school as thousands of schools were flooded or converted into temporary housing for displaced people (see Record Levels of Flooding in Africa Compounds Stress on Fragile Countries).

FLOODS IN MOROCCO AND ALGERIA

On 7–8 September an extratropical cyclone swept through the north-western Sahara, delivering heavy rainfall to typically arid areas in Morocco, Algeria, Tunisia, and Libya – regions that seldom experience such precipitation. NASA's Terra satellite captured images of floodwaters and evidence that some Saharan lakes, usually dry, had filled with water (see A Deluge for the Sahara). Satellite analysis showed that the cyclone brought more than 200 mm of rainfall

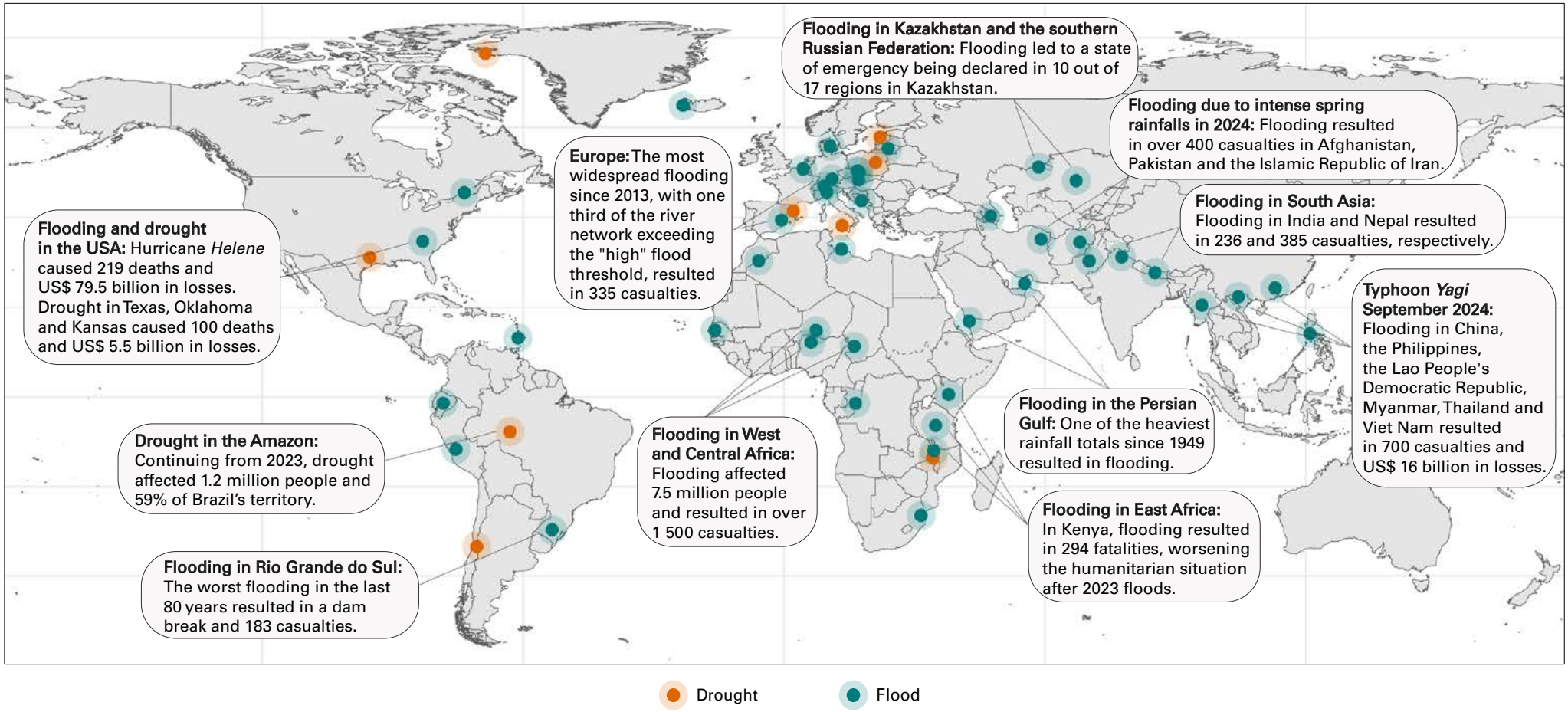

Figure 20. Selected most notable high-impact hydrological events across the globe in 2024

Note: The boundaries and names shown and the designations used do not imply official endorsement or acceptance by WMO or the United Nations.

to some areas on 7 and 8 September, which is about what the region receives in a year (see A Deluge for the Sahara). The event resulted in more than 20 casualties in Morocco and Algeria (see Morocco, Algeria – Floods, update (Direction de la Météorologie Nationale, Météo Algérie, media) (ECHO Daily Flash of 10 September 2024)).

FLOODS IN EUROPE

Europe experienced the most widespread flooding since 2013. Almost one third of the river network saw flooding that exceeded at least the "high" flood threshold.[7] Storms and flooding affected an estimated 413 000 people in Europe, with at least 335 lives lost (Copernicus Climate Report 2024).

In 2024, Latvia experienced two major flood events. The first occurred in late February, when an ice jam on the Daugava River between Jēkabpils and Zeļķi triggered a red flood warning. Peak water levels reached the highest since 2010 – causing damage to protective dams in the city of Pļaviņas and Gostiņi settlement. The second event took place on 28–29 July, when record-breaking rainfall (65.3 mm over two days) led to widespread flooding and flash flooding across the country, with 15 municipalities reporting over €8.4 million in damages. Emergency measures, hydrological monitoring, and a post-event municipal survey coordinated by the Ministry of Climate and Energy helped assess and manage both events.[8]

On 16 May 2024, severe storms brought intense rainfall to eastern France. Some areas, such as Scheibenhard and Berg-sur-Moselle, received over 100 mm of rain in 24 hours – precipitation levels not seen since 1885 (see Floods and storms in Western Europe, May 2024). The extreme weather also affected parts of Germany, with flash floods in Bavaria leading to water rescues in Nuremberg and mass evacuations in Saarland and Rhineland-Palatinate (see Floods and storms in Western Europe, May 2024).

In September, prolonged rainfall brought by storm Boris led to widespread flooding in Central and Eastern Europe. Between 12 and 16 September, Poland, Germany, Czechia and north-eastern Romania experienced rainfall equivalent to up to three months' worth of precipitation (see Aon estimates €1.65bn market loss from September Central Europe flooding). In the upper Danube basin, the highest five-day rainfall total ever (704.2 mm) was recorded at Loučná nad Desnou in Czechia, as well as a daily record of 385.6 mm, beating the previous record of 345 mm from 1897 (CHMI, 2024). The estimated economic loss of this event alone was €1.65 billion (see Aon estimates €1.65bn market loss from September Central Europe flooding).

Between 28 October and 4 November, catastrophic flooding was caused by prolonged intense rainfall in Valencia, Spain. It resulted in at least 232 fatalities (see Actualización de datos del Gobierno de España) and severe economic losses, totalling around €17.5 billion (*State of the Global Climate 2024* (WMO-No. 1368)).

[7] Copernicus Climate Report 2024 defines the "high" flood threshold as flooding with a five-year return period.

[8] Information based on direct communication from WMO Member.

FLOODS IN VIET NAM, CHINA, MYANMAR AND THE PHILIPPINES

Typhoon *Yagi* was one of the deadliest and most extreme events in South-east Asia in 2024. It hit China, the Philippines, the Lao People's Democratic Republic, Thailand, Myanmar, and especially Viet Nam, in early September (see 2024 Super Typhoon *Yagi*; *State of the Global Climate 2024* (WMO-No. 1368); Viet Nam: Typhoon *Yagi* and Floods - Situation Update No. 5 (as of 23 October 2024)). Typhoon *Yagi* brought several subsequent days of heavy rainfall: on the 6–12 September Nam Dan (Viet Nam) received 781 mm of rain, and many other stations exceeded 500 mm. Also in Myanmar, several stations observed 500 mm of rainfall within three days (*State of the Global Climate 2024* (WMO-No. 1368)), causing widespread flooding and landslides across 26 provinces in Viet Nam (see Viet Nam: Typhoon *Yagi* and Floods – Situation Update No. 5 (as of 23 October 2024)). In Viet Nam, 321 deaths, 24 missing people and 1 978 injured people (see Viet Nam: Typhoon *Yagi* and Floods – Situation Update No. 5 (as of 23 October 2024)) were reported after the event, and in Myanmar at least 328 deaths were reported (*State of the Global Climate 2024* (WMO-No. 1368)). In total, more than 700 people lost their lives due to the event across Viet Nam, China, the Lao People's Democratic Republic, China, Thailand and the Philippines (*State of the Global Climate 2024* (WMO-No. 1368)). The estimated economic loss reached 16 billion US dollars (US$) (see 2024 Super Typhoon *Yagi*).

FLOODS IN AFGHANISTAN, THE ISLAMIC REPUBLIC OF IRAN AND PAKISTAN

Afghanistan, the Islamic Republic of Iran and Pakistan were badly affected by intense spring rainfalls in 2024. In fact, spring precipitation over the region has become 25% heavier over the past 40 years, according to World Weather Attribution (see Increasing April–May rainfall, El Niño and high vulnerability behind deadly flooding in Afghanistan, Pakistan and Iran).

In the early months of 2024 in Afghanistan, more than 300 people lost their lives and 1 600 people were injured due to unusually heavy rains and extreme cold temperatures (see CRED, 2025; More than 300 killed in Afghanistan flash floods). In Pakistan, the intense rainfall began on 12 April and led to flooding which caused the death of 124 people, while another 153 were injured and over 6 000 houses were damaged (see Pakistan: Flash Floods Flash Update No. 3 (As of 30 April 2024)). The flash floods also severely affected large areas of agricultural land, especially wheat that was ready for harvest, leading to substantial economic losses for local farmers and communities (see Pakistan: Flash Floods Flash Update No. 3 (As of 30 April 2024)). Heavy rainfalls and flooding also affected the Islamic Republic of Iran, leading to 18 deaths (see Death Toll From Region-Wide Floods Rises To 18 In Southeast Iran; Iran: Floods – Feb 2024).

FLOODS IN NEPAL AND INDIA

Record-breaking precipitation in late September 2024 caused dramatic flooding and landslides in Nepal. Severe flooding occurred in the Kathmandu Valley, and the Narayani River at Devghat exceeded its previous record flood level by 3.5 m (*State of the Global Climate 2024* (WMO-No. 1368)). At least 236 people lost their lives, 173 were injured, and 19 were missing (see Floods and landslides in Nepal, late September 2024). Economic losses caused by the flood equalled 1% of Nepal's gross domestic product (see Floods and landslides in Nepal, late September 2024).

In India, 385 deaths were reported, caused by extreme rainfall on 30 July in Kerala, triggering extreme landslides (*State of the Global Climate 2024* (WMO-No. 1368)).

FLOODS IN THE UNITED ARAB EMIRATES

In April 2024, Dubai was hit by its heaviest rainfall in 75 years, delivering over a year's worth of rain (255 mm) in 24 hours, which resulted in widespread urban flooding, paralysis of infrastructure – including metro services and airports (1 244 cancelled flights), overwhelmed drainage, and five confirmed fatalities. The government swiftly deployed emergency services, evacuated affected residents, and mobilized both the public and private sectors to support relief efforts.

FLOODS AND DROUGHT IN BRAZIL

Rio Grande do Sul (southern Brazil) was affected by a record-breaking flood in May 2024 caused by extreme precipitation. Santa Maria and Soledad stations received 470.7 mm over three days and 498 mm over the five days from 1 to 5 May. Santa Maria station received 213.6 mm of rainfall on 1 May.

In total, 183 lives were lost and almost 2.4 million people were affected (see Brazil: Floods in Rio Grande do Sul – United Nations Situation Report, as of 20 September 2024; Simoes-Sousa et al., 2025). In Porto Alegre, capital of the state of Rio Grande do Sul and home to 1.3 million people, 12% of the population was affected by flooding (Simoes-Sousa et al., 2025). The flooding led to a dam break on the Barramansa River (Sun et al., 2025) and was the most destructive flood event to affect the country in the last 80 years (Alcantara et al., 2024; Pessoa, 2024; *State of the Global Climate 2024* (WMO-No. 1368)).

On the other hand, in the Amazon region, the drought that started in 2023 continued in 2024, driven by decreased precipitation due to effects of El Niño, and intensified by deforestation and climate change-induced temperature anomalies (see Climate change, not El Niño, main driver of exceptional drought in highly vulnerable Amazon River Basin). This drought has been recorded as the most intense and extensive drought since the agency began monitoring these events (see Wildfires and climate crisis: The 2023/2024 drought is the most severe in recent history, records show). It affected 1.2 million people (UNICEF, 2025) and 59% of Brazil's territory in 2023–2024, causing water shortages and a severe loss of livelihoods and crops (see ACAPS Thematic report – Brazil: Impact of drought in the Brazilian Amazon and 2025 outlook (28 January 2025)). On 9 to 12 October, the Rio Negro at Manaus hit a new record low level at 12.11 m, which is 0.59 m below the previous record set in 2023, and more than a metre below the lowest pre-2023 level (*State of the Global Climate 2024* (WMO-No. 1368)). The Madeira river hit a record low level of only 0.71 m on 10 September, the lowest level recorded since 1967 by the Geological Service of Brazil (SGB) (see Madeira River falls to 71 cm, below minimum level of 2023).

Drought created favourable conditions for forest fires: from 1 January to 22 September, about 11 million hectares were burned in the Amazon, which represents 2.8% of the biome (see Wildfires and climate crisis: The 2023/2024 drought is the most severe in recent history, records show).

FLOODS AND DROUGHT IN THE UNITED STATES

Hurricane *Helene* produced historic rainfall in late September 2024, with 781 mm three-day rainfall totals recorded from 25 to 27 September (*State of the Global Climate 2024* (WMO-No. 1368)), and caused the worst flooding in the south-east of the United States since 1916, especially in western North Carolina. Hurricane *Helene* was associated with 219 deaths (see Billion-Dollar Weather and Climate Disasters; *State of the Global Climate 2024* (WMO-No. 1368)) and US$ 79.5 billion in losses.

At the same time, Texas, Oklahoma and Kansas were impacted by a drought throughout the year. This region lost a high volume of crops, and, for a number of these states, the year was reported to be the hottest on record, with more than 100 deaths from excessive heat exposure and US$ 5.5 billion in economic losses (see Billion-Dollar Weather and Climate Disasters).

FLOODS IN KAZAKHSTAN AND THE RUSSIAN FEDERATION

Significant spring flooding occurred in late March and April in northern Kazakhstan and adjacent border areas of the Russian Federation, resulting from rapid melting of a heavier-than-normal snowpack after warm weather during second half of March (*State of the Global Climate 2024* (WMO-No. 1368)). In Kazakhstan, the flood displaced over 119 000 people, including 44 000 children (see Devastating Floods in Kazakhstan: A National Emergency). Local governments declared a state of emergency in 10 out of 17 regions in the country, launching massive relief and rescue operations (see Devastating Floods in Kazakhstan: A National Emergency).

FLOODS IN WEST AND CENTRAL AFRICA

An exceptionally wet monsoon season resulted in long-lived and extensive flooding during the second half of 2024 across large parts of the Sahel region and West and Central Africa (*State of the Global Climate 2024* (WMO-No. 1368)). Rainfall in 2024 was more than 50% above normal over much of the region, and flooding was reported in almost every country in the region, including Burkina Faso, Cameroon, the Central African Republic, Chad, Mali, Niger, Nigeria, Senegal and Sudan (*State of the Global Climate 2024* (WMO-No. 1368)). A total of 7.5 million people were affected by flooding across West and Central Africa (see West and Central Africa: Flooding Situation 2024 Overview – as of 10 February 2025), at least 1 526 deaths were reported (*State of the Global Climate 2024* (WMO-No. 1368); West and Central Africa: Flooding Situation 2024 Overview – as of 10 February 2025), 4 499 were injured, and 639 000 houses were damaged or destroyed (*State of the Global Climate 2024* (WMO-No. 1368)). More than 960 000 hectares of agricultural land has become unsuitable for farming and livestock production; 128 000 cows were also swept away by the floods. These events have worsened the overall humanitarian situation (see West and Central Africa: Flooding Situation 2024 Overview – as of 10 February 2025).

The Congo basin was badly affected by flooding in the beginning of 2024, following intense rains at the end of 2023. Nearly 300 lives were lost in the flood disaster zone, and 433 000 people were affected in 18 provinces (see République démocratique du Congo – Flash Update #2: De graves inondations affectent 18 provinces, Mis à jour au 6 février 2024 – Democratic Republic of the Congo).

FLOODS IN EAST AFRICA

Between March and May significant flooding events occurred across East Africa, specifically in Burundi, Ethiopia, Kenya, Rwanda, Somalia, the United Republic of Tanzania and Uganda (*State of the Global Climate 2024* (WMO-No. 1368)). In Kenya, 294 fatalities, 162 people missing and more than 100 000 affected households were reported (see Floods Operations, 2024). The flooding, coming after years of drought, increased overall displacement in East Africa and exacerbated acute food insecurity, disease outbreaks and damage to infrastructure (see 2024 East Africa Flooding and Cyclones). The 2024 floods, coming after flooding in 2023, are worsening an already critical humanitarian situation in Kenya.

FLOODS IN AUSTRALIA

In 2024, Australia experienced several significant rainfall and flooding events that impacted multiple regions and catchments. Iin early January, record-breaking rainfall (154.4 mm in 24 hours) in south-eastern Australia triggered major flood warnings for Victoria's rivers. February and March brought intense rainfall, thunderstorms and monsoonal activity across Queensland, New South Wales, the Northern Territory and northern Western Australia, leading to widespread flooding. Heavy rain resulted in widespread flash flooding in eastern New South Wales and south-eastern Queensland, and about 75 000 lightning strikes were recorded across Greater Sydney. Later in the year, prolonged rainfall caused major flooding in Tasmania during August–September, and in December, successive troughs produced severe thunderstorms and flash flooding across central and south-eastern Queensland (see Annual Statement 2024).

GLACIER OUTBURST FLOOD IN CANADA

In the summer of 2024, a glacial outburst flood (*jökulhlaup*) occurred in British Columbia, originating from the Place Glacier. The sudden release of meltwater inundated downstream areas, prompting the issuance of emergency alerts and evacuation protocols. While the affected region was rural – limiting the overall financial and social impact – the event caused notable infrastructure damage and altered downstream watercourses. This incident underscores the growing risk of glacial outburst floods in a warming climate and highlights the importance of monitoring glacier-fed systems. Though not classified as an extreme flood, the event has important implications for water resource management and underpins the importance of better monitoring, forecasting and early warning systems.

Outlook

The 2024 edition of the State of Global Water Resources report reflects significant progress in both reach and content. Feedback from our global user survey and the remarkable response from Members and international partners have been overwhelmingly positive. This is evident in the growing number of participating countries, the increase in data contributions, and the expanding list of partner organizations involved. The report now covers a wider range of hydrometeorological variables than ever before, underscoring the collective commitment to improving global water monitoring and reporting.

One notable development this year is the inclusion of infilled data in the streamflow chapter. While observational data are crucial to support effective water management, limitations of observational data availability and continuity do not need be a restricting factor in contributing to international reporting efforts like the State of Global Water Resources. Advances in machine learning, remote sensing and modelling techniques now allow us to bridge data gaps (as seen in the River discharge chapter) for many larger rivers with increasing confidence – strengthening our understanding of global water conditions even in data-scarce regions.

Looking ahead, we aim to enhance the automation of data flows through our data centres and the WMO Hydrological Observing System (WHOS), streamlining integration for future reporting cycles. The ongoing operationalization of the WMO Hydrological Status and Outlook System (HydroSOS) and associated capacity development activities will enable countries to produce monthly water resources status updates. This will provide WMO Members and stakeholders with timely, actionable information for water-related decision-making in an increasingly dynamic climatological and hydrological environment, in addition to the annual snapshot the State of Global Water Resources provides.

References

Alcântara, E.; Mantovani, J.; Baião, C. et al. Unprecedented Flooding in Porto Alegre Metropolitan Region (Southern Brazil) in May 2024: Causes, Risks, and Impacts. *Social Science Research Network* **2024** [preprint]. https://doi.org/10.2139/ssrn.4867780.

Alfieri, L.; Burek, P.; Dutra, E. et al. GloFAS – Global Ensemble Streamflow Forecasting and Flood Early Warning. *Hydrology and Earth System Sciences* **2013**, *17* (3), 1161–1175. https://doi.org/10.5194/hess-17-1161-2013.

Arheimer, B.; Pimentel, R.; Isberg, K. et al. Global Catchment Modelling Using World-Wide HYPE (WWH), Open Data, and Stepwise Parameter Estimation. *Hydrology and Earth System Sciences* **2020**, *24* (2), 535–559. https://doi.org/10.5194/hess-24-535-2020.

Becker, A.; Finger, P.; Meyer-Christoffer, A. et al. A Description of the Global Land-Surface Precipitation Data Products of the Global Precipitation Climatology Centre with Sample Applications Including Centennial (Trend) Analysis from 1901–Present. *Earth System Science Data* **2013**, *5* (1), 71–99. https://doi.org/10.5194/essd-5-71-2013.

Biswas, N. K.; Hossain, F.; Bonnema, M. et al. Towards a Global Reservoir Assessment Tool for Predicting Hydrologic Impacts and Operating Patterns of Existing and Planned Reservoirs. *Environmental Modelling & Software* **2021**, *140*, 105043. https://doi.org/10.1016/j.envsoft.2021.105043.

Boussetta, S.; Balsamo, G.; Arduini, G. et al. ECLand: The ECMWF Land Surface Modelling System. *Atmosphere* **2021**, *12* (6), 723. https://doi.org/10.3390/atmos12060723.

Centre for Research on the Epidemiology of Disasters (CRED). *EM-DAT*; CRED/UCLouvain: Brussels, Belgium. http://www.emdat.be.

Czech Hydrometeorological Institute (CHMI). Evaluation of the Flood in September 2024 (Vyhodnocení povodně v září 2024) [report in Czech]; CHMI: Prague, 2024; 150 p. https://www.chmi.cz/files/portal/docs/tiskove_zpravy/2025/Povoden_zari_2024.pdf.

Decharme, B.; Barbu, A. Crocus-ERA5 Daily Snow Product over the Northern Hemisphere at 0.25° Resolution; Version 2023; *Zenodo* **2024**. https://doi.org/10.5281/zenodo.10943718.

Dorigo, W.; Himmelbauer, I.; Aberer, D. et al. The International Soil Moisture Network: Serving Earth System Science for over a Decade. *Hydrology and Earth System Sciences* **2021**, *25* (11), 5749–5804. https://doi.org/10.5194/hess-25-5749-2021.

Dorigo, W. a.; Xaver, A.; Vreugdenhil, M. et al. Global Automated Quality Control of In Situ Soil Moisture Data from the International Soil Moisture Network. *Vadose Zone Journal* **2013**, *12* (3), vzj2012.0097. https://doi.org/10.2136/vzj2012.0097.

Dussaillant, I.; Hugonnet, R.; Huss, M. et al. Annual Mass Change of the World's Glaciers from 1976 to 2024 by Temporal Downscaling of Satellite Data with in Situ Observations. *Earth System Science Data* **2025**, *17* (5), 1977–2006. https://doi.org/10.5194/essd-17-1977-2025.

Eilander, D.; van Verseveld, W.; Yamazaki, D. et al. A Hydrography Upscaling Method for Scale-Invariant Parametrization of Distributed Hydrological Models. *Hydrology and Earth System Sciences* **2021**, *25* (9), 5287–5313. https://doi.org/10.5194/hess-25-5287-2021.

Elmi, O.; Tourian, M. J.; Saemian, P. et al. Remote Sensing-Based Extension of GRDC Discharge Time Series - A Monthly Product with Uncertainty Estimates. *Scientific Data* **2024**, *11* (1), 240. https://doi.org/10.1038/s41597-024-03078-6.

Global Precipitation Climatology Centre (GPCC). *2025 Precipitation Quantiles at 1.0°: Monthly Land-Surface Precipitation as Quantiles from Rain-Gauges built on GTS-based and Historic Data*; https://doi.org/10.5676/DWD_GPCC/QUANTILES_V2022_100.

González-Zamora, Á.; Sánchez, N.; Pablos, M. et al. CCI Soil Moisture Assessment with SMOS Soil Moisture and *in Situ* Data under Different Environmental Conditions and Spatial Scales in Spain. *Remote Sensing of Environment* **2019**, *225*, 469–482. https://doi.org/10.1016/j.rse.2018.02.010.

Grimaldi, S.; Salamon, P.; Russo, C. et al. GloFAS v4.0: Towards Hyper-resolution Hydrological Modelling at Global Scale. In *European Geosciences Union (EGU) Abstracts EGU General Assembly 2023*, Vienna, Austria, 23–28 April 2023. https://doi.org/10.5194/egusphere-egu23-3410.

Hales, R. C.; Nelson, E. J.; Souffront, M. et al. Advancing Global Hydrologic Modeling with the GEOGloWS ECMWF Streamflow Service. *Journal of Flood Risk Management* **2022**, *18* (1), e12859. https://doi.org/10.1111/jfr3.12859.

Hanazaki, R.; Yamazaki, D.; Yoshimura, K. Development of a Reservoir Flood Control Scheme for Global Flood Models. *Journal of Advances in Modeling Earth Systems* **2022**, *14* (3), e2021MS002944. https://doi.org/10.1029/2021MS002944.

Huang, Q.; Zhang, Y.; Ma, N. et al. Estimating Vegetation Greening Influences on Runoff Signatures Using a Log-Based Weighted Ensemble Method. *Water Resources Research* **2022**, *58* (12), e2022WR032492. https://doi.org/10.1029/2022WR032492.

Hugonnet, R.; McNabb, R.; Berthier, E. et al. Accelerated Global Glacier Mass Loss in the Early Twenty-First Century. *Nature* **2021**, *592* (7856), 726–731. https://doi.org/10.1038/s41586-021-03436-z.

Huss, M.; Hock, R. Global-Scale Hydrological Response to Future Glacier Mass Loss. *Nature Climate Change* **2018**, *8* (2), 135–140. https://doi.org/10.1038/s41558-017-0049-x.

Imhoff, R. O.; van Verseveld, W. J.; van Osnabrugge, B. et al. Scaling Point-Scale (Pedo)Transfer Functions to Seamless Large-Domain Parameter Estimates for High-Resolution Distributed Hydrologic Modeling: An Example for the Rhine River. *Water Resources Research* **2020**, *56* (4), e2019WR026807. https://doi.org/10.1029/2019WR026807.

Jasechko, S.; Seybold, H.; Perrone, D. et al. Rapid Groundwater Decline and Some Cases of Recovery in Aquifers Globally. *Nature* **2024**, *625* (7996), 715–721. https://doi.org/10.1038/s41586-023-06879-8.

Kuang, X.; Liu, J.; Scanlon, B. R. et al. The Changing Nature of Groundwater in the Global Water Cycle. *Science* **2024**, *383* (6686). https://doi.org/10.1126/science.adf0630.

Kumar, R.; Samaniego, L.; Attinger, S. Implications of Distributed Hydrologic Model Parameterization on Water Fluxes at Multiple Scales and Locations. *Water Resources Research* **2013**, *49* (1), 360–379. https://doi.org/10.1029/2012WR012195.

Landerer, F. W.; Flechtner, F. M.; Save, H. et al. Extending the Global Mass Change Data Record: GRACE Follow-On Instrument and Science Data Performance. *Geophysical Research Letters* **2020**, *47* (12), e2020GL088306. https://doi.org/10.1029/2020GL088306.

Leavesley, G.; David, O.; Garen, D. et al. A Modelling Framework for Improved Agricultural Water Supply Forecasting. In *AGU Fall Meeting Abstracts*, San Francisco, USA, 15–19 December 2008.

Lehner, B.; Verdin, K.; Jarvis, A. New Global Hydrography Derived from Spaceborne Elevation Data. *Eos, Transactions American Geophysical Union* **2008**, *89* (10), 93–94. https://doi.org/10.1029/2008EO100001.

Lehner, B.; Liermann, C. R.; Revenga, C. et al. High-Resolution Mapping of the World's Reservoirs and Dams for Sustainable River-Flow Management. *Frontiers in Ecology and the Environment* **2011**, *9* (9), 494–502. https://doi.org/10.1890/100125.

Luojus, K.; Moisander, M.; Pulliainen, J. et al. *ESA Snow Climate Change Initiative (Snow_cci): Snow Water Equivalent (SWE) Level 3C Daily Global Climate Research Data Package (CRDP) (1979–2020), version 2.0*; NERC EDS Centre for Environmental Data Analysis, 2022. https://doi.org/10.5285/4647cc9ad3c044439d6c643208d3c494.

Mudryk, L. R.; Chereque, A. E.; Derksen, C. et al. *Terrestrial Snow Cover: Arctic Report Card 2024*; Moon, T. A.; Druckenmiller, M. L.; Thoman, R. L., Eds.; NOAA Technical Report OAR ARC; 24-04; National Oceanic and Atmospheric Administration, 2024. https://doi.org/10.25923/4bb3-3f87.

Mudryk, L. R.; Elias Chereque, A.; Derksen, C. et al. Terrestrial Snow Cover [in "State of the Climate in 2024"]. *Bulletin of the American Meteorological Society* **2025**, *106* (8), S335–S338. https://doi.org/10.1175/BAMS-D-25-0104.1.

Müller Schmied, H.; Cáceres, D.; Eisner, S. et al. The Global Water Resources and Use Model WaterGAP v2.2d: Model Description and Evaluation. *Geoscientific Model Development* **2021**, *14* (2), 1037–1079. https://doi.org/10.5194/gmd-14-1037-2021.

Müller Schmied, H.; Trautmann, T.; Ackermann, S. et al. The Global Water Resources and Use Model WaterGAP v2.2e: Description and Evaluation of Modifications and New Features. *Geoscientific Model Development* **2024**, *17* (23), 8817–8852. https://doi.org/10.5194/gmd-17-8817-2024.

Muñoz Sabater, J. *ERA5-Land Hourly Data from 1950 to Present*; Copernicus Climate Change Service (C3S) Climate Data Store (CDS), 2019. https://doi.org/10.24381/cds.e2161bac.

Murray, A. M.; Jørgensen, G. H.; Godiksen, P. N. et al. DHI-GHM: Real-Time and Forecasted Hydrology for the Entire Planet. *Journal of Hydrology* **2023**, *620*, 129431. https://doi.org/10.1016/j.jhydrol.2023.129431.

National Aeronautics and Space Administration (NASA) Global Modeling and Assimilation Office (GMAO). *MERRA-2 tavg1_2d_lnd_Nx: 2d,1-Hourly, Time-Averaged, Single-Level, Assimilation, Land Surface Diagnostics V5.12.4*; GMAO, 2015. https://doi.org/10.5067/RKPHT8KC1Y1T.

Pessoa, G. S. Southern Brazil Hit by Worst Floods in Over 80 Years, Killing at Least 39 People. *Insurance* Journal, 6 May 2024. https://www.insurancejournal.com/news/international/2024/05/06/772932.htm.

Saemian, P.; Elmi, O.; Stroud, M. et al. Satellite Altimetry-Based Extension of Global-Scale in Situ River Discharge Measurements (SAEM). *Earth System Science Data* **2025**, *17* (5), 2063–2085. https://doi.org/10.5194/essd-17-2063-2025.

Samaniego, L.; Kaluza, M.; Kumar, R. et al. Mesoscale Hydrologic Model; *Zenodo*, **2019**. https://doi.org/10.5281/zenodo.3239055.

Samaniego, L.; Kumar, R.; Attinger, S. Multiscale Parameter Regionalization of a Grid-Based Hydrologic Model at the Mesoscale. *Water Resources Research* **2010**, *46* (5). https://doi.org/10.1029/2008WR007327.

Schaefer, G. L.; Cosh, M. H.; Jackson, T. J. The USDA Natural Resources Conservation Service Soil Climate Analysis Network (SCAN). *Journal of Atmospheric and Oceanic Technology* **2007**, *24* (12), 2073–2077. https://doi.org/10.1175/2007JTECHA930.1.

Schneider, U.; Becker, A.; Finger, P. et al. GPCC's New Land Surface Precipitation Climatology Based on Quality-Controlled in Situ Data and Its Role in Quantifying the Global Water Cycle. *Theoretical and Applied Climatology* **2014**, *115* (1), 15–40. https://doi.org/10.1007/s00704-013-0860-x.

Simoes-Sousa, I. T.; Camargo, C. M. L.; Tavora, J. et al. The May 2024 Flood Disaster in Southern Brazil: Causes, Impacts, and SWOT-Based Volume Estimation. *Geophysical Research Letters* **2025**, *52* (4), e2024GL112442. https://doi.org/10.1029/2024GL112442.

Sun, D.; Zhou, L.; Li, S. et al. Mapping and Analysis of the 2024 Brazil Record Flooding with Multi-Satellite Data. *Geomatics, Natural Hazards and Risk* **2025**, *16* (1), 2461063. https://doi.org/10.1080/19475705.2025.2461063.

Sutanudjaja, E. H.; van Beek, R.; Wanders, N. et al. PCR-GLOBWB 2: A 5 Arcmin Global Hydrological and Water Resources Model. *Geoscientific Model Development* **2018**, *11* (6), 2429–2453. https://doi.org/10.5194/gmd-11-2429-2018.

Tapley, B. D.; Watkins, M. M.; Flechtner, F. et al. Contributions of GRACE to Understanding Climate Change. *Nature Climate Change* **2019**, *9* (5), 358–369. https://doi.org/10.1038/s41558-019-0456-2.

United Nations Children's Fund (UNICEF). *Climate-related crisis in the Amazon region Flash Update No. 2*; UNICEF, 2025. https://www.unicef.org/media/165191/file/LACR-Flash-Update-11-November-2024.pdf.

van Verseveld, W. J.; Weerts, A. H.; Visser, M. et al. Wflow_sbm v0.7.3, a Spatially Distributed Hydrological Model: From Global Data to Local Applications. *Geoscientific Model Development* **2024**, *17* (8), 3199–3234. https://doi.org/10.5194/gmd-17-3199-2024.

Wimberly, F.; Ultee, L.; Schuster, L. et al. Inter-Model Differences in 21st Century Glacier Runoff for the World's Major River Basins. *The Cryosphere* **2025**, *19* (4), 1491–1511. https://doi.org/10.5194/tc-19-1491-2025.

World Glacier Monitoring Service (WGMS). *Global Glacier Change Bulletin No. 5 (2020–2021)*. Zemp, M.; Gärtner-Roer, I.; Nussbaumer, S. U. et al., Eds.; WGMS: Zurich, Switzerland, 2023, 134 pp. [publication based on database version: doi:10.5904/wgms-fog-2023-09]. https://wgms.ch/downloads/WGMS_GGCB_05.pdf.

World Meteorological Organization (WMO). *Global Climate 2024* (WMO-No. 1368); Geneva, 2025.

Yamazaki, D.; Kanae, S.; Kim, H. et al. A Physically Based Description of Floodplain Inundation Dynamics in a Global River Routing Model. *Water Resources Research* **2011**, *47* (4). https://doi.org/10.1029/2010WR009726.

Yuan, X.; Ji, P.; Wang, L. et al. High-Resolution Land Surface Modeling of Hydrological Changes Over the Sanjiangyuan Region in the Eastern Tibetan Plateau: 1. Model Development and Evaluation. *Journal of Advances in Modeling Earth Systems* **2018**, *10* (11), 2806–2828. https://doi.org/10.1029/2018MS001412.

Zemp, M.; Welty, E. Temporal Downscaling of Glaciological Mass Balance Using Seasonal Observations. *Journal of Glaciology* **2023**, 1–6. https://doi.org/10.1017/jog.2023.66.

Zhang, Y.; Kong, D.; Gan, R. et al. Coupled Estimation of 500 m and 8-Day Resolution Global Evapotranspiration and Gross Primary Production in 2002–2017. *Remote Sensing of Environment* **2019**, *222*, 165–182. https://doi.org/10.1016/j.rse.2018.12.031.

Ziese, M.; Schneider, U.; Meyer-Christoffer, A. et al. The GPCC Drought Index – a New, Combined and Gridded Global Drought Index. *Earth System Science Data* **2014**, *6* (2), 285–295. https://doi.org/10.5194/essd-6-285-2014.

Annex. Technical annex

METHODS

This annex provides high-level information on the main methodological steps applied to portray the state of global water resources in the year 2024.

For the 2024 State of Global Water Resources report, modelled data were based on 986 basins spanning the globe. The basin map was based on Hydrosheds level 4 data (Lehner et al., 2013). The original dataset contained about 1 300 basins. However, due to the resolution of global hydrological modelling systems (GHMSs), basins with a drainage area of less than 10 000 km^2 were removed in addition to some regions with modelling limitations (such as Greenland), leaving 986 basins (presented in Figure A1).

DATA SOURCES

Several sources of information on water resources were used to produce this report (refer also to the overview provided by Table A1); in particular:

- Precipitation provided by the Global Precipitation Climatology Centre (GPCC).
- Observed river discharge provided by National Meteorological and Hydrological Services (NMHSs), the Global Runoff Data Centre (GRDC) (see GRDC Data Portal), and enhanced streamflow observations using Earth system-based products (Elmi et al., 2024).
- Simulated river discharge data obtained from ten GHMSs for the selected hydrological basins. For more information on the models used, please refer to the section on Global hydrological modelling systems below.
- Inflow into selected reservoirs globally, obtained from Wflow_sbm (Verseveld et al., 2024), CaMa-Flood (Yamazaki et al., 2011) , Conjunctive Surface–Subsurface Process version 3 (CSSPv3) (Yuan et al., 2018) and World-Wide HYPE model (WWH) (Arheimer et al., 2020).
- Reservoir volume anomalies obtained from NASA, following the methodology described by Biswas et al. (2021).

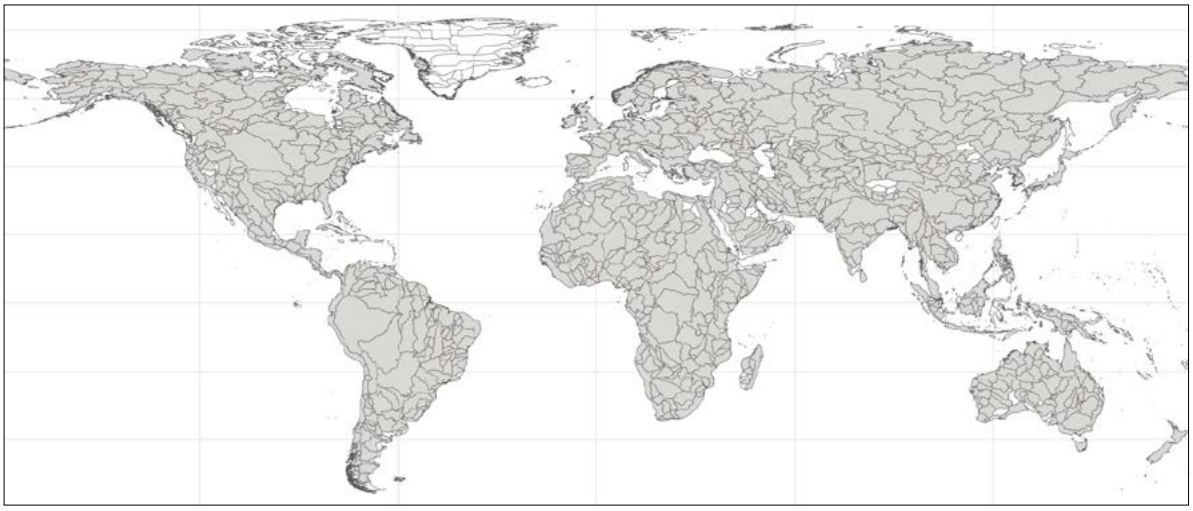

Figure A1. Global coverage of selected hydrological basins for modelled data

Note: The boundaries and names shown and the designations used do not imply official endorsement or acceptance by WMO or the United Nations.

Table A1. Data sources per chapter

Institution	*Model/product name*	*Key reference*	*Streamflow*	*Reservoirs*	*Soil moisture*	*Actual evapo-transpiration*	*Terrestrial water storage*	*Snow water equivalent*	*Lake level and temperature*	*Glaciers*	*Groundwater*	*Water quality*	*Precipitation*
Observed datasets													
NMHSs			■										
Global Runoff Data Centre (GRDC), Germany			■										
International Soil Moisture Network (ISMN), Germany	**Observed soil moisture**				■								
International Groundwater Resources Assessment Centre (IGRAC), Kingdom of the Netherlands	**Observed groundwater levels**										■		
European Space Agency, United Kingdom	**Lakes CCI project**								■				
GEMS/Water Data Centre, Germany												■	
Global Precipitation Climatology Centre (GPCC), Germany													■
World Glacier Monitoring Service (WGMS), Germany										■			

Institution	*Model/product name*	*Key reference*	*Streamflow*	*Reservoirs*	*Soil moisture*	*Actual evapo-transpiration*	*Terrestrial water storage*	*Snow water equivalent*	*Lake level and temperature*	*Glaciers*	*Groundwater*	*Water quality*	*Precipitation*
Models and Earth observation datasets													
Goethe University Frankfurt	**WaterGAP 2.2e**	Müller Schmied et al., 2021; Müller Schmied et al., 2023	■			■							
Institute of Atmospheric Physics, Chinese Academy of Sciences	**Conjunctive Surface–Subsurface Process version 3 (CSSPv3)**	Yuan et al., 2018	■	■	■	■	■	■					
Helmholtz Centre for Environmental Research – UFZ	**mesoscale Hydrologic Model (mHM)**	Kumar et al., 2013; Samaniego et al., 2010; Samaniego et al. 2019	■		■	■	■	■					
Swedish Meteorological and Hydrological Institute (SMHI)	**World-Wide HYPE (WWH) version 1.3.9**	Arheimer et al., 2020	■	■		■							
DHI	**DHI-GHM**	Murray et al., 2023	■										
University of Tokyo	**CaMa-Flood with Dam**	Hanazaki et al., 2022; Yamazaki et al., 2011	■	■									
European Commission Joint Research Centre (JRC)	**Global Flood Awareness System (GloFAS)**	Alfieri et al., 2013; Grimaldi et al., 2022	■										
European Centre for Medium-Range Weather Forecasts (ECMWF)	**ecLand: The ECMWF Land Surface Modelling System/GloFAS**	Boussetta et al., 2021	■										

Institution	*Model/product name*	*Key reference*	*Streamflow*	*Reservoirs*	*Soil moisture*	*Actual evapo-transpiration*	*Terrestrial water storage*	*Snow water equivalent*	*Lake level and temperature*	*Glaciers*	*Groundwater*	*Water quality*	*Precipitation*
Models and Earth observation datasets													
National Aeronautics and Space Administration (NASA)	**NASA-LISF-Noah MP**	Biswas et al., 2021			■								
Deltares	**Wflow_sbm**	Eilander et al., 2021; Imhoff et al., 2020; van der Laan et al., 2024; Verseveld et al., 2024	■	■		■							
Brigham Young University/ECMWF	**GEOGLOWS**	Hales et al., 2025	■										
Chinese Academy of Sciences, Institute of Geographic Sciences and Natural Resources Research	**HBV-PML**	Huang et al., 2022; Zhang et al., 2019	■			■	■						
Utrecht University	**PCR-GLOBWB 2**	Sutanudjaja et al., 2018	■										
GFZ Research Centre for Geosciences, Germany	**GRACE-based TWS**	Boergens et al., 2020; Landerer et al., 2020					■						
Environment and Climate Change Canada	**Crocus-ERA5**	Mudryk et al., 2024						■					
University of Stuttgart	**Remote Sensing-Based discharge (Extension of GRDC) (RSEG)**	Elmi et al., 2024	■										

- Lake levels and lake temperature provided by the European Space Agency (ESA) Lake CCI project.
- Groundwater data provided by the International Groundwater Resources Assessment Centre (IGRAC) for 47 selected countries
- Evaportanspiration data from six GHMSs.
- Soil moisture data from three GHMSs.
- Global terrestrial water storage (TWS) anomaly obtained from the Gravity Recovery and Climate Experiment (GRACE) project (Boergens et al., 2020; Landerer et al., 2020) globally.
- Glacier data from WMO Member States and Territories and the World Glacier Monitoring Service (WGMS).
- Snow water equivalent data from Environment and Climate Change Canada (Mudryk et al., 2024, 2025) and from two GHMSs: Today's Earth – Global (TEJRA55) (Ma et al., 2021; Yoshimura et al., 2008) and mesoscale Hydrologic Model (mHM) (Kumar et al., 2013; Samaniego et al., 2010, 2019).
- Water quality data provided by the Global Environment Monitoring System for Freshwater (GEMS/Water).
- Qualitative and quantitative information on high-impact events obtained from open data sources such as the EM-DAT database (CRED, 2025), ReliefWeb, WMO Climate Report and others.

VARIABLE RANKING (ANOMALY CALCULATION)

To provide a coherent picture across different datasets obtained, a consistent method of variable ranking was applied to the variables listed in the previous section: river discharge, inflow into reservoirs, groundwater level, soil moisture, evapotranspiration and TWS. Annual averages were calculated for each year for modelled and observed datasets over the given reference period. The resulting array was ranked. The annual average of the given variable for the year 2024 was then compared to this ranked array and classified according to the following rule:

much below normal:	$Q_{2024} \leq$ 10th percentile (exceptionally dry)
below normal:	10th $< Q_{2024} <$ 25th percentile
normal:	25th $\leq Q_{2024} \leq$ 75th percentile
above normal:	75th $< Q_{2024} <$ 90th percentile
much above normal:	$Q_{2024} \geq$ 90th percentile (exceptionally wet)

The historical reference period varied according to the variable in question, constrained by the data availability. Refer to Table A2 for selected historical reference periods and to dataset-specific chapters of the main report for more details.

For the modelled data, where several data sources (ensembles of models) have been used (specifically, for data from GHMSs on inflow into and storage in the reservoirs), the averaging of the variable ranking results was done at the basin level. For each model in the ensemble, the above-specified rankings were assigned an integer ("much below normal" = 1, "below normal" = 2, "normal" = 3, "above normal" = 4, "much above normal" = 5), and then an average was calculated across the outputs of the ensemble of models for each of the basins. The resulting number was rounded, and the average discharge ranking was derived for each basin, according to the thresholds listed above.

Table A2. Historical reference periods of selected datasets

Dataset	*Selected historical reference period*	*Length of historical reference period*
Precipitation	1991–2020	30 years
Simulated river discharge from GHMSs	1991–2020*	30 years
Observed river discharge from GRDC and NHMSs	<2001–2020	Varying between 20 to 30 years
Inflow into reservoirs	1991–2020	30 years
Reservoir storage	2000–2023	24 years
Lake level	1995–2020	26 years
Lake temperature	1995–2020	26 years
Groundwater level	2005–2024	20 years[a]
Evapotranspiration	1991–2020	30 years
Soil moisture modelled	1991–2020	30 years
Soil moisture observed	2009–2023	15 years
Snow water equivalent	1991–2020	30 years
Glaciers	1976–2024	49 years
Terrestrial water storage	2002–2020	19 years
Water quality	2012–2023	12 years

[a] Ten years for Brazil, Costa Rica, Iraq, Kenya and State of Palestine.

GLOBAL HYDROLOGICAL MODELLING SYSTEMS

The 2024 report uses GHMSs sourced from the modelling community. Despite improved availability, observed discharge data were not sufficient to ensure a comprehensive global overview, requiring the need for an alternative source for discharge data. The simulated discharge produced by multiple GHMSs was analysed using the subbasin map obtained after processing the level 4 Hydrosheds dataset (Figure A1).

In total, 12 GHMSs took part in the modelling exercise (in alphabetical order):

- CaMa-Flood with Dam (Hanazaki et al., 2022; Yamazaki et al., 2011)
- Conjunctive Surface–Subsurface Process version 3 (CSSPv3) (Yuan et al., 2018)
- DHI-GHM (Murray et al., 2023)
- ecLand (Boussetta et al., 2021)
- Global Flood Awareness System (GloFAS) (Alfieri et al., 2013; Grimaldi et al., 2023)
- HBV-PML (Huang et al., 2022; Zhang et al., 2019)
- mesoscale Hydrologic Model (mHM) (Kumar et al., 2013; Samaniego et al., 2010, 2019)
- PCR-GLOBWB 2 (Sutanudjaja et al., 2018)
- River Forecast System (GEOGLOWS) (Hales et al., 2025)
- WaterGAP 2.2e (Müller Schmied et al., 2021, 2024)
- World-Wide HYPE v1.3.9 (Arheimer et al., 2020)
- Wflow_sbm (Eilander et al., 2021; Imhoff et al., 2020; Verseveld et al., 2024)

The global hydrological modelling community was asked to provide historical simulations for the chosen 986 basins for the years 1991–2020 and the target year of 2024, using meteorological input data of their choice. Before submitting the outputs, the modelling teams were required to complete a modelling "fact sheet" to provide key information about the model, technical details and input data sources. An ensemble of models was used to address potential uncertainties in the simulations. The 2024 data were ranked for the simulated discharge and other variables (refer to Table A1) from each model for each basin, then averaged across all models for each basin (refer to the Variable ranking (anomaly calculation) section for more details). GHMS simulations are subject to uncertainties, largely due to three factors: uneven data coverage and quality across regions and variables, insufficient measurement of human impacts on the water cycle, and difficulties in adapting processes to diverse regional hydrological systems (Reinecke et al., 2025).

Table A3 shows a technical breakdown of the various global hydrological modelling systems, and the Validation of modelled results section summarizes the models' spatial coverage and provides a graphical representation of trends simulated by each model for each basin. Regarding climate forcing, all GHMSs used ERA5 reanalysis data (Hersbach et al., 2020), except for the HBV-PML, World-Wide HYPE v1.3.9 and TEJRA55 models, which were driven by the Multi-source Weighted-ensemble Precipitation (MSWEP) (Beck et al., 2019), HydroGFD (Berg et al., 2021) and JRA-55 datasets (Kobayashi, 2015), respectively.

Table A3. Characteristics of global hydrological modelling systems used in the report

Model name	*Institution*	*Spatial coverage*	*Spatial model resolution*	*Climate data product used*
WaterGAP 2.2e	Goethe University Frankfurt	Global	0.5° × 0.5°	GSWP3-ERA5
Conjunctive Surface–Subsurface Process version 3 (CSSPv3)	Institute of Atmospheric Physics, Chinese Academy of Sciences	Global	0.25°	ERA5, with precipitation replaced by MSWEPv2
mesoscale Hydrologic Model (mHM)	Helmholtz Centre for Environmental Research – UFZ	Two set-ups available: (1) global and (2) individually delineated and calibrated GRDC basins	Last version was based on the 0.25° resolution	ERA5
World-Wide HYPE (WWH) version 1.3.9	Swedish Meteorological and Hydrological Institute (SMHI)	All continents except Antarctica	On average 1 000 km^2	HydroGFD
DHI-GHM	DHI	The model covers land surface of the globe between 60°S and 80°N	0.1° × 0.1°	ERA5
CaMa-Flood with Dam	University of Tokyo	60°S–90N°, 180°W–180°E (without Greenland)	0.25° lat./lon. deg.	ERA5-land runoff
Global Flood Awareness System (GloFAS)	European Commission Joint Research Centre (JRC)	Global except for Antarctica (60°S–90°N, 180°W–180°E)	0.05° (~5 km, gridded)	ERA5
River Forecast System	GEOGLOWS	Global	Irregular grid, ~150 km^2	ERA5
Wflow_sbm	Deltares	Global	30 arcsec (0.0083° ~ 1 km)	ERA5, with precipitation replaced by MSWEPv2
ecLand	European Centre for Medium-Range Weather Forecasts (ECMWF)	Global	6 arcmin (~10 km)	ERA5
HBV-PML	Chinese Academy of Sciences, Institute of Geographic Sciences and Natural Resources Research	Global	0.1° × 0.1°	MSWEP
PCR-GLOBWB 2	Utrecht University	Global	5 arcmin (10 km at the equator)	ERA5

PRECIPITATION

The Global Precipitation Climatology Centre (GPCC) provides global precipitation analyses to support climate monitoring and research. It represents a German contribution to the World Climate Research Programme (WCRP) and the Global Climate Observing System (GCOS). GPCC provides a gridded (1° resolution) monthly precipitation dataset available from 1891 to present that is produced from quality-controlled, global station data.

Figure A2 shows anomalies in extreme precipitation, defined as the percentage proportion of annual precipitation in 2024 that exceeded the 95th percentile threshold calculated over the reference period 1991–2020. Areas with annual precipitation below 300 mm were masked and displayed in white, as anomalies over such low baseline values can result in exaggerated and potentially misleading signals. This is because in arid regions, precipitation typically occurs on only a few days per year, and even moderate rainfall events can exceed high percentiles. In 2024, notable areas where precipitation exceeded the 95th percentile threshold include parts of Australia and regions of India near the border with Pakistan.

DROUGHT INDEX

The GPCC Drought Index (GPCC-DI) (Ziese et al., 2014) is a combination of two drought indices – the Standardized Precipitation Index (SPI) and the Standardized Precipitation Evapotranspiration Index (SPEI) – and uses temperature and precipitation for the calculation of drought conditions. The combination of the two indices allows for an improved assessment of drought conditions at the global scale. Indeed, the SPEI performs better in dry, warm regions, whereas the SPI cannot be applied in such regions, while the SPI is applicable in cold regions, where calculation of evapotranspiration is problematic. Still, dry and cold regions like the Tibetan Plateau and southern Andes cannot be covered by either index and are, therefore, left blank. The combined index is calculated on a regular grid with 1° spatial resolution.

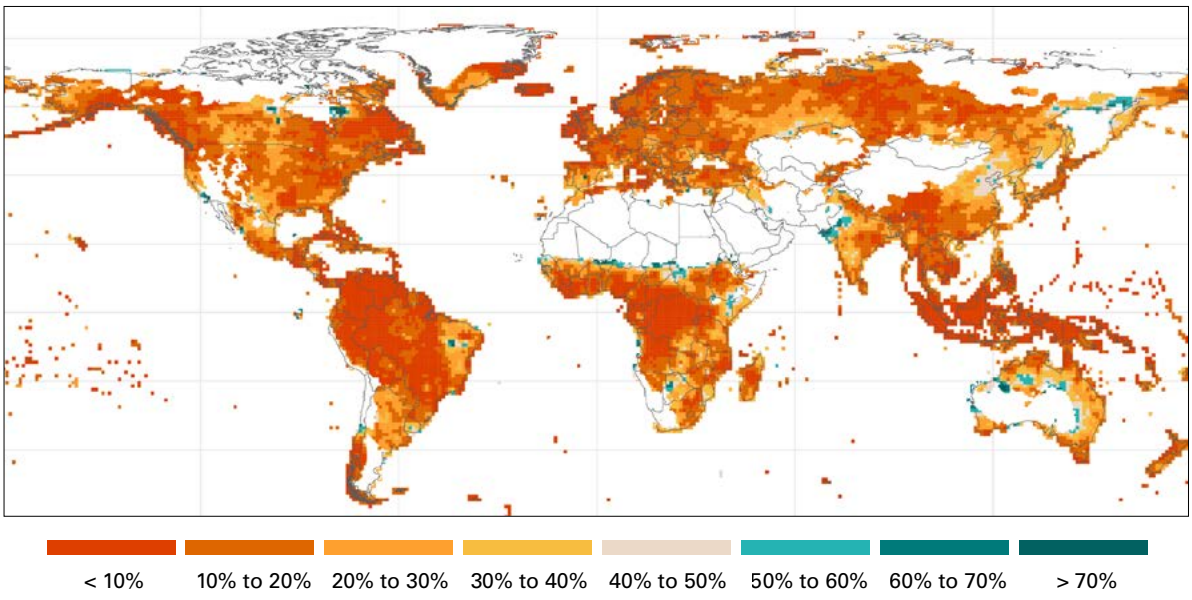

Figure A2. Percentage of the precipitation in 2024 that was above the annual 95th percentile for the historical period 1991–2020.

Note: The boundaries and names shown and the designations used do not imply official endorsement or acceptance by WMO or the United Nations.

RIVER DISCHARGE

OBSERVED DATA AND VALIDATION OF MODELLED RESULTS

Discharge data availability in GRDC and from NHMS for the year 2024

Observed discharge data were obtained from GRDC (see GRDC Data Portal) and received from the NMHSs. Two selection criteria were adjusted from last year to increase the potential volume of observed data: the number of missing values among the data points within the historical reference period had to be 10% or less, and for 2024 the data had to at least cover the 2024 hydrological year (until 31 October 2024). Similarly to last year, datasets not yet subjected to quality checks were included (in 2024, these included data from the United Kingdom (UK), Slovakia and Luxembourg). NMHSs were also able to supply calculated anomalies.

Observational data were collected from 2777 stations for the year 2024 from the GRDC database and NHMSs. Additionally, data from 473 stations were sourced from the Earth system-based in-filled remote-sensing-based discharge product (Elmi and Tourian, 2023; Tourian et al., 2022). The rationale for using remote-sensing-based methods to infill data is as follows: The number of active GRDC river gauge stations has declined since the 1980s. However, the rise of remote sensing technologies offered possibilities to estimate river discharge from space. Developing a mapping function between satellite-based river width/height and historical gauge data is among the most straightforward solutions to estimate discharge from space. Building on this idea, Elmi et al. (2024) and Saemian et al. (2025) developed the remote-sensing-based extension of the GRDC discharge records.

The total pool of 3 250 stations was used for evaluating the 2024 discharge anomaly. A subset of 278 stations was identified for validating the GHMS results, based on their proximity to the chosen HydroBASIN outlet, ensuring a closer match between the observed and modelled data. Given the spatial resolution of HydroBASINS outlets in the UK, an aggregated national UK outflow series was used (Marsh et al., 2015).

Figure A3 presents the location of 3250 gauges for which data were received from the GRDC database, NHMSs and the Remote Sensing-based discharge dataset, which were used for

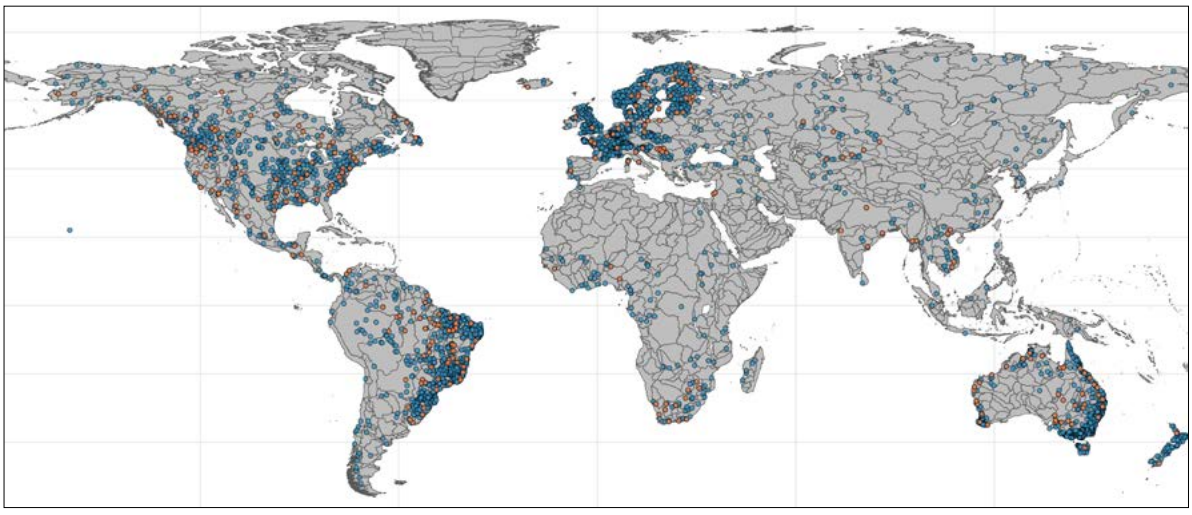

Figure A3. Location of gauges in the GRDC database, in the Remote Sensing-based Extension of GRDC (RSEG), and received from NHMSs (green points) in 2024; gauges selected to validate GHMSs (red points) and Hydrobasins

Note: The boundaries and names shown and the designations used do not imply official endorsement or acceptance by WMO or the United Nations.

discharge anomaly analysis for the year 2024 (green dots). The figure also shows gauges selected for validation of modelling results (red dots), including respective Hydrobasins where those were located. Note that the ranking of the streamflow for 2024 estimated from the ensemble of GHMSs might differ from the results obtained from the observed streamflow data, depending on the catchment area of the observed data and model performance. Therefore, WMO emphasizes the importance of the availability of local in situ data to support water resource management and the production of hydrological status products at the regional, national and basin scale as well as for producing accurate global products such as the assessments presented in this report.

VALIDATION OF MODELLED RESULTS

The discharge ranking obtained from the GHMS simulations was validated with the discharge ranking obtained from the observed data available. Annual averages of flow observations from 2024 were ranked against the hydrological normals (obtained from at least 20 years of flow observations) at each HydroBasin basin (where observed flow data were available). The discharge rankings from simulated and observed data for the year 2024 were classified by the sign of change with respect to the historical reference period (that is, "below", "above" or "normal") and then compared to each other. Note that in large basins, where some of the downstream units (according to the HydroBasins basin classification) import a considerable amount of water resources from the upstream catchments, the comparison/validations between results from modelled data and observations for only one gauge per WMO basin might lead to inaccurate results. Therefore, observations from intermediary gauges or redefining of the catchment areas must be considered in the future to minimize uncertainties in the results.

Figure A4 shows model agreement on the state of the annual river discharge with respect to the ensemble mean (above, below, normal – that is, no change) among GHMSs for each

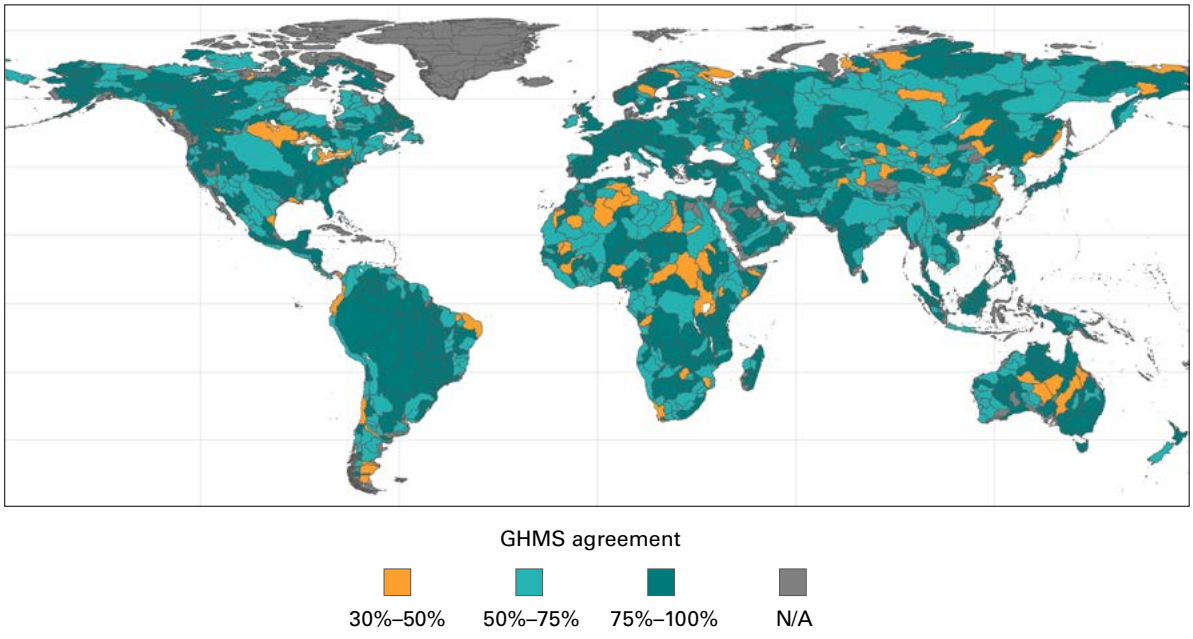

Figure A4. Share of GHMSs agreeing on the annual river discharge with respect to mean (above, below, normal) for each basin

Note: The boundaries and names shown and the designations used do not imply official endorsement or acceptance by WMO or the United Nations.

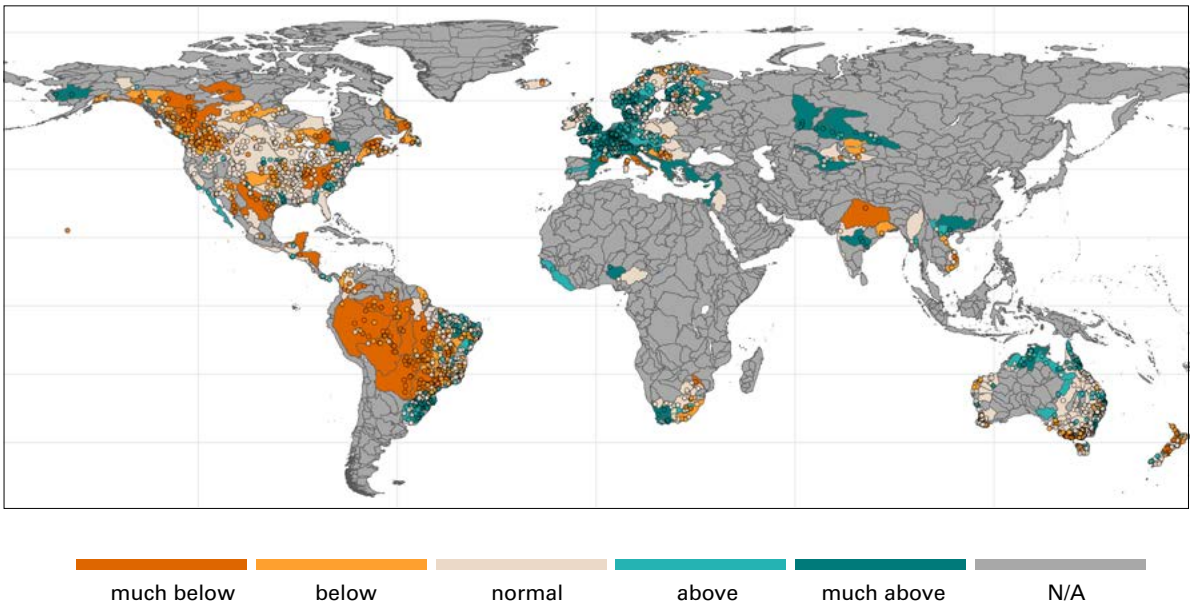

Figure A5. River discharge in 2024 as ranked with respect to the historic period 1991–2020. The results presented here were derived from the observed discharge data, which were obtained from NMHSs and the GRDC database (coloured basins + dots for gauge locations). Dots represent the location of observed gauges for which data were received. Grey areas indicate areas where discharge data were not available from NMHSs or GRDC for 2024.

Note: The boundaries and names shown and the designations used do not imply official endorsement or acceptance by WMO or the United Nations.

basin. The results show that more than 50% of GHMSs agree on the sign of trends for 98% of the area globally. The agreement for Australia, South America, East Africa (Nile basin, the Greater Horn of Africa), Northern Europe and other regions lies between 75% and 100% of the ensemble, while the agreement is lower (25%–50%) in West and North Africa and in some North American basins, Central Asia and China, as well as some parts of Australia.

Figure A5 presents river discharge anomalies for 2024 ranked against the historical period 1991–2020, using all gauges for which data were received from National Meteorological and Hydrological Services (NMHSs) and the Global Runoff Data Centre (GRDC). Coloured basins show the anomaly classes simulated by GHMSs, while dots mark the locations of the observational gauges, with their colour indicating the observed anomaly for 2024. Grey areas denote regions without available discharge data from NMHSs or GRDC in 2024. Figure A6 shows the validation of simulated discharge trends against observations for 2024 for selected gauges. Instead of the standard five classes, for validation purposes results are compared using three aggregated labels – normal, above-normal, and below-normal conditions, which included much-above- and much-below-normal, respectively. Areas where the simulated and observed classifications disagreed in the direction of change (for example, one indicating above-normal and the other below-normal discharge) are highlighted with diagonal hatching.

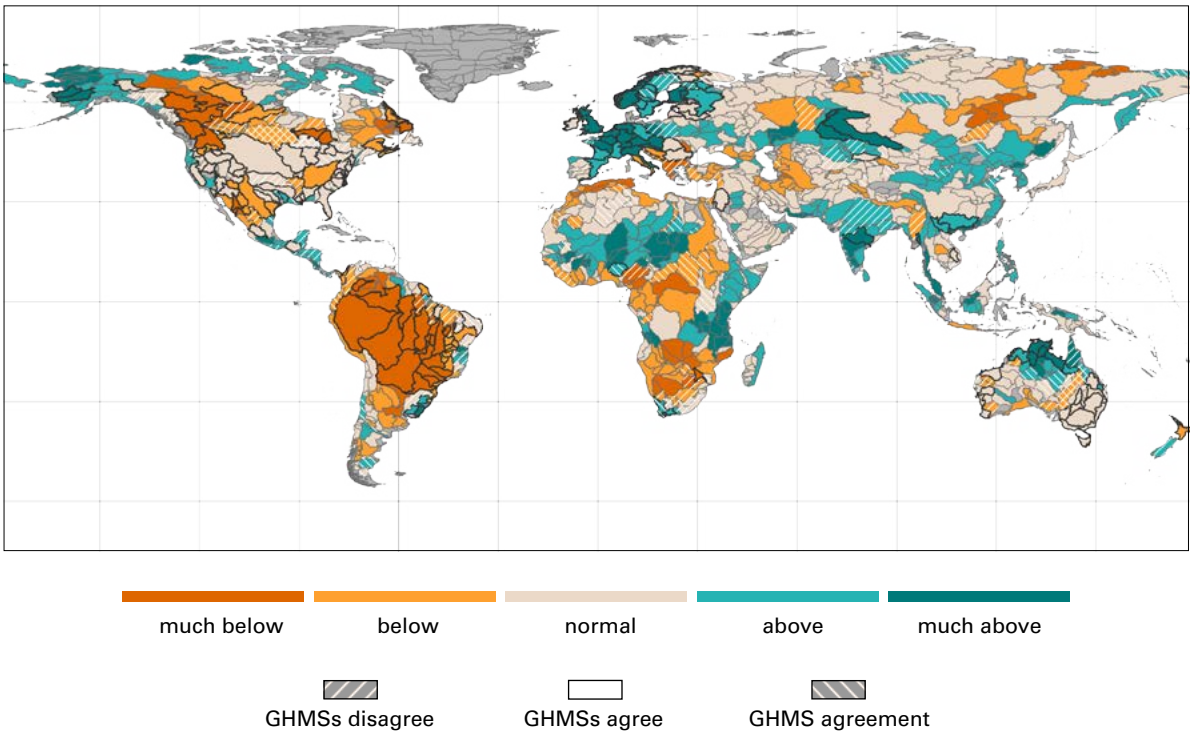

Figure A6. Validation of modelled discharge from GHMSs for the year 2024. Basins where simulated and observed data agree on the hydrological condition are indicated by a black bold outline. Areas where GHMSs disagree with each other are marked with left slanting hashing, and areas where GHMSs disagree with observations are marked with right slanting hashing. Basins where GHMS agreement is below 50% and the multi-model mean disagrees with observations are indicated by both patterns overlapping (cross-hatching).

Note: The boundaries and names shown and the designations used do not imply official endorsement or acceptance by WMO or the United Nations.

The validation of modelled results showed agreement between observed and simulated anomalies for the year 2024 in Australia, across North America (except for Nelson River basin), across South America (excluding smaller catchments along the coast of Brazil), and across Europe (excluding smaller catchments in Eastern Europe and parts of northern Sweden and Finland). As in 2023, results also disagree with observations in the southern part of Europe (for example, Greece and Albania), across Africa and in northern India. In general, GHMS simulations align with observations in >64% of the basins with available observational data.

In some areas, there was a mismatch (for example, the UK and Ireland) between the resolution of the models (catchments above 10 000 km^2 were selected for the analysis) and the observed datasets. The provision of a "national outflow" data series for the UK allowed for a simple validation of these model results, though this case underlines the importance of scale in small countries, and the need for better spatial representation of relevant catchments.

Figure A7 shows simulated discharge rankings for the year 2024 for each basin by each of the GHMSs grouped by region.

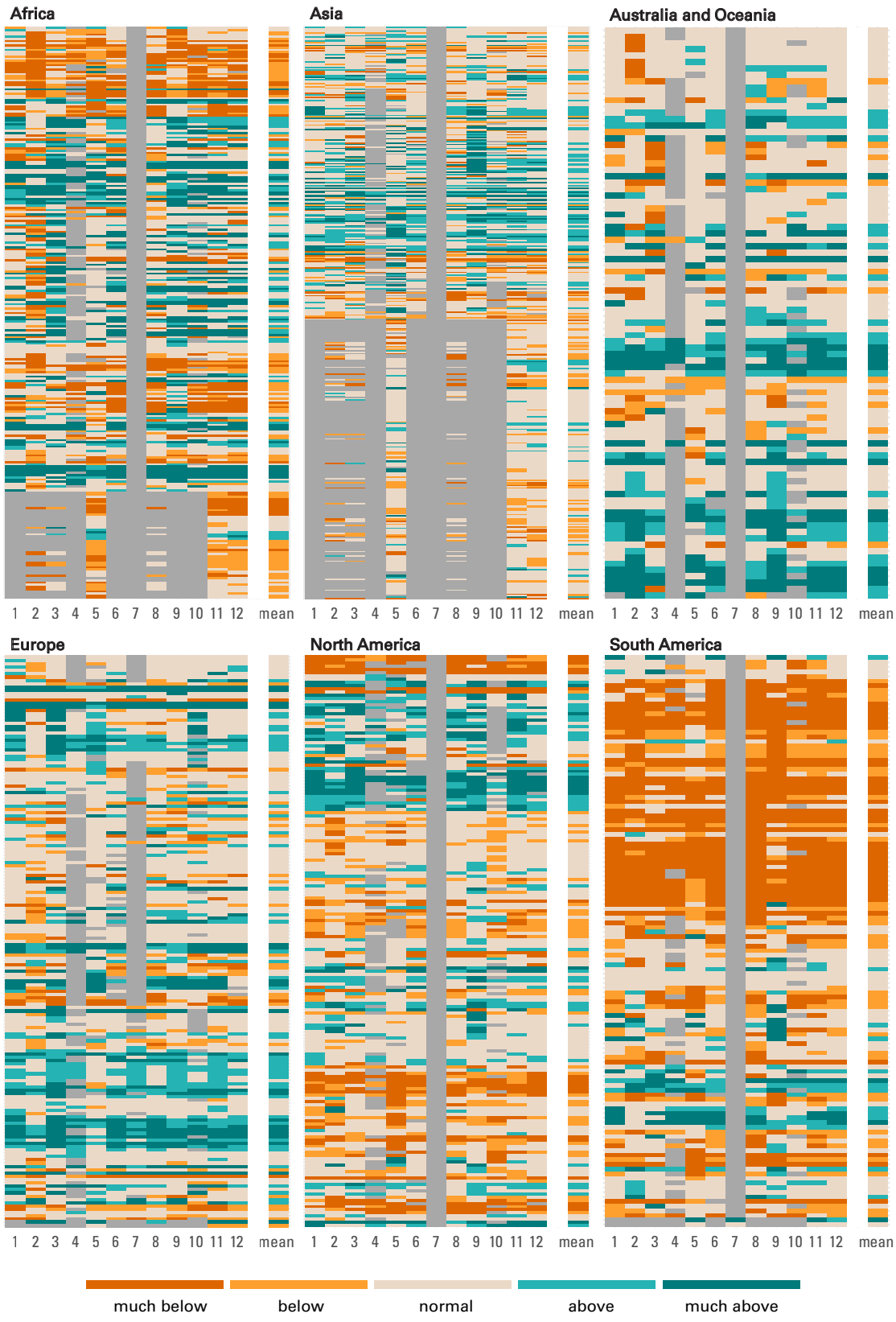

Figure A7. Simulated discharge rankings for the year 2024 for each basin by each of the GHMs grouped by region.

Note: 1 – WaterGAP 2.2e, 2 – CSSPv3, 3 – DHI-GHM, 4 – mHM, 5 – WWHv1310, 6 – CaMa-Flood, 7 – Wflow_sbm, 8 – PCRGLOBWB, 9 – HBV-PML, 10 – GEOGLOWS, 11 – GloFAS, 12 – ecLand. Grey indicates no data values for a specific basin.

RESERVOIRS

INFLOW INTO SELECTED RESERVOIRS

The modelled results for the inflow into 926 reservoirs globally were obtained from four main sources: Wflow_sbm (Verseveld et al., 2024), CaMa-Flood with Dam (Hanazaki et al., 2022; Yamazaki et al., 2011), the WWH model (Arheimer et al., 2020) and CSSPv3 (Yuan et al., 2018). The reservoirs were selected based on overlap between those three sources, based on their GRanD ID (Lehner et al. 2023). Daily inflow into selected GRanD reservoirs was provided from 1991 to 2023.

Wflow_sbm (Imhoff et al., 2024; van Verseveld et al., 2024): Daily inflow and reservoir volumes were derived for the period 1991–2023 for the selected GRanD reservoirs. Simulations were conducted at 1/120° (~1 km) and were forced with downscaled ERA5 reanalysis for total precipitation, 2 m temperature and potential evaporation using de Bruin et al. (2016) formulation. The set-up of the Wflow_sbm models (using hydromt 0.10.0 and hydromt_wflow 0.6.1) was similar to that used by van der Laan et al. (2024), who validated reservoir simulations against Earth observed surface water area and in-situ measured reservoir volume. For the anisotropy factor for lateral hydraulic conductivity we used the random forest global results from Ali et al. (2025). The simulations (using wflow.jl 0.8.1) were carried out on an onsite linux cluster using a snakemake workflow.

CaMa Flood with Dam: CaMa-Flood model (Yamazaki et al., 2011) along with the Dam operational scheme by Hanazaki et al. (2022) was implemented to conduct global simulations. The model can simulate river flows encompassing 2 169 global dams and reservoirs with a drainage area of at capacity and drainage area) in the model is based on GRanD (Lehner et al., 2011). The model configuration, done by Hanazaki et al. (2022 least 1 000 km^2. The information for each reservoir (such as the dam's name, coordinates, storage), enables global simulations at a spatial resolution of 0.25° using MERIT Hydro (Yamazaki et al., 2019) as a baseline topography. The same model configuration settings, utilizing ERA5-Land reanalysis data (Muñoz Sabater, 2019) from 1991 to 2024 as a runoff forcing, have been used for the current global simulations. The temporal resolution of the Model is 1 hour. However, keeping in view the reporting requirements, the outputs have been prepared at 24-hour intervals.

Calibration of the model with the Dam operational scheme is unavailable. However, Hanazaki et al., 2022 conducted model validation based on simulations spanning 2001 to 2019. Validation for the model is accessible for the daily streamflow discharge of 687 gauges (located downstream of dams) from GRDC and other institutions worldwide. The accuracy of discharge hydrographs compared to observations was evaluated by calculating Nash–Sutcliffe efficiency (NSE) (Nash and Sutcliffe, 1970) and peak discharge error (PDE) (Hanazaki et al., 2022). In addition to the 687 global gauges, validation is also available for inflow, outflow and storage of the Seminoe and Trinity reservoirs using in-situ observation data.

World-Wide HYPE v1.3.9: Daily inflow to GRanD reservoirs and daily reservoir volume have been delivered for the period of 1991–2023. The World-Wide HYPE model was calibrated in a stepwise manner using 2 475 discharge gauges and evaluated against an additional 2 863 independent discharge gauges (Arheimer et al., 2020). The model includes around 13 000 lakes and 2 500 reservoirs. These are described in a general fashion based on information from the GRanD database. Except for a handful of places, the operating routines of the reservoirs have not yet been calibrated in WWH.

Conjunctive Surface–Subsurface Process version 3 (CSSPv3) (Yuan et al., 2018): In CSSPv3, reservoir outflow is calculated based on current inflow, long-term average inflow and storage. The model further considers multiple beneficial functions such as hydropower, flood control and irrigation water supply.

RESERVOIR STORAGE

Reservoir storage anomalies were prepared in line with the methodology described by Biswas et al. (2021). A total number of 50 068 reservoirs were selected worldwide from different dam datasets (Donchyts et al., 2022; Lehner et al., 2011; Lehner and Döll, P., 2004; Messager et al., 2016; Wang et al., 2022). For each of the selected reservoirs, the area-elevation curve was generated using the SRTM elevation dataset following the methodology described in the Global Reservoir Assessment Tool (Biswas et al., 2021). From the area-elevation curve, the accumulated storage for each elevation band was calculated using Equation 1 to form a complete area-elevation-storage curve for individual reservoirs. Secondly, water extent area time series for each of the reservoirs were extracted using the application programming interface (API) and the Global Water Watch (GWW) (Donchyts et al., 2022) time-series data.

$$S_{i+1} = \frac{A_i + A_{i+1}}{2} \cdot (h_{i+1} - h_i) + S_i \quad \text{for } i = 0 \text{ to } n-1 \tag{1}$$

where S is the reservoir's storage, A is the reservoir's area and h indicates the reservoir's water elevation.

The water extent area time series were prepared from multiple satellites (Landsat series, Sentinel 2). The surface water extent time series data were then converted into monthly median time series spanning from 2000 to 2023. From the surface water extent area time series of the individual reservoir, monthly storage was calculated using the area-elevation-storage curve (shown in Figure A8). The reservoirs were filtered first to include only those in the GrandID database and then to include only those above a volume threshold of 100 million m^3.

The annual mean of monthly storage values for selected reservoirs for the reference period (2000–2023) of modelled data was calculated for each year and then ranked according to the rule described in the Data sources and Variable ranking (anomaly calculation) sections.

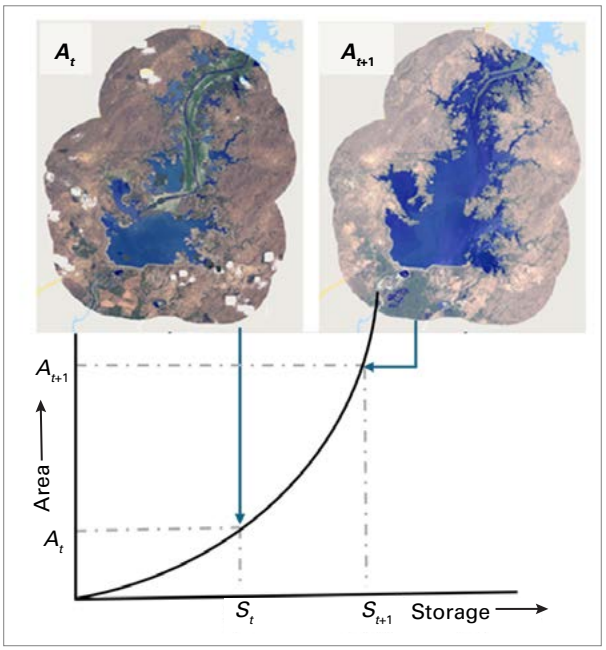

Figure A8. Surface water extent at timestamp t and $t+1$, and the area-elevation-storage curve used for calculation of monthly storage

GROUNDWATER

The methodology used to report on groundwater levels was developed and consolidated in 2023 (*State of Global Water Resources 2023* (WMO-No. 1362). It is described in a methodology report, which is available for downloading following the following link: https://un-igrac.org/data/resources/state-of-global-water-resources-2025-quantitative-status-of-groundwater-methodology-report/.

Groundwater level monitoring data were collected from 47 countries. The data were downloaded from the websites of the institutions in charge of groundwater monitoring, where available; otherwise the data were directly requested from the countries. Table A4 indicates how the data were collected for each country. Where data are open or we have permission to share the raw data, they are made available for downloading on the Global Groundwater Monitoring Network (GGMN) platform. Data from Taiwan, province of China were downloaded from https://opendata.wra.gov.tw/ListOpenDataView.

Table A4. Groundwater data sources per country

#	Country		Data source	Link
1	Australia		Requested	Bureau of Meteorology (BOM)
2	Austria*		Downloaded	https://ehyd.gv.at/#
3	Belgium	Brussels	Downloaded	https://geodata.environnement.brussels/client/bruwater/index
		Wallonia	Downloaded	https://piezometrie.wallonie.be/home.html
		Flanders	Downloaded	https://www.dov.vlaanderen.be/portaal/
4	Brazil		Requested	Geological Survey of Brazil (SGB)
5	Canada		Requested	Natural Resources Canada (NRCan/RNCan)
6	Chile		Requested	General Directorate of Water (DGA)
7	Costa Rica		Requested	Ministry of Environment and Energy – Department of Water Development
8	Croatia		Requested	Hrvatske vode (Croatian water)
9	Cuba		Requested	National Institute of Hydraulic Resources (INRH)
10	Czech Republic		Requested	Czech Hydrometeorological Institute
11	Denmark		Downloaded	https://data.geus.dk/JupiterWWW/
12	El Salvador		Requested	Ministry of Environment
13	Estonia		Requested	Geologic Survey of Estonia
14	Finland		Requested	Finnish Environment Institute (SYKE)
15	France*		Downloaded	https://ades.eaufrance.fr/
16	Germany§		Downloaded	https://gruvo.bgr.de/website/fss
17	Hungary		Requested	Hungarian Hydrological Forecasting Service

#	Country	Data source	Link
18	India	Requested	India Water Resources Information System (WIRIS)
19	Iraq	Requested	Ministry of Water Resources – General Commission for Groundwater
20	Ireland*	Downloaded	https://www.epa.ie/
21	Israel	Requested	Hydrological Service
22	Jamaica	Requested	Water Resources Authority
23	Jordan	Requested	Ministry of Water and Irrigation
24	Kenya	Requested	Water Resources Authority (WRA)
25	Latvia	Downloaded	https://videscentrs.lvgmc.lv/noverojumu-arhivs/pazemes/
26	Lithuania	Requested	Lithuanian Geological Survey
27	Luxembourg	Requested	Water Management Administration
28	Mexico	Requested	National Water Commission (CONAGUA)
29	Namibia	Requested	Ministry of Agriculture, Fisheries, Water and Land Reform – Department of Water Affairs – Geohydrology Division
30	Kingdom of the Netherlands	Downloaded	https://service.pdok.nl/bzk/bro-gminsamenhang-karakteristieken/atom/bro_grondwatermonitoring_gm_in_samenhang_karakteristieken.xml
31	New Zealand	Requested	GNS Science
32	Norway*	Downloaded	https://www.nve.no/english/
33	Palestine	Requested	Palestinian Water Authority (PWA)
34	Poland	Downloaded	https://www.pgi.gov.pl/psh/materialy-informacyjne-psh/
35	Portugal	Downloaded	https://snirh.apambiente.pt/
36	Slovakia	Requested	Slovak Hydrometeorological Institute
37	Slovenia	Requested	Slovenian Environment Agency - Meteorology, Hydrology and Oceanography Office - Hydrological Analysis and Modelling Division
38	South Africa	Requested	Department of Water and Sanitation (DWS)
39	South Korea	Requested	Ministry of Environment – K-water
40	Spain	Requested	Ministry for the Ecological Transition and the Demographic Challenge (MITECO)
41	Sweden*	Downloaded	https://www.sgu.se/grundvatten/grundvattennivaer/matstationer/
42	Switzerland	Requested	Swiss Federal Office for the Environment (FOEN)

#	Country	Data source	Link
43	Thailand	Requested	Department of Groundwater Resources (DGR)
44	UK	Requested	British Geological Survey (BGS)
45	United States*	Downloaded	https://cida.usgs.gov/ngwmn/index.jsp
46	Vietnam	Requested	Ministry of Natural Resources and Environment – National Center for Water Resources Planning and Investigation (NAWAPI)

* Groundwater level database is connected to Global Groundwater Monitoring Network (GGMN) – IGRAC through an API.

§ The website identifies reference monitoring stations in the country and provides the links to the states' websites where the data can be downloaded.

The data selection procedure (as described in the methodology report) works with a threshold, to specify the minimum number of years for which at least one specific month has data available across all the selected years. The threshold was set by default to 80%, which means that the time series that are selected have data for at least 16 years out of 20. However, in the case of Namibia and Iraq, the threshold was lowered to 60% to accommodate for the data gaps.

VISUALIZATION OF RESULTS

The analysis results for groundwater levels are mapped at both monitoring-station and grid levels (0.5° grid cells). For the grid-level visualization, the rankings of groundwater levels in individual wells were averaged within each corresponding grid cell, after which each grid cell was categorized based on the same classification scheme. While the grid-level maps are included in the main report, the station-level maps are presented below to provide additional details.

Regarding the station-level mapping, several boreholes are located at the same site to monitor different aquifers at various depths. To provide a clear representation of overlapping boreholes, a geographical information system (GIS) tool called "displacement tool" was used. This tool slightly offsets overlapping points, positioning them next to each other, as shown in Figure A9. In the first example in the figure, three different boreholes are at the same location; the average groundwater level in 2024 is "normal" in two of them and "above normal" in the third one. In the second example, two boreholes are at the same location; the average groundwater level in 2024 is "below normal" in both of them.

Figure A9. Representation of overlapping boreholes

MAPS AT GROUNDWATER STATION LEVEL

The maps in Figure A10 show point (station wise) data for groundwater collected from 47 countries.

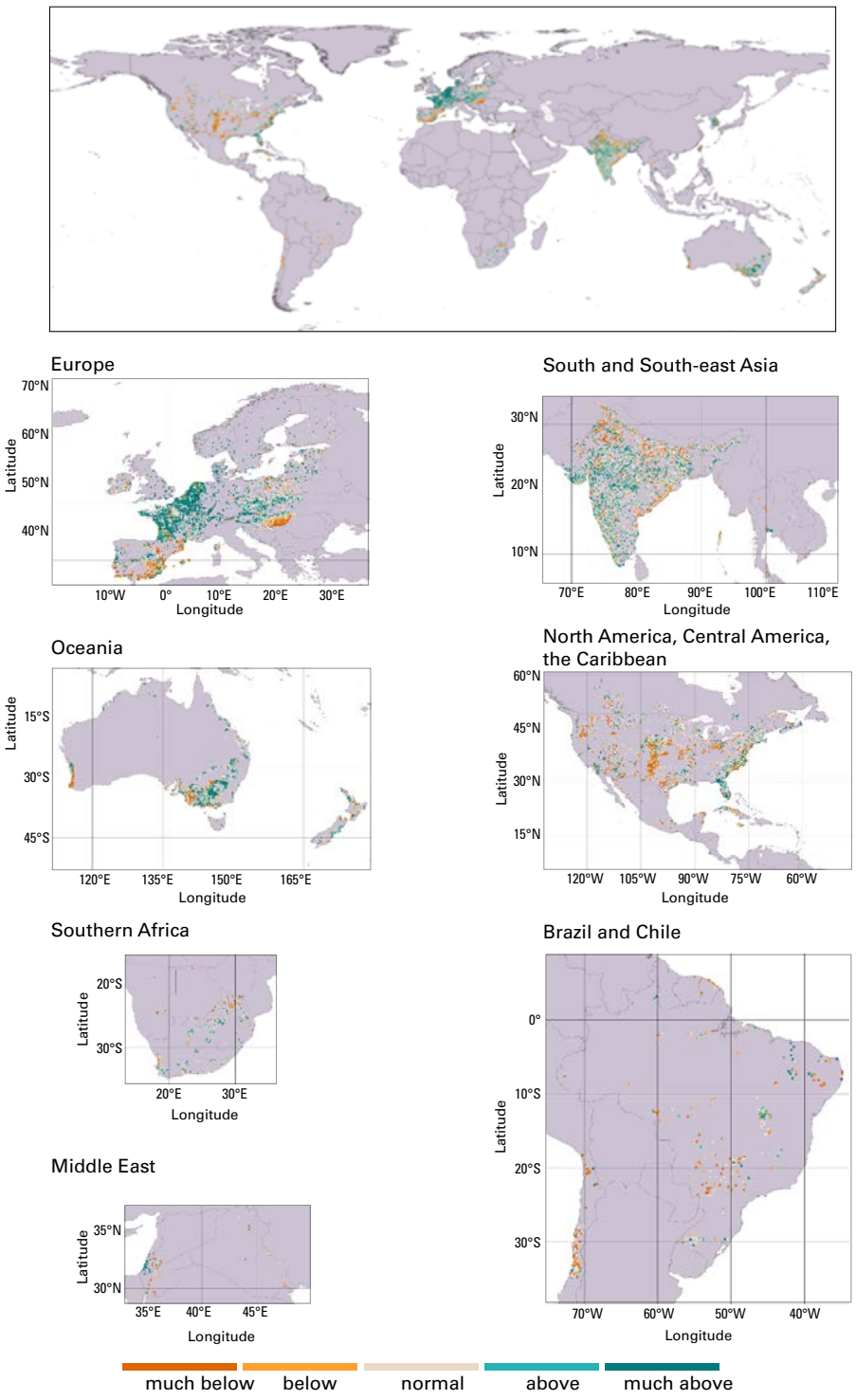

Figure A10. Mean groundwater levels per station in 2024 as compared with the historical period 2004–2024 (2015–2024 for Brazil, Costa Rica, Iraq, Kenya, State of Palestine)

Note: The boundaries and names shown and the designations used do not imply official endorsement or acceptance by WMO or the United Nations.

SOIL MOISTURE

The anomaly in surface soil moisture in 2023 has been obtained from three GHMSs (see Table A1 for model names) and ranked relative to the historical period 1991–2020 (Figure 14 in the main report) on a monthly basis to understand root zone soil moisture patterns at 1 m depth.

OBSERVED SOIL MOISTURE

In 2024 the majority of stations in the United States and Spain showed normal soil moisture conditions between March and October at both soil depths of 0–11 cm and 0–51 cm, as shown in Figure A11. However, this pattern shifted starting in November, with a noticeable increase in the fraction of stations experiencing below-normal conditions in the shallow soil layer. Notably, most of the stations under these conditions were located in Spain (7 and 8 in November and December, respectively, out of 9 stations). The fraction of stations under below-normal conditions approximately doubles compared to earlier months, as shown in the left-hand panel of Figure A12.

In October, predominantly dry conditions were reported across the United States (see NCEI Products). However, this pattern was not fully reflected in the ISMN data, as many of the analysed stations are concentrated in a few regions – such as the north-western states and Utah – where dry conditions were not observed. Despite this limitation, a drying tendency is still apparent, particularly in the deeper soil layer (down to 51 cm) (right panel of Figure 12), where many stations shifted from above-normal to normal or below-normal moisture levels.

Monthly analyses throughout 2024 support findings from other sources (see NCEI Products). In both the United States and Spain, the spatial pattern of soil moisture conditions is quite diverse, with strong local differences. During the summer months (June, July, August), the number of stations reporting below-normal and above-normal conditions were roughly equal (approximately 20 each), while normal conditions are predominant. As an example, Figure A11 illustrates this behaviour within the upper soil layer.

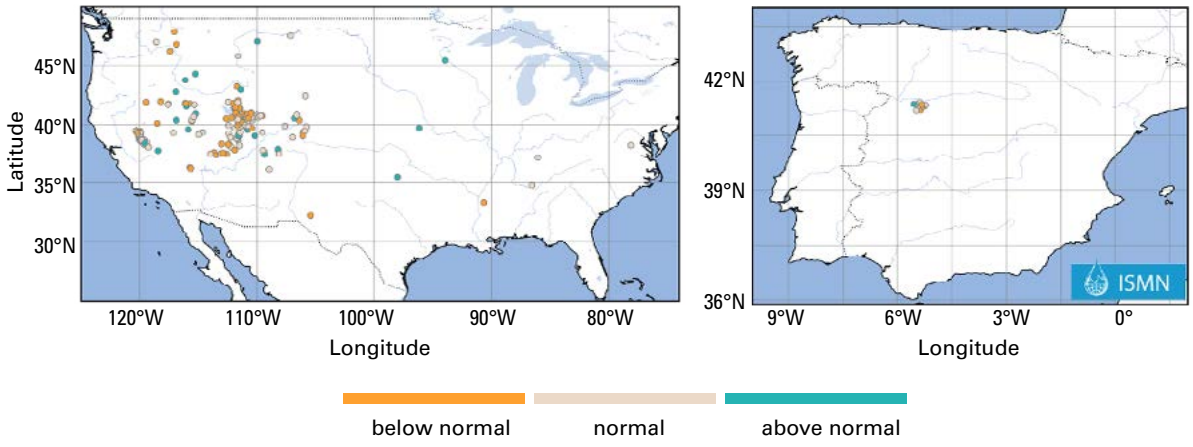

Figure A11. Soil moisture conditions in July 2024 compared to the 15-year reference period (July 2009–2023) for the topsoil layer (0–0.11 m depth). The left panel shows the state of soil moisture in the contiguous United States (CONUS) whereas Spain is shown on the right. Data availability is limited (176 stations, 164 in CONUS and 12 in Spain, which are displayed in the maps above), because only limited temporal coverage is achieved by using in situ soil moisture data.

Note: The boundaries and names shown and the designations used do not imply official endorsement or acceptance by WMO or the United Nations.

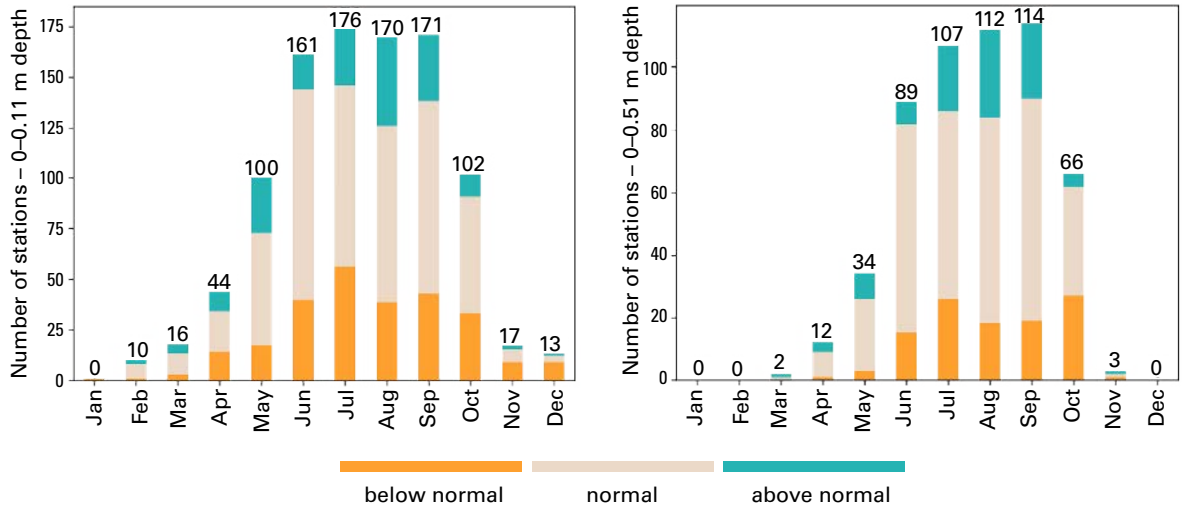

Figure A12, Number of stations reporting below-normal, normal, and above-normal soil moisture conditions. The left panel represents shallow soil moisture (0–11 cm), while the right panel represents a deeper soil column (0–51 cm). These stations are distributed across the United States (up to 165 stations) and Spain (up to 13 stations). Please note that the station locations may differ between the months, which is caused by the filtering method applied. One station can have data in August but might not be considered in September due to missing data or for data quality considerations. Indications of the location of the stations can be seen in Figure A11 above.

EVAPOTRANSPIRATION

The actual evapotranspiration at the global scale for four seasons in 2024 with respect to the historical period 1991–2020 was derived from six GHMSs (listed in Table A1) and averaged over the river basins derived from the Hydrobasins level 4 delineation (Lehner et al., 2013).

SNOW WATER EQUIVALENT

The daily snow water equivalent (SWE) output was obtained from the Crocus-ERA5 snow model (Decharme and Barbu, 2024) and aggregated over a given land region to produce a daily snow mass time series. Peak snow mass values were then calculated for each water year, and the resulting series of values were used to calculate 2024 percentiles relative to the 1991–2020 reference period.

Ensemble-mean March SWE fields over the 1991–2020 period were calculated using data from four individual gridded products:

- The European Space Agency Snow CCI SWE version 2 product derived through a combination of satellite passive microwave brightness temperatures and climate station snow depth observations (Luojus et al., 2022);
- The Modern-Era Retrospective Analysis for Research and Applications version 2 (MERRA-2) (GMAO, 2015) daily SWE fields;

- SWE output from the ERA5-Land analysis (Muñoz Sabater, 2019);
- The physical snowpack model Crocus (Decharme and Barbu, 2024) driven by ERA5 meteorological forcing.

March-mean fields from each product were regridded to a common 0.5° × 0.5° regular grid and averaged together. This is the same suite of products used to produce annually updated SWE data for the Arctic Report Card (see, for example, Mudryk et al., 2024) and the Bulletin of the American Meteorological Society (BAMS) State of the Climate Report (see, for example, Mudryk et al., 2025). March 2024 SWE values were converted to percentiles using the 1991–2020 reference period on a pixel-wise basis.

In addition, the March SWE in the northern hemisphere was obtained for 2024 and compared to the reference period from 1991 to 2020 based on two GHMSs: mHM and TEJRA55. Results are presented in Figure A13.

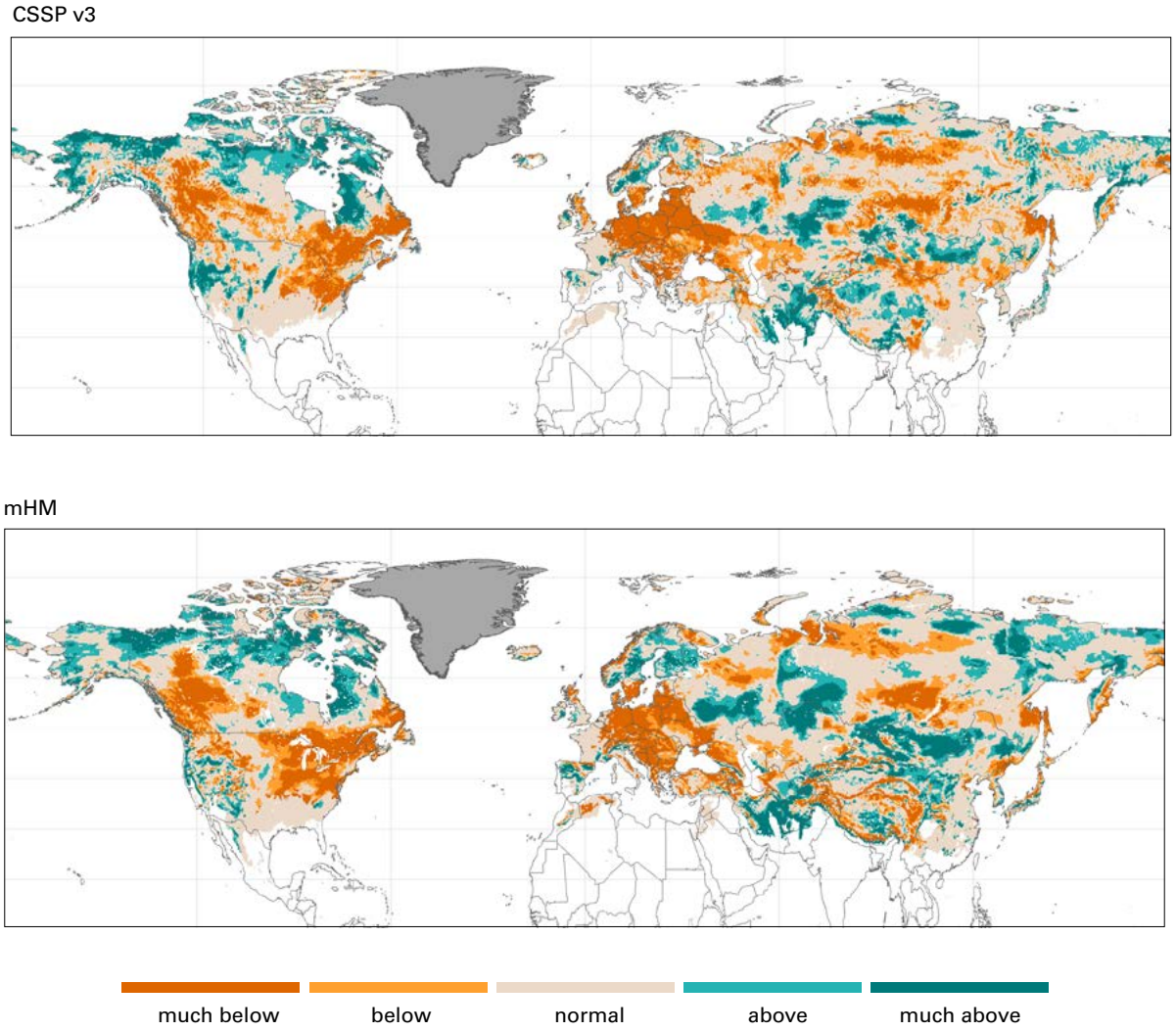

Figure A13. March 2024 snow water equivalent expressed as anomalies compared with the 1991–2020 reference period based on the mHM and CSSPv3 models

Note: The boundaries and names shown and the designations used do not imply official endorsement or acceptance by WMO or the United Nations.

TERRESTRIAL WATER STORAGE

GLOBAL

Satellite gravimetry is the only remote-sensing-based method capable of observing the whole water column, including surface water, soil moisture, groundwater, and snow and ice. This report presents an analysis of the terrestrial water storage (TWS) anomaly between the years 2002 and 2021, observed with the Gravity Recovery and Climate Experiment (GRACE) mission (2002–2017) and its successor GRACE-Follow-On (Grace-FO) (since 2018) (Landerer et al., 2020; Tapley et al., 2019). GRACE provides the TWS anomaly compared with the baseline of 2004–2009, and then Equation 2 is used to adjust the TWS anomaly compared with the baseline of 2002–2020.

The TWS anomaly in equivalent water heights in centimetres was calculated according to Equation 2:

$$TWS_{\text{anomaly}} = TWS_t - \bar{X} \tag{2}$$

where TWS_t (cm) is the TWS value at month t of the current year and $\bar{X}$ is the long-term average TWS (cm), as calculated for 2002–2020. Equivalent water height is the theoretical mean height of the water column over the whole area being considered.

TWS for the year 2021 was ranked in a manner similar to that used for the discharge. However, the time series of TWS were too short (19 years) to perform ranking on the yearly values, therefore the index for each month was computed and then aggregated to the yearly mean values.

GLACIERS

The present assessment of global glacier mass loss is based on a combination of glaciological field measurements (~500 glaciers or 1% of global glaciers) and geodetic satellite measurements (>200 000 glaciers or 96% of global glaciers) derived from the Fluctuations of Glaciers (FoG) database compiled by the World Glacier Monitoring Service (Dussaillant et al., 2025; WGMS, 2025). Winter and summer regional balances are calculated by downscaling the annual values using seasonal observations from FoG and the sine function analytical model proposed by Zemp and Welty (2023). Seasonal and annual balances follow the hydrological year, which is not the same for the northern hemisphere (NH), the southern hemisphere (SH) and the tropical (low-latitude) regions. A hydrological year cycle starts at the beginning of winter, finishes at the end of summer and is given the name of the year at the end of the cycle. For the NH, we assumed that winter lasts from October to March and summer from April to September. For the SH, we assumed that winter lasts from April to September and summer from October to March. For the low latitudes, we assumed no seasonality and, hence, plotted the annual values only. Regional winter and summer seasonal estimates are representative of the regional hydrological cycles. Therefore, seasonal balance bars are plotted with respect to their time of occurrence. On the other hand, because winter and summer occur at a different time globally, the global winter and summer seasonal estimates correspond to global hydrological years, with winter and summer global balance bars corresponding to the sum of winter and summer balances in the NH and SH regions, respectively.

GLACIER CONTRIBUTION TO SEASONAL RIVER RUNOFF

The annual mass balance of a glacier is calculated as the difference between the snow accumulation in winter (mass gain) and the melt of ice and snow during summer (mass loss) over a hydrological year, reflecting the prevalent atmospheric conditions. When measured over a long period, trends in glaciers' mass change are an indicator of climate change. The global net loss of glacier mass contributes to sea-level rise. Seasonal melting of ice and snow contributes to runoff. Therefore, glaciers contribute to seasonal runoff even in years with balanced conditions, or positive annual mass balance. This can be seen in Figure 21 in the main report, where seasonal mass balances are shown. Negative summer mass balance values (that is, ice mass loss) contribute to river flow even in years where regions experience a net positive annual mass balance (blue bars).

In general, depending on the region, precipitation and snowmelt play a larger role in modulating seasonal streamflow than glacier mass balance. However, glaciers do matter in some regions and during warm and dry months of the year. In arid and semiarid regions there is a delay between the moment when water is stored in a glacier (winter), and the moment when the meltwater is produced and released to the rivers (summer). For these regions, this seasonally delayed runoff plays a crucial role in sustaining river flows during the driest months of the year and during periods of extreme drought, compensating for otherwise reduced flows due to lack of rain and snowmelt (Dussaillant et al., 2019; Huss and Hock, 2018; Kaser et al., 2010; Pritchard et al., 2019; Radić and Hock, 2014).

When a glacier is balanced with its climate, its annual contribution to streamflow will only depend on the yearly summer balance. Contrarily, when a glacier is exposed to a climatic warming, its volume will decrease in time as water is released from its long-term storage. As a consequence, glacier runoff is expected to increase with climate change until reaching a maximum "peak water" contribution beyond which runoff starts to gradually decrease, as the reduced glacier volume cannot support high melt rates anymore (Huss and Hock, 2018; Wimberly et al., 2025). If temperatures continue to increase, the glacier will disappear, and with it, its hydrological contribution (Figure A14).

Concerning the future of glacier meltwater availability, Huss and Hock (2018) assessed the hydrological consequences of glacier decline around the world. The largest summer month

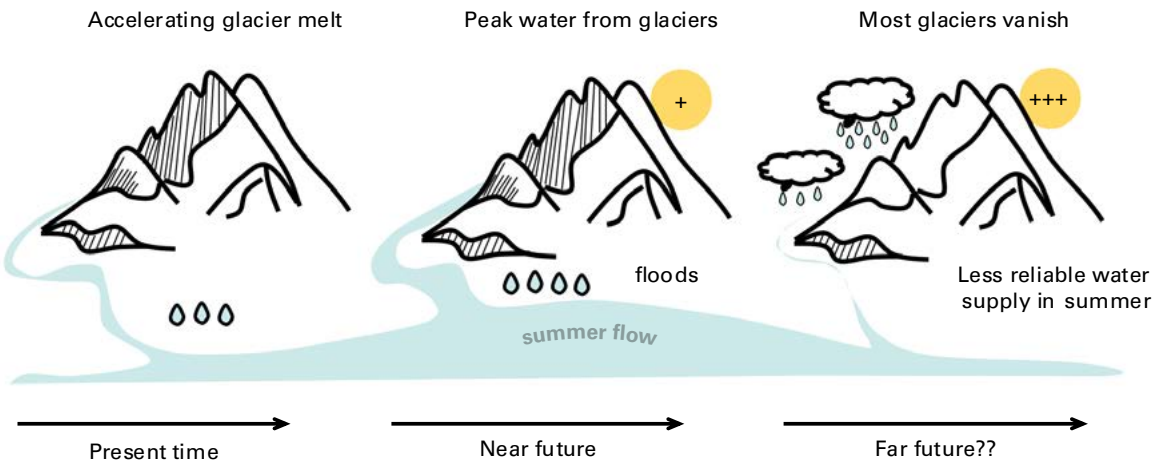

Figure A14. Schematic view of expected runoff changes under ongoing climate change affecting total glacier meltwater contribution as well as the seasonality in water availability

Source: Adapted from Barandun et al. (2020)

reductions in glacier runoff by the end of the century are expected in Central Asia and the tropical and central Andes. Notably, these are the only regions where more than 50% of the total basin runoff comes from snow and ice. The net contribution of water melt depends on the glacier area, with larger regions (such as Alaska) releasing larger water volumes. However, if observed in relation to the glacier surface, the impact of glacial meltwater is independent of glacier volume and is also recognizable in regions with lower glaciation. In the European Alps, for example, glaciers also significantly contribute to runoff during summer months and help mitigate the negative hydrological effects of drought years (Huss, 2011; Huss et al., 2017).

WATER QUALITY

OBSERVED RIVER WATER QUALITY

- Water quality was included for the first time in this report series: observed daily measurements for river water temperature, dissolved oxygen, pH and electrical conductivity from 472 stations in six countries were included in the assessment.

- More than half of the monitoring stations in rivers showed above- or much-above-normal water temperatures following similar spatial patterns as air temperature anomalies.

- Dissolved oxygen levels were more equally distributed, with 35% of the monitoring stations having normal levels, 32% above- or much-above-normal levels and 33% below- or much-below-normal levels.

- Similar to air temperature, more than half of the monitoring stations had above- or much-above-normal pH levels (55%), 34% normal and 11% below- and much-below-normal levels.

- Electrical conductivity levels were normal at 40% of the monitoring stations, with 30% of the stations showing above- or much-above-normal levels and 30% below- and much-below-normal levels.

This section provides the status of water temperature, dissolved oxygen, pH and electrical conductivity in rivers in 2024 compared to a 10-year reference period between 2011 and 2023. In order to align the assessment of water quality with the methodologies of other in situ variables as closely as possible, only water quality sensor data with daily temporal resolution have been included in this year's report.

The data were obtained from national water agencies and subsequently filtered to comply with the data coverage requirements, limiting the amount of data available for analysis to 472 stations covering one or more water quality variables in six countries, as presented in Table A4 and Figure A15. Further details on the methodology and its imitations are provided below.

METHODOLOGY

The quality of inland freshwater bodies depends on physical, chemical and biological characteristics of their water and sediment, usually assessed in relation to its suitability for a particular purpose such as drinking, swimming, agriculture, industrial use or its capacity to sustain aquatic ecosystems. Water quality is measured using a combination of field tests, laboratory analysis, and more recently sensor-based monitoring. While laboratory analyses allow for the evaluation of hundreds of different characteristics, the complexity of sampling

and laboratory analysis and their related costs prevent high spatial and temporal resolutions for these measurements in many parts of the world. In-situ sensor-based methods are limited to a few physical and chemical characteristics but can measure at high temporal frequencies, enabling the analysis of short-term variations in water quality.

In order to align the assessment of water quality with other observed variables in this report, only daily time series data from automatic monitoring networks for water temperature, dissolved oxygen, pH and electrical conductivity were considered. Due to the fact that automatic sensor networks only became more widely used in the 2010s, a reference period of 10 years was selected.

The data were either downloaded from online sources or requested from the data providers. Times series data with temporal resolutions higher than one day (for example, recordings every 10 minutes) were aggregated to daily mean values.

The data were filtered for data completeness using the following criteria:

- Only time series for which at least 80% of daily values were valid in a 10-year reference period and the 2024 reporting year were included.
- During the reference period one calendar month of consecutive missing daily values per year was permitted as long as the other reference years contained valid data for this calendar month.
- For each country, a suitable 10-year reference period was selected based on the maximum number of stations with time series complying with above criteria. This resulted in different reference periods for the countries included.

Due to time constraints, no further quality assurance of the data could be carried out. Out of 1 063 stations in seven countries for which data were initially collected, 438 stations in six countries satisfied the completeness criteria. The spatial distribution of the stations is presented in Figure A15, with the countries, their respective reference periods and number of stations listed in Table A5.

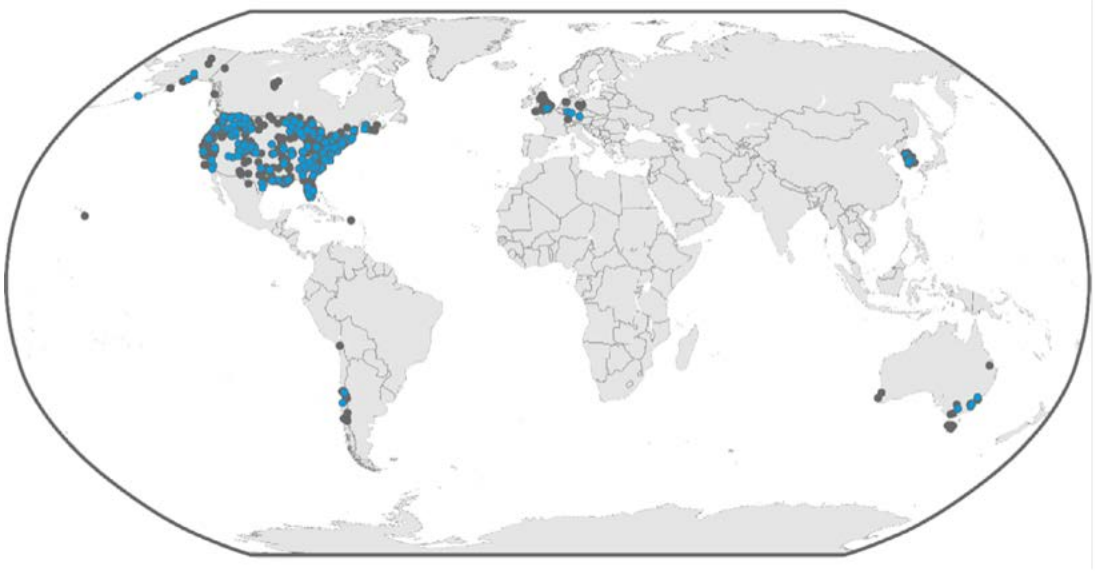

Figure A15. Locations of the monitoring stations for which data were used (in blue) and excluded (in grey) from the report

Table A5. Reference periods and number of monitoring stations used for the six countries included in the water quality report

Country	*Reference period*	*Number of stations*				
		Water temperature	*Dissolved oxygen*	*pH*	*Electrical conductivity*	*Total*
Australia	2013–2022	8		5	6	8
Chile	2014–2023	1	2	1	1	2
Germany	2011–2020	4	4[a]	4	4	4
United Kingdom	2014–2023	3	7	4	3	7
Republic of Korea	2013–2022	9	8[a]	8	8	9
United States of America	2012–2021	407	212[a]	87	194	438

[a] Including both dissolved concentration and saturation measurements.

WATER TEMPERATURE

Water temperature is a key water quality variable because it directly affects the physical, chemical and biological processes in aquatic environments. Many aquatic species have narrow temperature ranges for growth and reproduction. Warmer water holds less oxygen than cooler water, which can stress or kill aquatic species. Higher temperatures also accelerate chemical reactions, which can increase the toxicity of pollutants and affect nutrient levels due to accelerated breakdown of organic matter.

In 2024, above- and much-above-normal river water temperature was observed at 55%, normal temperature at 41% and below- and much-below-normal temperature in 4% of the monitoring stations (as shown in Figure A16).

Although river water temperature is mostly controlled by incoming solar radiation and depends on other natural and anthropogenic factors such as water volume, local conditions influencing solar exposure and thermally modified effluents, it often correlates to air temperature. Earth's

Water temperature anomalies in rivers in 2024

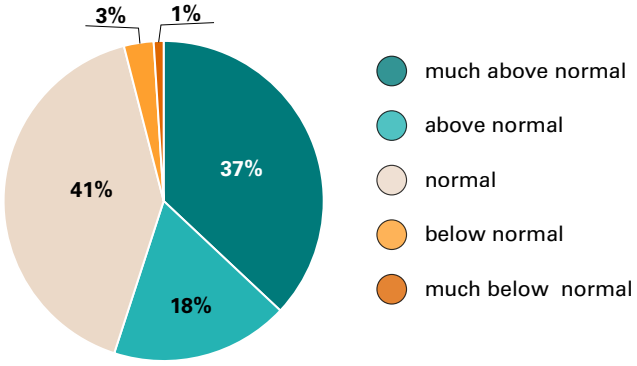

Figure A16. Water temperature anomalies in rivers in 2024 compared to a 10-year reference period between 2011 and 2023 (varying reference periods depending on the data source) across all monitoring stations analysed (432 stations in six countries)

average near-surface temperature in 2024 was the warmest on record *State of the Global Climate 2024* (WMO-No. 1368), and river water temperatures show similar spatial warming patterns as those for air temperature in many temperate and subtropical rivers in the United States, United Kingdom, Germany and Republic of Korea, as shown in Figure A17.

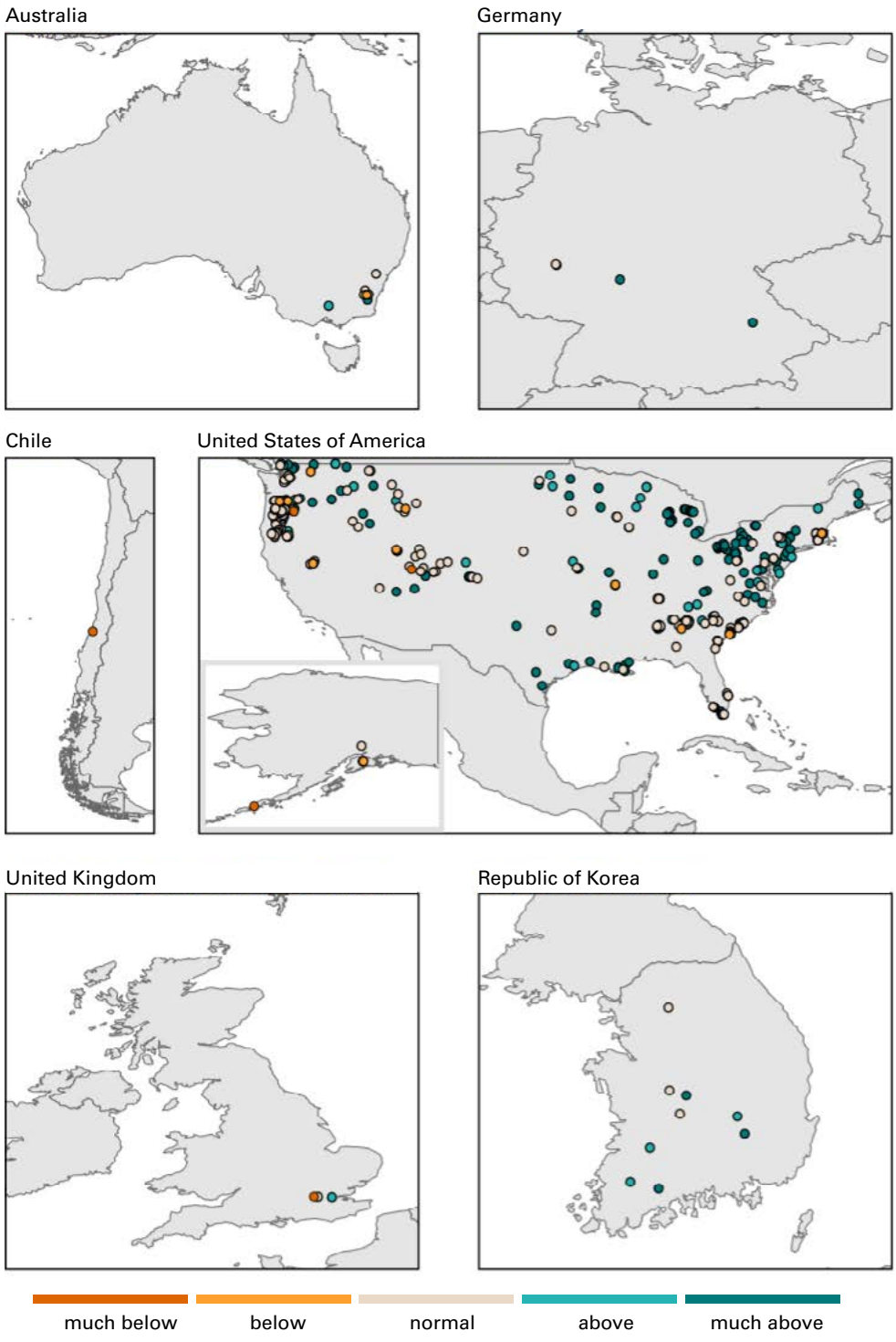

Figure A17. Water temperature anomalies in rivers in 2024 compared to a 10-year reference period between 2011 and 2023 (note: varying reference periods were applied depending on the data availability, see Table A5)

Note: The boundaries and names shown and the designations used do not imply official endorsement or acceptance by WMO or the United Nations.

DISSOLVED OXYGEN

Similar to water temperature, dissolved oxygen is a key water quality characteristic because it directly affects the health of aquatic ecosystems. Aquatic organisms such as fish and invertebrates need oxygen to survive. Low levels of dissolved oxygen can cause hypoxia stressing or killing these organisms. Bacteria consume oxygen when decomposing organic matter, reducing dissolved oxygen and increasing nutrient levels. This can lead to eutrophication, which can cause algal blooms that further deplete oxygen.

In 2024, above- and much-above-normal dissolved oxygen levels were observed at 32% of monitoring stations, with 35% of stations showing normal and 33% below- and much-below-normal levels (Figure A18).

Dissolved oxygen can be measured as concentration or saturation. For those monitoring stations where both concentration and water temperature data were available, saturation values were calculated using Equation 3:

$$DO\ (\%\ Saturation) = 100 \cdot C^{O_2} \div C_{eq}^{O_2} \quad (3)$$

where

C^{O_2} = Oxygen concentration in mg/l

$C_{eq}^{O_2}$ = Equilibrium oxygen concentration at standard pressure of 101.325 kpa in mg/l

defined as: $C_{eq}^{O_2} = e^{7.7117 - 1.31403*\ln(T+45.93)}$

Lower-than-normal dissolved oxygen levels occurred in rivers in Chile and across different rivers in the United States, potentially affecting aquatic organisms in these rivers (Figure A19).

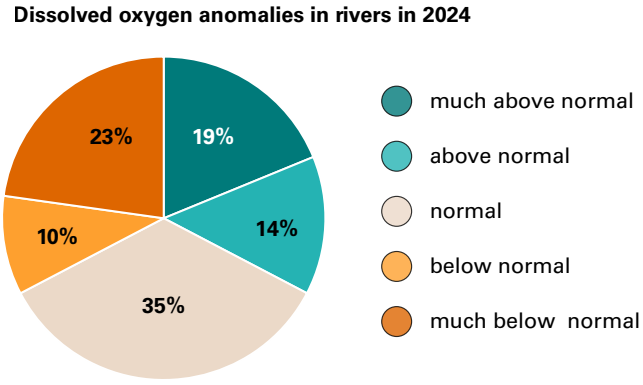

Figure A18. Dissolved oxygen anomalies in rivers in 2024 compared to a 10-year reference period between 2011 and 2023 (note: varying reference periods were applied depending on the data availability) across all monitoring stations analysed (235 stations with dissolved concentration or saturation measurements in 5 countries)

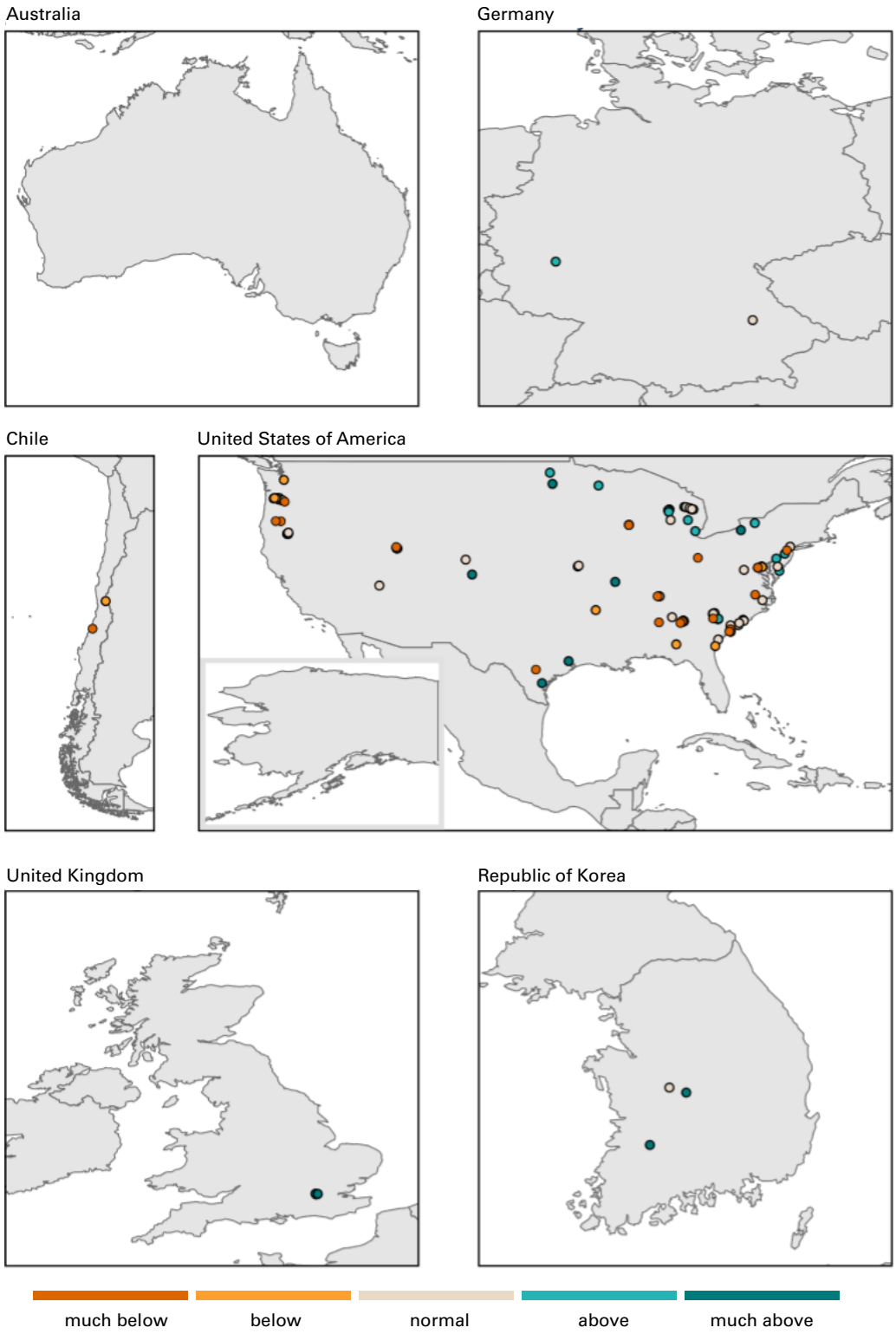

Figure A19. Dissolved oxygen anomalies in rivers in 2024 compared to a 10-year reference period between 2011 and 2023 (note: varying reference periods were applied depending on the data availability). Data include both dissolved oxygen concentration and saturation measurements.

Note: The boundaries and names shown and the designations used do not imply official endorsement or acceptance by WMO or the United Nations.

pH

The hydrogen potential (pH), a measure of the acidity or basicity of water, affects chemical and biological processes in water such as the solubility and availability of nutrients and metals. In acidic water (low pH), toxic metals become more soluble and harmful, whereas in alkaline water (high pH) the availability of certain nutrients is reduced. pH also affects aquatic organisms, which often require a pH range between 6.5 and 8.5 to flourish. River water pH is shaped by geology, biological activity, climate and hydrological conditions, and can be further influenced by human activities such as agriculture, wastewater discharge and atmospheric deposition.

The majority (55%) of the 109 stations analysed in 2024 showed above- and much-above-normal pH levels, 34% normal and 11% below- and much-below-normal levels (Figures A20 and A21). Although only six stations showed pH above or below the recommended pH range (6.5–8.5) with respect to the annual average pH levels, additional analyses of the exceedance times based on the daily measurements would be required to assess potential negative effects on aquatic organisms.

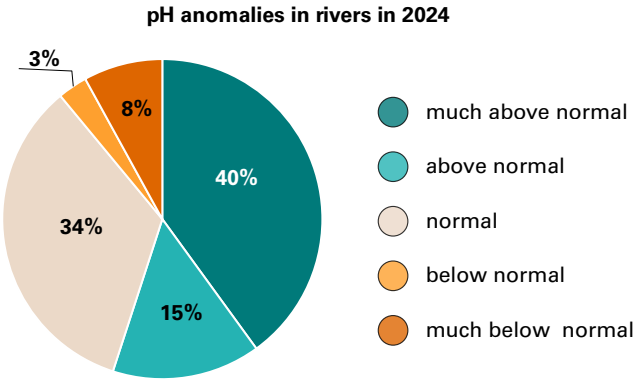

Figure A20. pH anomalies in rivers in 2024 compared to a 10-year reference period between 2011 and 2023 (note: varying reference periods were applied depending on the data availability) across all monitoring stations analysed (109 stations in six countries)

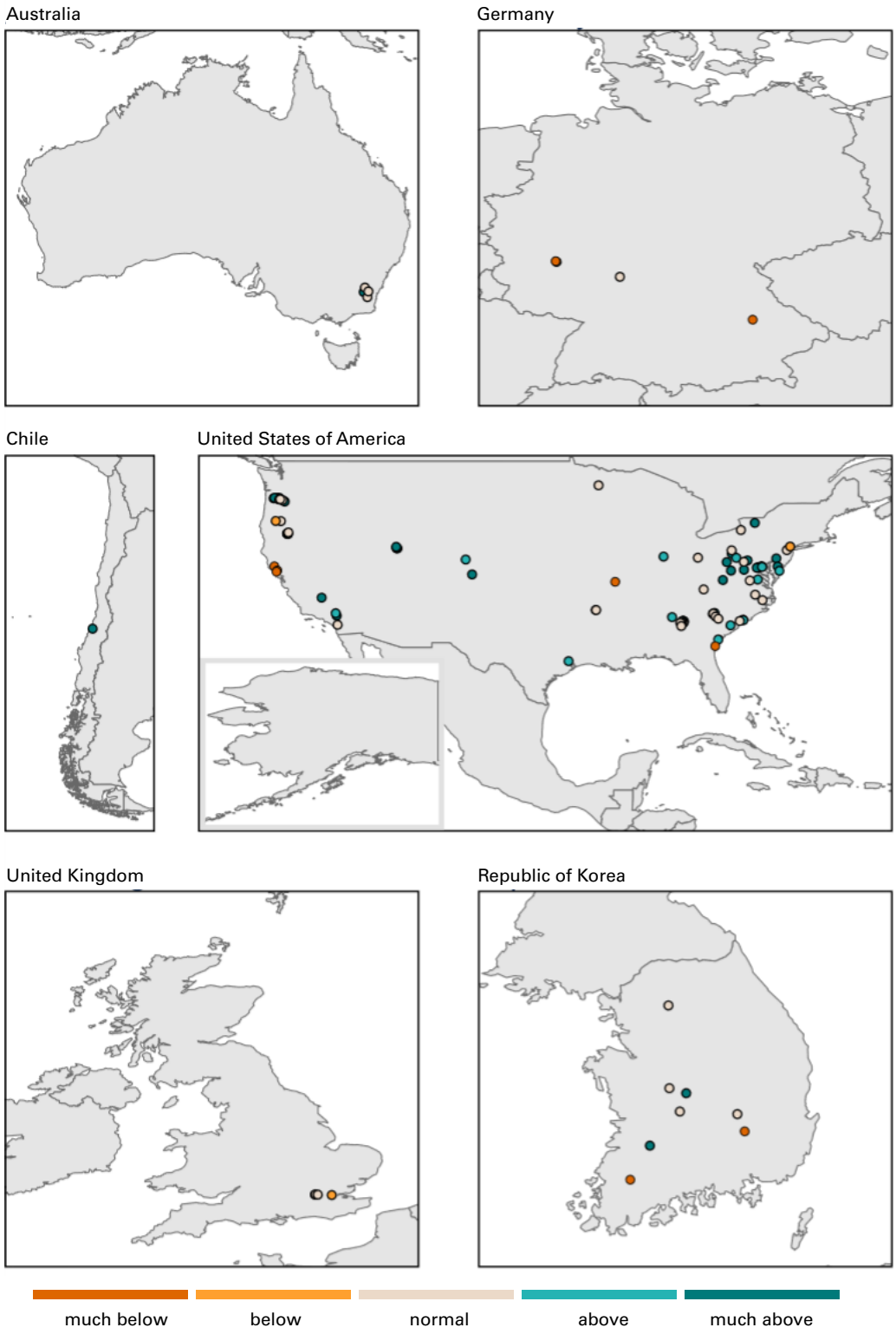

Figure A21. pH anomalies in rivers in 2024 compared to a 10-year reference period between 2011 and 2023 (note: varying reference periods were applied depending on the data availability)

Note: The boundaries and names shown and the designations used do not imply official endorsement or acceptance by WMO or the United Nations.

ELECTRICAL CONDUCTIVITY

Electrical conductivity reflects the amount of dissolved salts and ions in water, which can affect ecosystem health and water usability. Many aquatic organisms are sensitive to changes in salinity, especially if they occur suddenly. High levels of electrical conductivity can limit the suitability of water for drinking, irrigation or industrial uses. River water conductivity generally increases with higher concentrations of dissolved salts and nutrients from geology, evaporation or human inputs, and decreases when waters are diluted by rainfall, snow melt or low mineral runoff.

Electrical conductivity above and much above normal levels occurred at 30% of the monitoring stations analysed in 2024, whereas 40% of the stations showed normal levels and 30% below- or much-below-normal levels (see Figures A22 and A23).

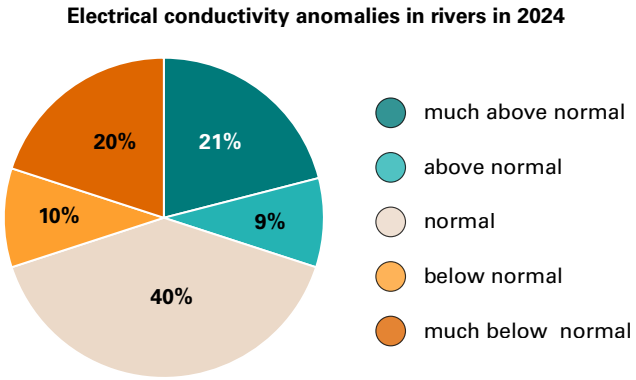

Figure A22. Electrical conductivity anomalies in rivers in 2024 compared to a 10-year reference period between 2011 and 2023 (note: varying reference periods were applied depending on the data availability) across all monitoring stations analysed (217 stations in six countries)

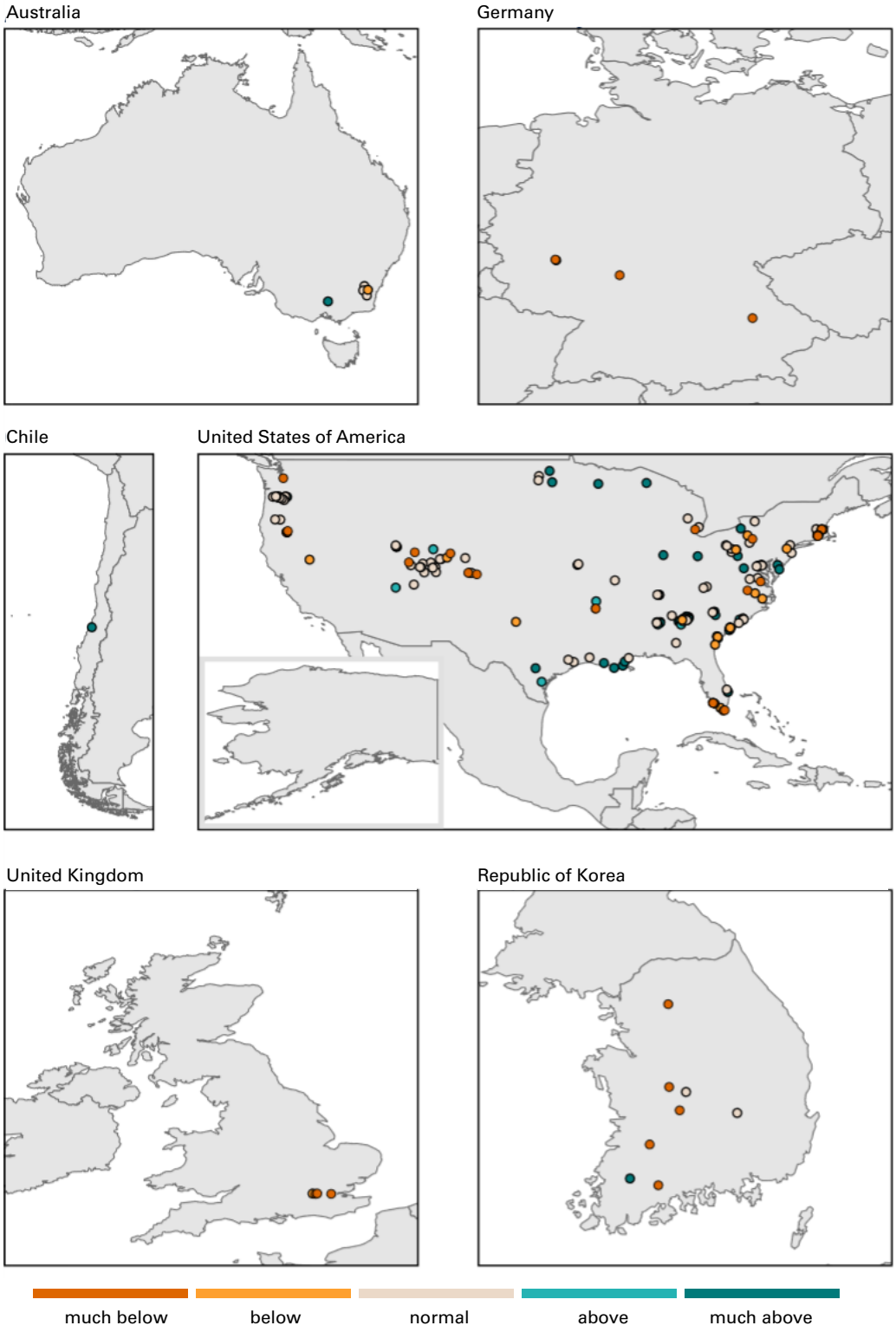

Figure A23. Electrical conductivity anomalies in rivers in 2024 compared to a 10-year reference period between 2011 and 2023 (note: varying reference periods were applied depending on the data availability)

Note: The boundaries and names shown and the designations used do not imply official endorsement or acceptance by WMO or the United Nations.

References

Alfieri, L.; Burek, P.; Dutra, E. et al. GloFAS – Global Ensemble Streamflow Forecasting and Flood Early Warning. *Hydrology and Earth System Sciences* **2013**, *17* (3), 1161–1175. https://doi.org/10.5194/hess-17-1161-2013.

Ali, A. N. A. M.; Imhoff, R. O.; Weerts, A. H. Machine Learning for Predicting Spatially Variable Lateral Hydraulic Conductivity: A Step towards Efficient Hydrological Model Calibration and Global Applicability. *ESS Open Archive* **2025**. https://essopenarchive.org/doi/full/10.22541/essoar.174016989.99005964.

Arheimer, B.; Pimentel, R.; Isberg, K. et al. Global Catchment Modelling Using World-Wide HYPE (WWH), Open Data, and Stepwise Parameter Estimation. *Hydrology and Earth System Sciences* **2020**, *24* (2), 535–559. https://doi.org/10.5194/hess-24-535-2020.

Barandun, M.; Fiddes, J.; Scherler, M. et al. The State and Future of the Cryosphere in Central Asia. *Water Security* **2020**, *11*, 100072. https://doi.org/10.1016/j.wasec.2020.100072.

Beck, H. E.; Wood, E. F.; Pan, M. et al. MSWEP V2 Global 3-Hourly 0.1° Precipitation: Methodology and Quantitative Assessment. *Bulletin of the American Meteorological Society* **2019**, *100* (3), 473–500. https://doi.org/10.1175/BAMS-D-17-0138.1.

Berg, P.; Almén, F.; Bozhinova, D. HydroGFD3.0 (Hydrological Global Forcing Data): A 25 Km Global Precipitation and Temperature Data Set Updated in near-Real Time. *Earth System Science Data* **2021**, *13* (4), 1531–1545. https://doi.org/10.5194/essd-13-1531-2021.

Biswas, N. K.; Hossain, F.; Bonnema, M. et al. Towards a Global Reservoir Assessment Tool for Predicting Hydrologic Impacts and Operating Patterns of Existing and Planned Reservoirs. *Environmental Modelling & Software* **2021**, *140*, 105043. https://doi.org/10.1016/j.envsoft.2021.105043.

Boergens, E.; Güntner, A.; Dobslaw, H. et al. Quantifying the Central European Droughts in 2018 and 2019 With GRACE Follow-On. *Geophysical Research Letters* **2020**, *47* (14), e2020GL087285. https://doi.org/10.1029/2020GL087285.

Boussetta, S.; Balsamo, G.; Arduini, G. et al. ECLand: The ECMWF Land Surface Modelling System. *Atmosphere* **2021**, *12* (6), 723. https://doi.org/10.3390/atmos12060723.

Centre for Research on the Epidemiology of Disasters (CRED). *EM-DAT*; CRED/UCLouvain: Brussels, Belgium. http://www.emdat.be.

Decharme, B.; Barbu, A. Crocus-ERA5 Daily Snow Product over the Northern Hemisphere at 0.25° Resolution; Version 2023; *Zenodo* **2024**. https://doi.org/10.5281/zenodo.10943718.

Donchyts, G.; Winsemius, H.; Baart, F. et al. High-Resolution Surface Water Dynamics in Earth's Small and Medium-Sized Reservoirs. *Scientific Reports* **2022**, *12* (1), 13776. https://doi.org/10.1038/s41598-022-17074-6.

Dussaillant, I.; Berthier, E.; Brun, F. et al. Two Decades of Glacier Mass Loss along the Andes. *Nature Geoscience* **2019**, *12* (10), 802–808. https://doi.org/10.1038/s41561-019-0432-5.

Dussaillant, I.; Hugonnet, R.; Huss, M. et al. Annual Mass Change of the World's Glaciers from 1976 to 2024 by Temporal Downscaling of Satellite Data with in Situ Observations. *Earth System Science Data* **2025**, *17* (5), 1977–2006. https://doi.org/10.5194/essd-17-1977-2025.

Eilander, D.; van Verseveld, W.; Yamazaki, D. et al. A Hydrography Upscaling Method for Scale-Invariant Parametrization of Distributed Hydrological Models. *Hydrology and Earth System Sciences* **2021**, *25* (9), 5287–5313. https://doi.org/10.5194/hess-25-5287-2021.

Elmi, O.; Tourian, M. J. Retrieving Time Series of River Water Extent from Global Inland Water Data Sets. *Journal of Hydrology* **2023**, *617*, 128880. https://doi.org/10.1016/j.jhydrol.2022.128880.

Elmi, O.; Tourian, M. J.; Saemian, P. et al. Remote Sensing-Based Extension of GRDC Discharge Time Series - A Monthly Product with Uncertainty Estimates. *Scientific Data* **2024**, *11* (1), 240. https://doi.org/10.1038/s41597-024-03078-6.

Global Modeling and Assimilation Office (GMAO). *inst3_3d_asm_Cp: MERRA-2 3D IAU State, Meteorology Instantaneous 3-hourly (p-coord, 0.625x0.5L42)*, version 5.12.4; Goddard Space Flight Center Distributed Active Archive Center (GSFC DAAC): Greenbelt, USA, 2015. https://doi.org/10.5067/VJAFPLI1CSIV.

Grimaldi, S.; Salamon, P.; Russo, C. et al. GloFAS v4.0: Towards Hyper-resolution Hydrological Modelling at Global Scale. In *European Geosciences Union (EGU) Abstracts EGU General Assembly 2023*, Vienna, Austria, 23–28 April 2023. https://doi.org/10.5194/egusphere-egu23-3410.

Hales, R. C.; Nelson, E. J.; Souffront, M. et al. Advancing Global Hydrologic Modeling with the GEOGloWS ECMWF Streamflow Service. *Journal of Flood Risk Management* **2022**, *18* (1), e12859. https://doi.org/10.1111/jfr3.12859.

Hanazaki, R.; Yamazaki, D.; Yoshimura, K. Development of a Reservoir Flood Control Scheme for Global Flood Models. *Journal of Advances in Modeling Earth Systems* **2022**, *14* (3), e2021MS002944. https://doi.org/10.1029/2021MS002944.

Hersbach, H.; Bell, B.; Berrisford, P. et al. The ERA5 Global Reanalysis. *Quarterly Journal of the Royal Meteorological Society* **2020**, *146* (730), 1999–2049. https://doi.org/10.1002/qj.3803.

Huang, Q.; Zhang, Y.; Ma, N. et al. Estimating Vegetation Greening Influences on Runoff Signatures Using a Log-Based Weighted Ensemble Method. *Water Resources Research* **2022**, *58* (12), e2022WR032492. https://doi.org/10.1029/2022WR032492.

Huss, M. Present and Future Contribution of Glacier Storage Change to Runoff from Macroscale Drainage Basins in Europe. *Water Resources Research* **2011**, *47* (7). https://doi.org/10.1029/2010WR010299.

Huss, M.; Hock, R. Global-Scale Hydrological Response to Future Glacier Mass Loss. *Nature Climate Change* **2018**, *8* (2), 135–140. https://doi.org/10.1038/s41558-017-0049-x.

Huss, M.; Bookhagen, B.; Huggel, C. et al. Toward Mountains without Permanent Snow and Ice. *Earth's Future* **2017**, *5* (5), 418–435. https://doi.org/10.1002/2016EF000514.

Imhoff, R. O.; van Verseveld, W. J.; van Osnabrugge, B. et al. Scaling Point-Scale (Pedo)Transfer Functions to Seamless Large-Domain Parameter Estimates for High-Resolution Distributed Hydrologic Modeling: An Example for the Rhine River. *Water Resources Research* **2020**, *56* (4), e2019WR026807. https://doi.org/10.1029/2019WR026807.

Kaser, G.; Großhauser, M.; Marzeion, B. Contribution Potential of Glaciers to Water Availability in Different Climate Regimes. *Proceedings of the National Academy of Sciences* **2010**, *107* (47), 20223–20227. https://doi.org/10.1073/pnas.1008162107.

Kobayashi, S.; Ota, Y.; Harada, Y. et al. The JRA-55 Reanalysis: General Specifications and Basic Characteristics. *Journal of the Meteorological Society of Japan. Ser. II* **2015**, *93* (1), 5–48. https://doi.org/10.2151/jmsj.2015-001.

Kumar, R.; Samaniego, L.; Attinger, S. Implications of Distributed Hydrologic Model Parameterization on Water Fluxes at Multiple Scales and Locations. *Water Resources Research* **2013**, *49* (1), 360–379. https://doi.org/10.1029/2012WR012195.

Landerer, F. W.; Flechtner, F. M.; Save, H. et al. Extending the Global Mass Change Data Record: GRACE Follow-On Instrument and Science Data Performance. *Geophysical Research Letters* **2020**, *47* (12), e2020GL088306. https://doi.org/10.1029/2020GL088306.

Lehner, B.; Döll, P. Development and Validation of a Global Database of Lakes, Reservoirs and Wetlands. *Journal of Hydrology* **2004**, *296* (1), 1–22. https://doi.org/10.1016/j.jhydrol.2004.03.028.

Lehner, B.; Liermann, C. R.; Revenga, C. et al. High-Resolution Mapping of the World's Reservoirs and Dams for Sustainable River-Flow Management. *Frontiers in Ecology and the Environment* **2011**, *9* (9), 494–502. https://doi.org/10.1890/100125.

Lehner, B.; Reidy Liermann, C.; Revenga, C. et al. *Global Reservoir and Dam Database, Version 1 (GRanDv1): Dams, Revision 01*; NASA Socioeconomic Data and Applications Center (SEDAC), 2011. https://doi.org/10.7927/H4N877QK.

Lehner, B.; Grill, G. Global River Hydrography and Network Routing: Baseline Data and New Approaches to Study the World's Large River Systems. *Hydrological Processes* **2013**, *27* (15), 2171–2186. https://doi.org/10.1002/hyp.9740.

Luojus, K.; Moisander, M.; Pulliainen, J. et al. *ESA Snow Climate Change Initiative (Snow_cci): Snow Water Equivalent (SWE) Level 3C Daily Global Climate Research Data Package (CRDP) (1979–2020), version 2.0*; NERC EDS Centre for Environmental Data Analysis, 2022. https://doi.org/10.5285/4647cc9ad3c044439d6c643208d3c494.

Ma, W.; Ishitsuka, Y.; Takeshima, A. et al. Applicability of a Nationwide Flood Forecasting System for Typhoon Hagibis 2019. *Scientific Reports* **2021**, *11* (1), 10213. https://doi.org/10.1038/s41598-021-89522-8.

Marsh, T.; Sanderson, F.; Swain, O. *Derivation of the UK National and Regional Runoff Series*; National Environment Research Council (NERC): Wallingford, UK, 2015. https://nora.nerc.ac.uk/id/eprint/510580/.

Messager, M. L.; Lehner, B.; Grill, G. et al. Estimating the Volume and Age of Water Stored in Global Lakes Using a Geo-Statistical Approach. *Nature Communications* **2016**, *7* (1), 13603. https://doi.org/10.1038/ncomms13603.

Mudryk, L. R.; Chereque, A. E.; Derksen, C. et al. Terrestrial Snow Cover: Arctic Report Card 2024; Moon, T. A.; Druckenmiller, M. L.; Thoman, R. L., Eds.; NOAA Technical Report OAR ARC; 24-04; National Oceanic and Atmospheric Administration, 2024. https://doi.org/10.25923/4bb3-3f87.

Mudryk, L. R.; Elias Chereque, A.; Derksen, C. et al. Terrestrial Snow Cover [in "State of the Climate in 2024"]. *Bulletin of the American Meteorological Society* **2025**, *106* (8), S335–S338. https://doi.org/10.1175/BAMS-D-25-0104.1.

Müller Schmied, H.; Cáceres, D.; Eisner, S. et al. The Global Water Resources and Use Model WaterGAP v2.2d: Model Description and Evaluation. *Geoscientific Model Development* **2021**, *14* (2), 1037–1079. https://doi.org/10.5194/gmd-14-1037-2021.

Müller Schmied, H.; Trautmann, T.; Ackermann, S. et al. The Global Water Resources and Use Model WaterGAP v2.2e: Description and Evaluation of Modifications and New Features. *Geoscientific Model Development* **2024**, *17* (23), 8817–8852. https://doi.org/10.5194/gmd-17-8817-2024.

Muñoz Sabater, J. *ERA5-Land Hourly Data from 1950 to Present; Copernicus Climate Change Service (C3S) Climate Data Store (CDS)*, 2019. https://doi.org/10.24381/cds.e2161bac.

Murray, A. M.; Jørgensen, G. H.; Godiksen, P. N. et al. DHI-GHM: Real-Time and Forecasted Hydrology for the Entire Planet. *Journal of Hydrology* **2023**, *620*, 129431. https://doi.org/10.1016/j.jhydrol.2023.129431.

Nash, J. E., & Sutcliffe, J. V. River flow forecasting through conceptual models Part I—A discussion of principles. *Journal of Hydrology* **1970**, *10* (3), 282–290. https://doi.org/10.1016/0022-1694(70)90255-6.

Pritchard, H. D. Asia's Shrinking Glaciers Protect Large Populations from Drought Stress. *Nature* **2019**, *569* (7758), 649–654. https://doi.org/10.1038/s41586-019-1240-1.

Radić, V.; Hock, R. Glaciers in the Earth's Hydrological Cycle: Assessments of Glacier Mass and Runoff Changes on Global and Regional Scales. *Surveys in Geophysics* **2014**, *35* (3), 813–837. https://doi.org/10.1007/s10712-013-9262-y.

Reinecke, R.; Stein, L.; Gnann, S. et al. Uncertainties as a Guide for Global Water Model Advancement. *WIREs Water* **2025**, *12* (3), e70025. https://doi.org/10.1002/wat2.70025.

Saemian, P.; Elmi, O.; Stroud, M. et al. Satellite Altimetry-Based Extension of Global-Scale in Situ River Discharge Measurements (SAEM). *Earth System Science Data* **2025**, *17* (5), 2063–2085. https://doi.org/10.5194/essd-17-2063-2025.

Samaniego, L.; Kaluza, M.; Kumar, R. et al. Mesoscale Hydrologic Model; *Zenodo*, **2019**. https://doi.org/10.5281/zenodo.3239055.

Samaniego, L.; Kumar, R.; Attinger, S. Multiscale Parameter Regionalization of a Grid-Based Hydrologic Model at the Mesoscale. *Water Resources Research* **2010**, *46* (5). https://doi.org/10.1029/2008WR007327.

Sutanudjaja, E. H.; van Beek, R.; Wanders, N. et al. PCR-GLOBWB 2: A 5 Arcmin Global Hydrological and Water Resources Model. *Geoscientific Model Development* **2018**, *11* (6), 2429–2453. https://doi.org/10.5194/gmd-11-2429-2018.

Tapley, B. D.; Watkins, M. M.; Flechtner, F. et al. Contributions of GRACE to Understanding Climate Change. *Nature Climate Change* **2019**, *9* (5), 358–369. https://doi.org/10.1038/s41558-019-0456-2.

Tourian, M. J.; Elmi, O.; Shafaghi, Y. et al. HydroSat: Geometric Quantities of the Global Water Cycle from Geodetic Satellites. *Earth System Science Data* **2022**, *14* (5), 2463–2486. https://doi.org/10.5194/essd-14-2463-2022.

van der Laan, E.; Hazenberg, P.; Weerts, A. H. Simulation of Long-Term Storage Dynamics of Headwater Reservoirs across the Globe Using Public Cloud Computing Infrastructure. *Science of The Total Environment* **2024**, *931*, 172678. https://doi.org/10.1016/j.scitotenv.2024.172678.

van Verseveld, W. J.; Weerts, A. H.; Visser, M. et al. Wflow_sbm v0.7.3, a Spatially Distributed Hydrological Model: From Global Data to Local Applications. *Geoscientific Model Development* **2024**, *17* (8), 3199–3234. https://doi.org/10.5194/gmd-17-3199-2024.

Wang, J.; Walter, B. A.; Yao, F. et al. GeoDAR: Georeferenced Global Dams and Reservoirs Dataset for Bridging Attributes and Geolocations. *Earth System Science Data* **2022**, *14* (4), 1869–1899. https://doi.org/10.5194/essd-14-1869-2022.

Wimberly, F.; Ultee, L.; Schuster, L. et al. Inter-Model Differences in 21st Century Glacier Runoff for the World's Major River Basins. *The Cryosphere* **2025**, *19* (4), 1491–1511. https://doi.org/10.5194/tc-19-1491-2025.

World Glacier Monitoring Service (WGMS). *Global Glacier Change Bulletin No. 5 (2020–2021)*. Zemp, M.; Gärtner-Roer, I.; Nussbaumer, S. U. et al., Eds.; WGMS: Zurich, Switzerland, 2023, 134 pp. [publication based on database version: doi:10.5904/wgms-fog-2023-09]. https://wgms.ch/downloads/WGMS_GGCB_05.pdf.

Yamazaki, D.; Kanae, S.; Kim, H. et al. A Physically Based Description of Floodplain Inundation Dynamics in a Global River Routing Model. *Water Resources Research* **2011**, *47* (4). https://doi.org/10.1029/2010WR009726.

Yamazaki, D.; Ikeshima, D.; Sosa, J. et al. MERIT Hydro: A High-Resolution Global Hydrography Map Based on Latest Topography Dataset. *Water Resources Research* **2019**, *55* (6), 5053–5073. https://doi.org/10.1029/2019WR024873.

Yoshimura, K.; Sakimura, T.; Oki, T. et al. Toward Flood Risk Prediction: A Statistical Approach Using a 29-Year River Discharge Simulation over Japan. *Hydrological Research Letters* **2008**, *2*, 22–26. https://doi.org/10.3178/hrl.2.22.

Yuan, X.; Ji, P.; Wang, L. et al. High-Resolution Land Surface Modeling of Hydrological Changes Over the Sanjiangyuan Region in the Eastern Tibetan Plateau: 1. Model Development and Evaluation. *Journal of Advances in Modeling Earth Systems* **2018**, *10* (11), 2806–2828. https://doi.org/10.1029/2018MS001412.

Zemp, M.; Welty, E. Temporal Downscaling of Glaciological Mass Balance Using Seasonal Observations. *Journal of Glaciology* **2023**, 69 (278), 1–6. https://doi.org/10.1017/jog.2023.66.

Zhang, Y.; Kong, D.; Gan, R. et al. Coupled Estimation of 500 m and 8-Day Resolution Global Evapotranspiration and Gross Primary Production in 2002–2017. *Remote Sensing of Environment* **2019**, *222*, 165–182. https://doi.org/10.1016/j.rse.2018.12.031.

Ziese, M.; Schneider, U.; Meyer-Christoffer, A. et al. The GPCC Drought Index – a New, Combined and Gridded Global Drought Index. *Earth System Science Data* **2014**, *6* (2), 285–295. https://doi.org/10.5194/essd-6-285-2014.

For more information, please contact:

World Meteorological Organization

7 bis, avenue de la Paix – P.O. Box 2300 – CH 1211 Geneva 2 – Switzerland

Strategic Communications Office
Cabinet Office of the Secretary-General

Tel: +41 (0) 22 730 83 14 – Fax: +41 (0) 22 730 80 27

Email: media@wmo.int

wmo.int

JN 25789